Novel Photophysical Properties Based on the Association of Luminescent Metal Complex with DNA

February 2021

Haruki Minami

Graduate School of Science and Engineering

Chiba University

（千葉大学審査学位論文）

Novel Photophysical Properties Based on the Association of Luminescent Metal Complex with DNA

February 2021

Haruki Minami

Graduate School of Science and Engineering

Chiba University

Preface

The functional materials that show optical changes in response to various stimulations are fascinating and expected to be applied to luminescent devices, chemical sensors, bio-imaging, and other fields.   Especially, luminescent metal complexes have attracted much attention of many researchers in various fields.   In addition, the chiral luminescence (circularly polarized luminescence: CPL) provides advanced information based on the difference in intensity between right and left component and is expected not only to improve the precise sensing of chiral molecules and biomolecules as well as structural analyses of biopolymers but also to lead to the development of multifunctional displays, security paints, and optical communication.   However, the simultaneous achievement of both strong emission intensity and brilliant luminescent chirality was difficult in the metal complex-based systems.

The luminescent properties of the metal complexes significantly change under the alteration of the structure and ligand field around the central metal ion.   Thus, this thesis focused on the association of metal complex with DNA toward the development of novel photo-functional materials showing both strong emission intensity and brilliant luminescent chirality.   DNA is well known biopolymer having unique helical structure and have ability to incorporate other molecules through various types of interaction mode leading the structural change of incorporated molecules.   First, Δ- and Λ-Ru(phen)$_3{}^{2+}$ were associated with DNA toward the fabrication of novel photo functional material. These molecules formed associations thorough different interaction modes and exhibited enantioselective emission enhancement whereas CPL was not observed.   Then, Eu(III) complex, which show luminescence due to f-f transition, were employed in order to obtain CPL.   When Eu(tta)$_3$(H$_2$O)$_2$ was associated with DNA-CTMA, induced CPL was observed because of change in coordination structure.   In addition, an emission enhancement and higher dissymmetry factor were simultaneously observed upon the association of Eu(D-facam)$_3$ with DNA.   Finally, I successfully achieved novel photo functional material showing strong luminescence and high luminescent dissymmetry simultaneously by associating chiral metal complex with DNA.

Haruki Minami

Acknowledgement

Haruki Minami

Contents

Chapter 1

Introduction for the DNA-based photo functional materials

1.1 Luminescent metal complexes and its application

1.1.1 Luminescence from transition metal complexes

The functional materials that show optical changes in response to various stimulations are fascinating and expected to be applied to luminescent devices, chemical sensors, bio-imaging, and other fields.[1-7] Especially, luminescent metal complexes have attracted much attention of many researchers in various fields. The first luminescence from metal transition complexes was reported in the middle of 19th century in the platinum(II) complex. However, subsequent research on luminescent metal complexes was relatively limited, and the main research targets were polypyridine ruthenium(II) (Ru(II)) complexes and metal porphyrins.[8-10] In the late 1990s, it was discovered that iridium(III) complexes are very useful as light emitting materials for organic electro-luminescence devices (OLEDs).[11] With this as a trigger, the search for new luminescent metal complexes has become active all over the world, and the types of luminescent metal complexes and their applications have rapidly developed. The characteristics of the luminescent metal complex are mainly the following two. 1) It emits phosphorescence. 2) It has a variety of luminescent states. In the luminescent metal complex with d-block elements, the singlet excited state generated by photoexcitation causes intersystem crossing due to strong spin-orbit interaction by heavy metal ions, leading to easy relaxation to triplet excited state. As a result, most d-metal complexes exhibit phosphorescence. The lowest excited triplet state, which is the luminescent state of a transition metal complex, has various origins. It is known that there are various type of excited states based on metal-to ligand charge transfer (MLCT), ligand-to-metal charge transfer (LMCT), ligand-to-ligand charge transfer (LLCT), etc. due to the difference in the combination of central metal ion and ligand. Of course, the excited state in the ligand (intraligand: IL) such as the $\pi\pi^*$ state can also be the luminescent state. Furthermore, in recent years, complexes using 3d-metals, which are cheaper than precious metals have attracted much attention as promising candidate for the luminescent material. In this way, the variety of light emitting states of metal complexes is further expanding. Various light emissions due to ligand field (LF) excited states represented by d-d transitions, other metal centered (MC) transitions, and cluster centered (CC) excited states are widely known, and research on delayed light fluorescence as well as phosphorescence is very active.

Luminescent metal complexes with d^6 electron configuration

Various studies have been conducted on tris(2,2'-bipyridine)ruthenium(II) ($[Ru(bpy)_3]^{2+}$) for many years as a representative of metal complexes having triplet state of metal-to-ligand charge transfer (^{3}MLCT) as a luminescent state.[12,13] Figure 1-1 shows the structure of $Ru(bpy)_3^{2+}$. $Ru(bpy)_3^{2+}$ shows a relatively long-life red emission even in an aqueous solution at room temperature (λ_{max} = 610 nm, τ = ca. 600 ns, Φ = ca. 0.06). The ^{3}MLCT excited state having such properties is very useful for photoreaction. Since the excited state of $Ru(bpy)_3^{2+}$ obtained with photoexcitation exhibits strong reducing ability and oxidizing ability, it has been widely utilized as a photosensitizer and a photocatalyst. In connection with this, various polypyridin ruthenium(II) complexes have been synthesized and their emission characteristics have been investigated. For example, tris(3,3'-biisoquinoline)ruthenium(II) ($[Ru(i\text{-}biq)_3]^{2+}$: Figure 1-1) has the same ligand field intensity as $Ru(bpy)_3^{2+}$, but has interesting luminescence properties different from $Ru(bpy)_3^{2+}$ due to the difference in the extension of the π-conjugation.[14] Although the lowest excited singlet state of $Ru(i\text{-}biq)_3^{2+}$ is the ^{1}MLCT from ruthenium(II) ion to ligand same as in $Ru(bpy)_3^{2+}$, its absorption band appears at shorter wavelengths (λ_{max} = 392 nm) than that of $Ru(bpy)_3^{2+}$ (λ_{max} = 450 nm). On the other hand, since the $^1\pi\pi^*$ absorption band of $Ru(i\text{-}biq)_3^{2+}$ has a lower energy of about 5000 cm^{-1} than that of $Ru(bpy)_3^{2+}$, the MLCT state and the $\pi\pi^*$ state are close to each other in $Ru(i\text{-}biq)_3^{2+}$ (Figure 1-2). As a result, the energy level reversed in the triplet state of $Ru(i\text{-}biq)_3^{2+}$, and the emission spectrum shows the peaks with clear vibrational structure derived from the $^3\pi\pi^*$ state with a clear vibrational structure (Figure 1-3). In addition, since the emission of ^{3}MLCT is thermal equilibrium emission from three sub-levels with different radiative rate, the magnitude of sub-level splitting without the influence of magnetic field
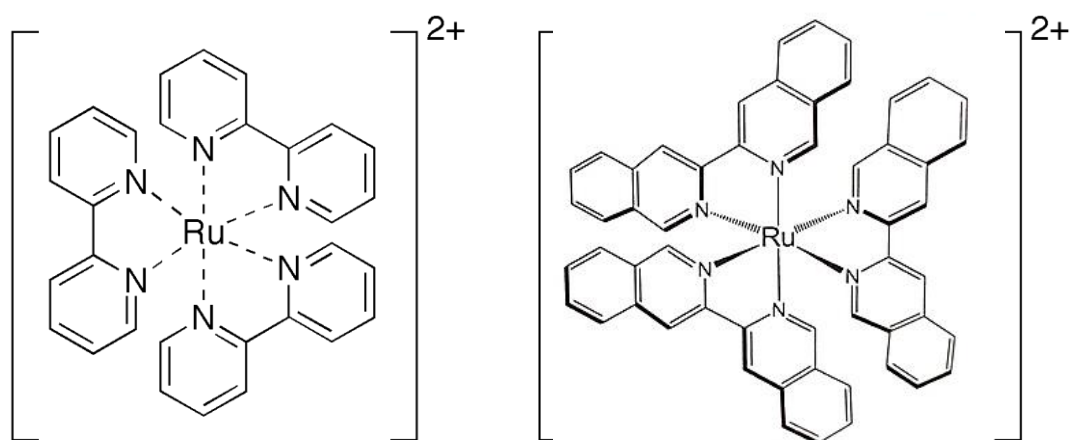
Figure 1-1. The structure of $Ru(bpy)_3^{2+}$ (left) and $Ru(i\text{-}biq)_3^{2+}$ (right).

(zero-field splitting) is very large in Ru(II) complexes (ca. 10-100 cm^{-1}). Therefore, it is known that the obvious temperature dependence of the emission lifetime is observed in the cryogenic region of 77 K or less. In the case of Ru(bpy)$_3^{2+}$, the emission lifetime is ca. 4 µs at 77 K and ca. 100 µs at 4.2 K. In contrast, in $^3\pi\pi^*$ emission with small zero-field splitting, such temperature dependence of emission lifetime is hardly observed.

Such changes in luminescence properties depending on the structure of the complex have also been investigated in detail in the ^{3}MLCT emission of tris(2-phenylpyridinate)iridium(II) (Ir(ppy)$_3$), which has played an important role as a material for various luminescence devices. Ir(ppy)$_3$ is a representative of cyclometalated ligands and forms a stable chelate coordination with deprotonated carbon located at the 2-position of the phenyl group and nitrogen of the pyridine ring.[15-17] This complex has geometric

Figure 1-2. Absorption spectra of Ru(*i*-biq)$_3^{2+}$ (full line), Ru(bpy)$_3^{2+}$ (dotted line) in AN solution. (reused from ref. 14)
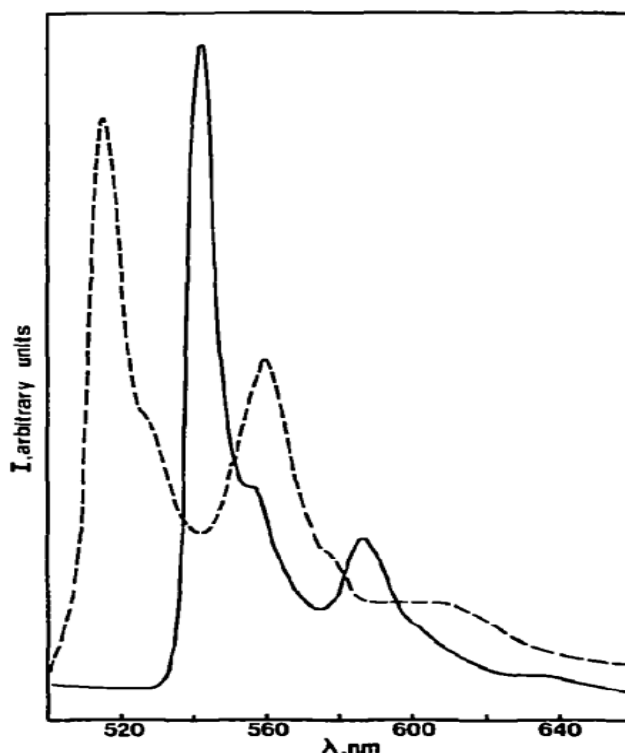
Figure 1-3. Emission spectra of Ru(*i*-biq)$_3^{2+}$ in MeOH-EtOH (4:1, v/v) (full line) and *i*-biq in C$_2$H$_5$I (dashed line) at 77K. (reused from ref. 14)

isomers of a *facial* body (*fac*) in which three carbons are arranged on the same plane of the octahedral coordination structure and a *meridional* form (*mer*) in which three carbons are arranged on the meridian (Figure 1-4). Each of these geometric isomers is produced as a thermodynamic and kinetic product. Interestingly, although the *fac* form shows

strong green phosphorescence at room temperature, the *mer* form emits much weaker light than the *fac* form.　Early studies have shown that the *fac*-Ir(ppy)$_3$ has a quantum yield of 0.40 and the *mer*-Ir(ppy)$_3$ has a quantum yield of 0.036.[15]　However, more detailed research in recent years has revealed that the *fac*-Ir(ppy)$_3$ has a quantum yield close to 1 (0.97 in 2-MeTHF solution at room temperature).[16,17]　Since a thin film of neutral Ir(ppy)$_3$ can be prepared by a deposition method, many OLEDs using Ir(ppy)$_3$ have been reported.　These strong phosphorescent properties are thought to be due to that the energy level of the *dd* excited state rises because of the large ligand field splitting based on the strong σ donating property of the cyclometalated ligand, and the non-radiative deactivation from there is suppressed.　Other metal complexes with a d^6-electron configuration that exhibit luminescence include rhenium(I) complex, osmium(II) complex, and rhodium(III) complex, and those that exhibit a high emission quantum yield of 0.1 or more have been reported.[18,19]
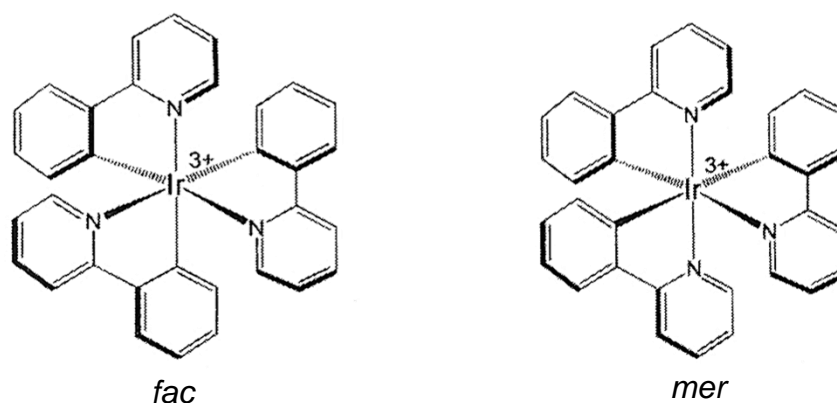
Figure 1-4. Structure of *fac*- (left) and *mer*- (right) Ir(ppy)$_3$

1.1.2 Luminescence from rare earth materials

The rare earth elements that construct the rare earth complex include lanthanide (atomic numbers are 58 to 71), lanthanum, scandium, and yttrium (Figure 1-5). Especially, trivalent lanthanide ions are known to exhibit characteristic luminescence. Luminophores using rare earths are extremely important for developing not only in various modern industrial technology fields such as fluorescent materials of fluorescent lamps and televisions, lasers, and optical communication elements, but also in medical-related fields and security-related fields.[20,21] The luminescence from rare earth ions are attributed to the electronic transition between f orbitals. Since the spatial position of the f orbital is inside the 5s and 5p orbitals, it is less affected by changes in electronic structure than organic compounds and transition metal ions. This is called the internal shielding effect. Therefore, even if the surrounding environment such as an organic ligand changes, its emission color and emission wavelength are hardly affected. In addition, since the Stokes shift hardly occurs between the ground state and the excited state due to this internal shielding effect, the rare earth ion exhibits high color purity (the half width of the emission spectrum is narrow). This emission properties with high color purity are preferably utilized as a material for displays such as televisions. In addition, since it is possible to generate an ideal strong luminescence state by exciting rare earth ions with strong light, it will be possible to realize applications in various modern science and technology fields such as laser materials and optical information communication materials. Rare earth complexes that combine rare earth ions and organic ligands has a high potential as a next-generation light-emitting material, because of "having high solubility in organic media" and "can be excited by utilizing the high absorbance of the ligand".

Figure 1-5. Types of rare earth elements

Photosensitizing effect from ligand

Rare earth complexes with aromatic ligands have a large absorption band in the ultraviolet light region of 400 nm or less due to the π-π^* transition of the ligand. This light absorption process is an allowed transition like normal luminescent dyes, and its absorption coefficient exceeds 10^4. On the other hand, the absorption coefficient of rare earths such as Eu(III) and Nd(III) is 10 or less because absorption due to electronic transitions in the f orbital is a forbidden transition. Thus, the ability of aromatic ligands to absorb light is more than 1000 times higher than that of rare earth ions. When the Eu(III) complex coordinated with an aromatic ligand is irradiated with light corresponding to the $\pi\pi^*$ transition of the ligand, the excited state of the ligand is firstly generated (process 1 in Figure 1-6). Since the Eu(III) ion is a heavy atom, the spin-orbit interaction is strong, and the excited state of the ligand changes to the triplet state (process 2). Next, energy transfer from the triplet excited state of ligand to the f orbital of Eu(III) ions occurs, and Eu(III) ions generate an excited state (process 3). After that, the excited electrons relax to the emission level in the Eu(III) ion and emit red emission due to the electronic transition in the f orbital (process 4). The emission due to this photosensitizing energy transfer shows 100-1000 times stronger intensity than the case that Eu(III) ions are directly excited.[21] These photosensitizing energy transfer from the $\pi\pi^*$ transition is peculiar to rare earth complexes, and this energy transfer process is currently the subject of academic research.
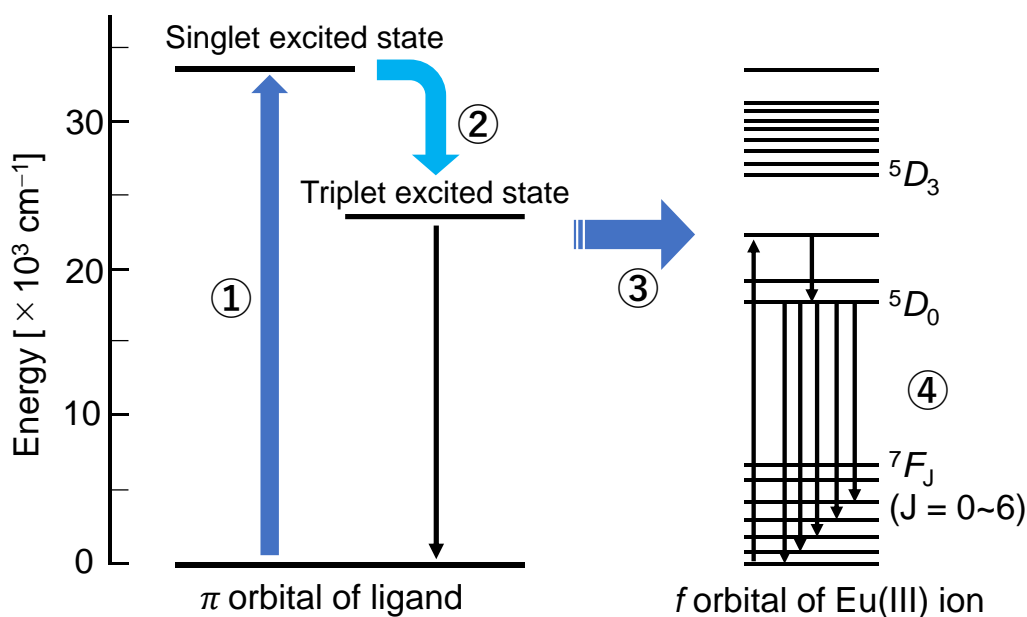
Figure 1-6. Photosensitizing process of Eu(III) complex

Promotion of electronic transitions by forming asymmetric structure

The shape of the 4f orbital of rare earth ions is anti-object to the inversion center. The direct product representing the f-f transition is as follows.

$$u \, (f \text{ orbital}) \; \times \; u \, (f \text{ orbital}) = g$$

Therefore, the $4f$-$4f$ transition of rare earth ions are Laporte forbidden transition. This forbidden transition is allowed by making the environment (ligand field) around rare earth ions to asymmetrical structure. The relax of forbiddance in the electric dipole transition by this asymmetry of the ligand field is explained by the Judd-Ofelt theory.[22,23]

In the case of the Eu(III) complex, a magnetic dipole transition of 590 nm ($^5D_0 \rightarrow ^7F_1$: ΔJ forbiddance = 1) and an electric dipole transition of 615 nm ($^5D_0 \rightarrow ^7F_2$: $\Delta J = 2$) are observed in its emission spectrum. This electric dipole transition increases as the asymmetry of the coordination structure of the complex increases. Figure 1-7 shows emission spectra of Eu(III) complexes with various ligands in PMMA.[24] Complex 2 (Eu(hfa$_3$(TPPO)$_2$, hfa: hexafluoro-acetylacetonate, TPPO: triphenyl-phosphune oxide) forms an asymmetric octacoordinated square antiprism structure, and complex 5 (Eu(hfa$_3$(DMSO)$_6$, DMSO: dimethyl-sulfoxide) forms a more symmetric pseudo-octahedron structure. Complex 2 with an asymmetric coordination structure relaxes the prohibition of electronic transitions, and the intensity of electric dipole transitions (613 nm) increases.
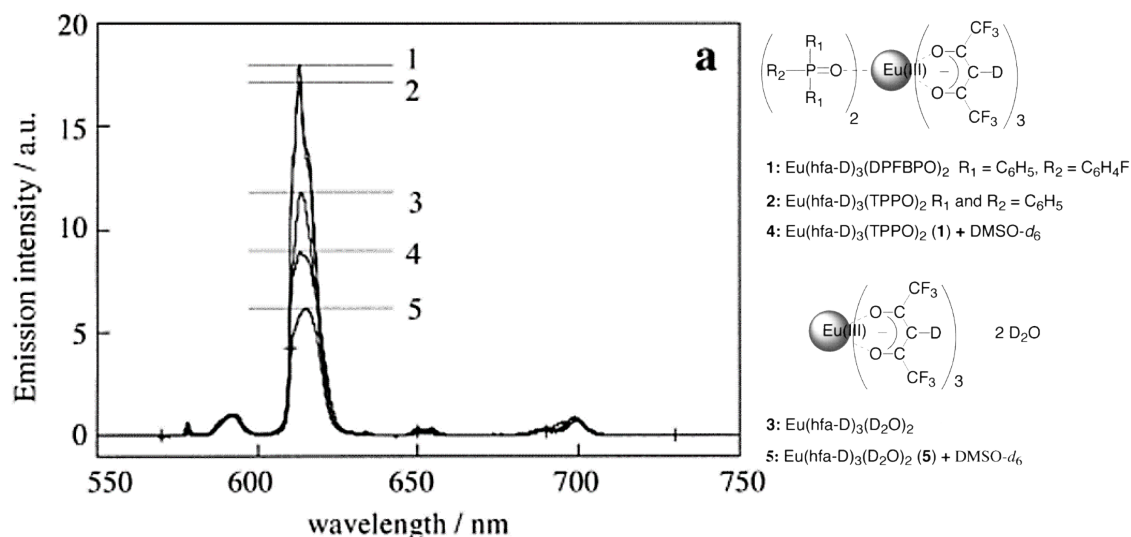
Figure 1-7. Emission spectra of Eu(III) complexes with various ligands in PMMA (Eu: 0.7 w%). The excitation at 465 nm is due to the $^7F_0 \rightarrow ^5D_2$ transition. (reused from ref. 24)

14

1.2 DNA-Based Photo-Functional Materials

As described above, the luminescent properties of the metal complexes significantly change under the influence of the structure and ligand field around the central metal ion. Such changes in the ligand field can induced not only by the difference in the structure of the ligand but also by the interaction between the metal complex and other molecules.[25-29] Therefore, this study focused on the method of associating a metal complex with deoxyribonucleic acid (DNA) in order to fabricate a novel photo-functional material while taking advantage of the characteristic luminescence properties of the metal complexes. DNA is well known biopolymer having unique helical structure and have ability to incorporate other molecules through various types of interaction mode. These interactions are highly specific to the substance and highly selective. By associating luminescent metal complex into the helical structure of DNA, it is expected that the ligand field of the complex is affected by the chiral structure and exhibit chiral optical properties such as circular dichroism (CD) and circularly polarized luminescence (CPL).

1.2.1 Structure of DNA

Deoxyribonucleic acid: DNA is an important biopolymer responsible for the transmission of genetic information and protein synthesis. Chargaff's rule was proposed after the discovery of nucleic acids by F. Miescher in 1869. Chargaff's rule is that DNA is composed of the bases adenine (A) and thymine (T), and guanine (G) and cytosine (C), and their quantity ratios are A = T and C = G.[30] When the double helix model of DNA was proposed by J.D. Watson and F.H.C. Crick in 1953, scientific research on nucleic acids began in earnest.[31] Subsequent further research has elucidated the genetic information of DNA and established a semi-conservative replication method, which has greatly contributed to the fields of medicine, biology, and medicinal chemistry.

Basic skeleton

DNA is composed of deoxyribose (Figure 1-8a), base, and phosphoric acid. A base bound to the 1'position of deoxyribose is called a deoxy nucleoside (Figure 1-8b), and a phosphate bound to the 5'position of deoxyribose is called a deoxynucleotide (Figure 1-8c). This deoxynucleotide is the smallest unit of DNA, and long-term linkage of deoxynucleotides results in a chain polymer. At this time, the deoxynucleotides are linked by a phosphodiester bond via a phosphate group. This bond is a strong covalent

(a) Deoxyribose   (b) Deoxy nucleoside   (c) Deoxy nucleotide
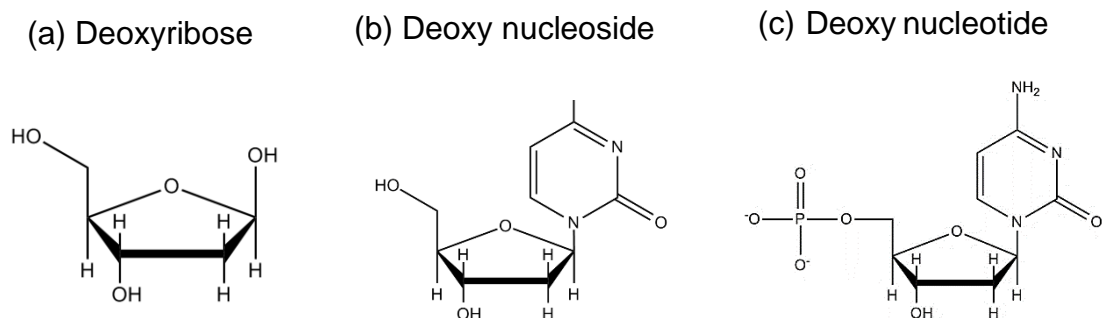
Figure 1-8. Basic skeleton of DNA.

bond in which two or more esters are bonded to a phosphorus atom, thus the phosphate group has a strong negative charge.   The double helix structure of DNA is formed by stabilizing two deoxynucleotide chains through hydrogen bonds between their respective bases.   The inside of the DNA double helix is hydrophobic because of the hydrophobic interaction between these bases. On the other hand, the periphery of the DNA double helix becomes hydrophilic due to the negative charge of the phosphate group.

Base

   Figure 1-9a shows the structures of the four bases that make up DNA: adenine (A), guanine (G), cytosine (C), and thymine (T).   Adenine and thymine are purine derivatives, and cytosine and thymine are pyrimidine derivatives, respectively, and the sequences of these bases provide the genetic information of DNA.   Hydrogen bonds between bases occur with a combination of adenine and thymine (A-T), guanine and cytosine (G-C), and there are no other combinations.   The hydrogen bonds between bases contribute to the stabilization of the double helix structure of DNA.   As shown in Figure 1-9b, A-T has two hydrogen bonds and G-C has three hydrogen bonds.   In this way, DNA has the property that when one base of adenine, guanine, cytosine, and thymine is determined, the base to be paired is also determined, and the hydrogen bond of this base connects the two deoxynucleotide chains.

16
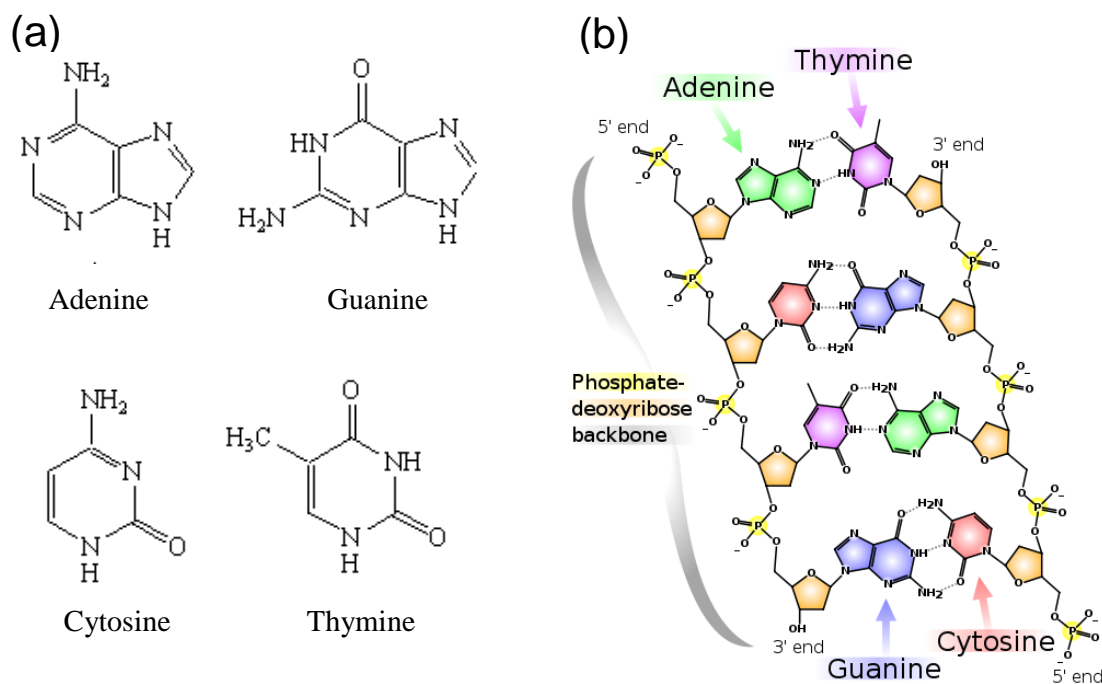
Figure 1-9. (a) Structure of bases.　　(b) Structure of nucleotide and DNA.

1.2.2 Interaction with other molecules

　　DNA has a right-handed double helix structure in which two nucleotide-bound strands are twisted together, and it interacts with other substances through various forms.　　Fig. 1-10 shows a schematic diagram of (a) electrostatic interaction, (b) intercalation, (c) groove binding, which are typical interaction form of DNA.　　By associating DNA with other functional molecules through these interaction modes, it is possible to add functionality to DNA, expanding its application as a functional material.　　Each form of interaction has its own characteristics, and the molecules that cause the interaction are also different, so they are described in detail below.

Electrostatic interaction

　　Since the phosphate groups in the DNA side chain have a negative charge, it can be said that DNA is a polyanion.　　Therefore, DNA can bind to positively charged cationic molecules via phosphate groups electrostatically.[32]　　This is called an "electrostatic interaction" (Figure1-10a).

17
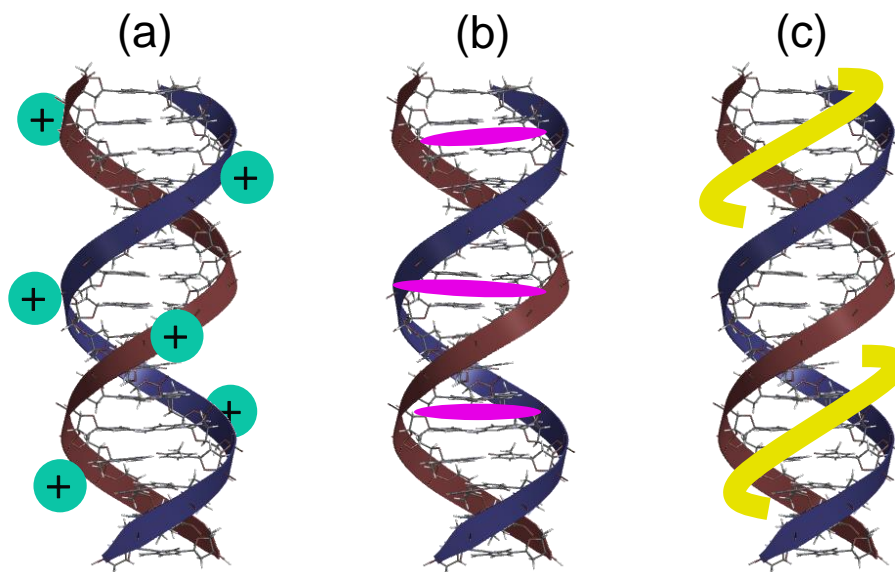
Figure 1-10. Schematic images of (a) electrostatic interaction, (b) intercalation and (c) groove binding.

Intercalation

Inside the helical structure of DNA, base pairs bound by hydrogen bonds are stacked in layers. The insertion of a molecule having a flat plate structure between layers of these base pairs is called "intercalation" (Figure 1-10b).[33] When other molecules intercalate between base pairs, the distance between base pairs are spatially separated, and the helical structure of DNA is unwound. Therefore, it is known that the viscosity of the DNA complex intercalated with other molecules increases more than usual. Further, since stacking occurs between the plate molecule and the base pair, the absorption band of the plate molecule may cause a red shift or a hypochromic effect. Typical intercalators include Ethidium Bromide and Acridine Orange, both are dyes used to stain DNA

Groove binding

As mentioned above, DNA has hydrophobic main-groove and sub-groove in its double helix structure, so that it can interact with other hydrophobic molecules. The binding that occurs when another molecule interact with groove of DNA is called "groove binding" (figure 1-10c).[34] Distamycin A is a well-known molecule that groove-binds to DNA. This Distamycin A is known to specifically interact with DNA in the sub-groove of a sequence in which A-T base pairs are lined up. Therefore, it is used as a probe for detecting base pair A-T in DNA.[35]

1.2.3 Association of DNA with luminescent materials and their functional potential

As described above, DNA has the unique feature to incorporate various types of functional materials like luminescent metal complexes,[36,37] organic dyes,[38-40] and conductive polymers,[41-43] thus resulting enhancement of their photo-functional properties. Especially, by associating metal complexes like Ru(II) complex, DNA-based color tunable OLEDs, and electrochemiluminescent materials
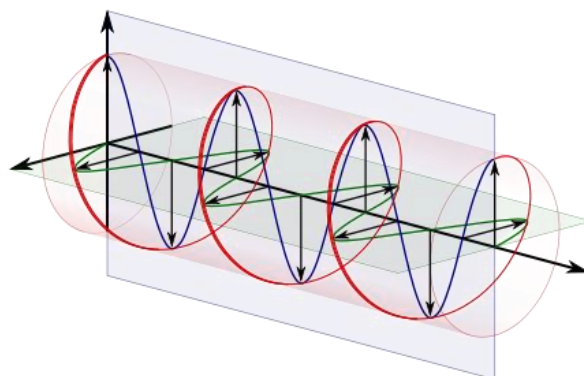
Figure 1-11. Circularly polarized luminescence.

utilizing the unique features of DNA-based functional materials were also reported.[44-47] In addition, it has been reported that luminescent materials that incorporated into chiral polymers express chiral optical properties like circular dichroism (CD) and circularly polarized luminescence (CPL).[48-51] CPL, which corresponds to the luminescence generated in response to electromagnetic waves with different rotation, provides advanced information based on the difference in intensity between right and left component (figure 1-11). The CPL is expected not only to improve the precise sensing of chiral molecules and biomolecules as well as structural analyses of biopolymers but also to lead to the development of multifunctional displays, security paints, and optical communication. Currently, CPL is generated by utilizing optical devices such as a combination of linear polarizer and quarter wave retarder.[52] On the other hand, the reduction in emission intensity remains an intrinsic demerit, thus self-luminescent materials that do not need optical devices to obtain CPL are in demand.

By utilizing the structural chirality of DNA that is attributed to its helical structure, it is expected to improve the luminescent chirality of luminescent metal complexes. Therefore, this study aimed to develop the novel photo functional material showing both strong emission and high luminescent dissymmetry by associating DNA and luminescent metal complexes. First, Ru(II) complexes, which have unique pho-electrochemical properties, were associated with DNA toward the development of novel chiral-photo-functional material, and their luminescent properties were investigated.

References of Chapter 1

1. Beer, P. D.; Gale, P. A. Anion Recognition and Sensing: The State of the Art and Future Perspectives. *Angew. Chemie - Int. Ed.* **2001**, *40* (3), 486–516. https://doi.org/10.1002/1521-3773(20010202)40:3<486::AID-ANIE486>3.0.CO;2-P.

2. Sangeetha, N. M.; Maitra, U. Supramolecular Gels: Functions and Uses. *Chem. Soc. Rev.* **2005**, *34* (10), 821–836. https://doi.org/10.1039/b417081b.

3. Hu, Z.; Deibert, B. J.; Li, J. Luminescent Metal-Organic Frameworks for Chemical Sensing and Explosive Detection. *Chem. Soc. Rev.* **2014**, *43* (16), 5815–5840. https://doi.org/10.1039/c4cs00010b.

4. Kim, H. N.; Lee, M. H.; Kim, H. J.; Kim, J. S.; Yoon, J. A New Trend in Rhodamine-Based Chemosensors: Application of Spirolactam Ring-Opening to Sensing Ions. *Chem. Soc. Rev.* **2008**, *37* (8), 1465–1472. https://doi.org/10.1039/b802497a.

5. Hembury, G. A.; Borovkov, V. V.; Inoue, Y. Chirality-Sensing Supramolecular Systems. *Chem. Rev.* **2008**, *108* (1), 1–73. https://doi.org/10.1021/cr050005k.

6. Kato, M.; Ito, H.; Hasegawa, M.; Ishii, K. Soft Crystals: Flexible Response Systems with High Structural Order. *Chem. - A Eur. J.* **2019**, *25* (20), 5105–5112. https://doi.org/10.1002/chem.201805641.

7. Medintz, I. L.; Uyeda, H. T.; Goldman, E. R.; Mattoussi, H. Quantum Dot Bioconjugates for Imaging, Labelling and Sensing. *Nat. Mater.* **2005**, *4* (6), 435–446. https://doi.org/10.1038/nmat1390.

8. Kober, E. M.; Meyer, T. J. Concerning the Absorption Spectra of the Ions $M(Bpy)_3^{2+}$ (M = Fe, Ru, Os; Bpy = 2,2′-Bipyridine). *Inorg. Chem.* **1982**, *21* (11), 3967–3977. https://doi.org/10.1021/ic00141a021.

9. Felix, F.; Ferguson, J.; Güdel, H. U.; Ludi, A. Electronic Spectra of $M(Bipy)_3^{2+}$ Complexions (M = Fe, Ru and Os). *Chem. Phys. Lett.* **1979**, *62* (1), 153–157. https://doi.org/10.1016/0009-2614(79)80432-7.

10. Juris, A.; Balzani, V.; Barigelletti, F.; Campagna, S.; Belser, P.; von Zelewsky, A. Ru(II) Polypyridine Complexes: Photophysics, Photochemistry, Eletrochemistry, and Chemiluminescence. *Coord. Chem. Rev.* **1988**, *84* (C), 85–277. https://doi.org/10.1016/0010-8545(88)80032-8.

11. Baldo, M. A.; an dY. You, D. F. O.; Shoustikov, A.; Sibley, S.; Thompson, M. E.; Forrest, S. R. Highly Efficient Phosphorescent Emission from Organic Electroluminescent Devices. *Nature* **1998**, *395* (September), 151.

12. Abrahamsson, M.; Jäger, M.; Kumar, R. J.; Österman, T.; Persson, P.; Becker, H. C.; Johansson, O.; Hammarström, L. Bistridentate Ruthenium(II)Polypyridyl-Type Complexes

with Microsecond 3MLCT State Lifetimes: Sensitizers for Rod-like Molecular Arrays. *J. Am. Chem. Soc.* **2008**, *130* (46), 15533–15542. https://doi.org/10.1021/ja804890k.

13. Sun, Y.; Collins, S. N.; Joyce, L. E.; Turro, C. Unusual Photophysical Properties of a Ruthenium(II) Complex Related to [Ru(Bpy)$_2$(Dppz)]$^{2+}$. *Inorg. Chem.* **2010**, *49* (9), 4257–4262. https://doi.org/10.1021/ic9025365.

14. Belser, P.; Zelewsky, A. V. O. N.; Juris, A.; Baricellemi, F.; Tucci, A.; Balzani, V. Ligand-centered luminescence from a ruthenium(II) complex. *Chem. Phys. Lett.* **1982**, *89* (2), 0–3.

15. Tamayo, A. B.; Alleyne, B. D.; Djurovich, P. I.; Lamansky, S.; Tsyba, I.; Ho, N. N.; Bau, R.; Thompson, M. E. Synthesis and Characterization of Facial and Meridional Tris-Cyclometalated Iridium(III) Complexes. *J. Am. Chem. Soc.* **2003**, *125* (24), 7377–7387. https://doi.org/10.1021/ja034537z.

16. Endo, A.; Suzuki, K.; Yoshihara, T.; Tobita, S.; Yahiro, M.; Adachi, C. Measurement of Photoluminescence Efficiency of Ir(III) Phenylpyridine Derivatives in Solution and Solid-State Films. *Chem. Phys. Lett.* **2008**, *460* (1–3), 155–157. https://doi.org/10.1016/j.cplett.2008.05.064.

17. Sajoto, T.; Djurovich, P. I.; Tamayo, A. B.; Oxgaard, J.; Goddard, W. A.; Thompson, M. E. Temperature Dependence of Blue Phosphorescent Cyclometalated Ir(III) Complexes. *J. Am. Chem. Soc.* **2009**, *131* (28), 9813–9822. https://doi.org/10.1021/ja903317w.

18. Kober, E. M.; Sullivan, B. P.; Dressick, W. J.; Caspar, J. V.; Meyer, T. J. Highly Luminescent Polypyridyl Complexes of Osmium(II). *J. Am. Chem. Soc.* **1980**, *102* (24), 7383–7385. https://doi.org/10.1021/ja00544a048.

19. Sacksteder, L. A.; Demas, J. N.; Lee, M.; DeGraff, B. A. Long-Lived, Highly Luminescent Rhenium(I) Complexes as Molecular Probes: Intra- and Intermolecular Excited-State Interactions. *J. Am. Chem. Soc.* **1993**, *115* (18), 8230–8238. https://doi.org/10.1021/ja00071a036.

20. Bixon, M.; Jortner, J. Long Radiative Lifetimes of Small Molecules. *J. Chem. Phys.* **1969**, *50* (8), 3284–3290. https://doi.org/10.1063/1.1671552.

21. Eliseeva, S. V.; Bünzli, J. C. G. Lanthanide Luminescence for Functional Materials and Bio-Sciences. *Chem. Soc. Rev.* **2010**, *39* (1), 189–227. https://doi.org/10.1039/b905604c.

22. Opelt, G. S. Intensities of Crystal Spectra of Rare-Earth Ions. *J. Chem. Phys.* **1962**, *37* (3), 511–520. https://doi.org/10.1063/1.1701366.

23. Judd, B. R. Optical Absorption Intensities of Rare-Earth Ions. *Phys. Rev.* **1962**, *127* (3), 750–761. https://doi.org/10.1103/PhysRev.127.750.

24. Hasegawa, Y.; Yamamuro, M.; Wada, Y.; Kanehisa, N.; Kai, Y.; Yanagida, S. Luminescent Polymer Containing the Eu(III) Complex Having Fast Radiation Rate and High Emission

Quantum Efficiency. *J. Phys. Chem. A* **2003**, *107* (11), 1697–1702. https://doi.org/10.1021/jp022397u.

25. Yam, V. W. W.; Li, C. K.; Chan, C. L. Proof of Potassium Ions by Luminescence Signaling Based on Weak Gold - Gold Interactions in Dinuclear Gold(I) Complexes. *Angew. Chemie - Int. Ed.* **1998**, *37* (20), 2857–2859. https://doi.org/10.1002/(SICI)1521-3773(19981102)37:20<2857::AID-ANIE2857>3.0.CO;2-G.

26. Wadas, T. J.; Wang, Q. M.; Kim, Y. J.; Flaschenreim, C.; Blanton, T. N.; Eisenberg, R. Vapochromism and Its Structural Basis in a Luminescent Pt(II) Terpyridine-Nicotinamide Complex. *J. Am. Chem. Soc.* **2004**, *126* (51), 16841–16849. https://doi.org/10.1021/ja047955s.

27. Kato, M. Luminescent Platinum Complexes Having Sensing Functionalities. *Bull. Chem. Soc. Jpn.* **2007**, *80* (2), 287–294. https://doi.org/10.1246/bcsj.80.287.

28. Vickery, J. C.; Olmstead, M. M.; Fung, E. Y.; Balch, A. L. Communications [3]. **1997**, 1996–1998.

29. Rawashdeh-Omary, M. A.; Omary, M. A.; Fackler, J.; Galassi, R.; Pietroni, B. R.; Burini, A. Chemistry and Optoelectronic Properties of Stacked Supramolecular Entities of Trinuclear Gold(I) Complexes Sandwiching Small Organic Acids [9]. *J. Am. Chem. Soc.* **2001**, *123* (39), 9689–9691. https://doi.org/10.1021/ja016279g.

30. Elson, D.; Chargaff, E. On the deoxyribonucleic acid content of sea urchin gametes. *Experientia*. **1952**, *8* (4): 143–145.

31. Watson, J.; Crick, F. Molecular Structure of Nucleic Acids. *Nature.* **1953**, *171* (4356), 737–738. https://doi.org/10.1038/171737a0.

32. Matulis, D.; Rouzina, I.; Bloomfield, V. A. Thermodynamics of DNA Binding and Condensation: Isothermal Titration Calorimetry and Electrostatic Mechanism. *J. Mol. Biol.* **2000**, *296* (4), 1053–1063. https://doi.org/10.1006/jmbi.1999.3470.

33. Long, E. C.; Barton, J. K. On Demonstrating DNA Intercalation. *Acc. Chem. Res.* **1990**, *23* (9), 271–273. https://doi.org/10.1021/ar00177a001.

34. Krowicki, K.; Balzarini, J.; De Clercq, E.; Newman, R. A.; William Lown, J. Novel DNA Groove Binding Alkylators: Design, Synthesis, and Biological Evaluation. *J. Med. Chem.* **1988**, *31* (2), 341–345. https://doi.org/10.1021/jm00397a012.

35. Sugiyama, H.; Lian, C.; Isomura, M.; Saito, I.; Wang, A. H. J. Distamycin A Modulates the Sequence Specificity of DNA Alkylation by Duocarmycin A. *Proc. Natl. Acad. Sci. U. S. A.* **1996**, *93* (25), 14405–14410. https://doi.org/10.1073/pnas.93.25.14405.

36. Lin, S.; Lu, L.; Kang, T. S.; Mergny, J. L.; Leung, C. H.; Ma, D. L. Interaction of an Iridium(III) Complex with G-Quadruplex DNA and Its Application in Luminescent Switch-

On Detection of Siglec-5. *Anal. Chem.* **2016**, *88* (20), 10290–10295. https://doi.org/10.1021/acs.analchem.6b03128.

37. Pages, B. J.; Ang, D. L.; Wright, E. P.; Aldrich-Wright, J. R. Metal Complex Interactions with DNA. *Dalt. Trans.* **2015**, *44* (8), 3505–3526. https://doi.org/10.1039/c4dt02700k.

38. Mukae, M.; Ihara, T.; Tabara, M.; Jyo, A. Anthracene-DNA Conjugates as Building Blocks of Designed DNA Structures Constructed by Photochemical Reactions. *Org. Biomol. Chem.* **2009**, *7* (7), 1349–1354. https://doi.org/10.1039/b821869b.

39. Chovelon, B.; Fiore, E.; Faure, P.; Peyrin, E.; Ravelet, C. A Lifetime-Sensitive Fluorescence Anisotropy Probe for DNA-Based Bioassays: The Case of SYBR Green. *Biosens. Bioelectron.* **2017**, *90* (November 2016), 140–145. https://doi.org/10.1016/j.bios.2016.11.049.

40. Kahn, J. S.; Freage, L.; Enkin, N.; Garcia, M. A. A.; Willner, I. Stimuli-Responsive DNA-Functionalized Metal–Organic Frameworks (MOFs). *Adv. Mater.* **2017**, *29* (6), 1–6. https://doi.org/10.1002/adma.201602782.

41. Mondal, P. C.; Fontanesi, C.; Waldeck, D. H.; Naaman, R. Spin-Dependent Transport through Chiral Molecules Studied by Spin-Dependent Electrochemistry. *Acc. Chem. Res.* **2016**, *49* (11), 2560–2568. https://doi.org/10.1021/acs.accounts.6b00446.

42. Watson, S. M. D.; Hedley, J. H.; Galindo, M. A.; Al-Said, S. A. F.; Wright, N. G.; Connolly, B. A.; Horrocks, B. R.; Houlton, A. Synthesis, Characterisation and Electrical Properties of Supramolecular DNA-Templated Polymer Nanowires of 2,5-(Bis-2-Thienyl)-Pyrrole. *Chem. - A Eur. J.* **2012**, *18* (38), 12008–12019. https://doi.org/10.1002/chem.201201495.

43. Sakurai, K.; Uezu, K.; Numata, M.; Hasegawa, T.; Li, C.; Kaneko, K.; Shinkai, S. β-1,3-Glucan Polysaccharides as Novel One-Dimensional Hosts for DNA/RNA, Conjugated Polymers and Nanoparticles. *Chem. Commun.* **2005**, No. 35, 4383. https://doi.org/10.1039/b506673p.

44. Nakamura, K.; Ishikawa, T.; Nishioka, D.; Ushikubo, T.; Kobayashi, N. Color-Tunable Multilayer Organic Light Emitting Diode Composed of DNA Complex and Tris(8-Hydroxyquinolinato)Aluminum. *Appl. Phys. Lett.* **2010**, *97* (19), 2008–2011. https://doi.org/10.1063/1.3512861.

45. Kobayashi, N.; Uemura, S.; Kusabuka, K.; Nakahira, T.; Takahashi, H. An Organic Red-Emitting Diode with a Water-Soluble DNA-Polyaniline Complex Containing $Ru(Bpy)_3^{2+}$. *J. Mater. Chem.* **2001**, *11* (7), 1766–1768. https://doi.org/10.1039/b102882k.

46. Tsuneyasu, S.; Takahashi, R.; Minami, H.; Nakamura, K.; Kobayashi, N. Ultrafast Response in AC-Driven Electrochemiluminescent Cell Using Electrochemically Active $DNA/Ru(Bpy)_3^{2+}$ Hybrid Film with Mesoscopic Structures. *Sci. Rep.* **2017**, *7* (1), 1–7. https://doi.org/10.1038/s41598-017-09123-2.

47. Hagen, J. A.; Li, W.; Steckl, A. J.; Grote, J. G. Enhanced Emission Efficiency in Organic Light-Emitting Diodes Using Deoxyribonucleic Acid Complex as an Electron Blocking Layer. *Appl. Phys. Lett.* **2006**, *88* (17), 1–4. https://doi.org/10.1063/1.2197973.

48. Li, J.; Peng, X.; Huang, C.; Qi, Q.; Lai, W. Y.; Huang, W. Control of Circularly Polarized Luminescence from a Boron Ketoiminate-Based π-Conjugated Polymer via Conformational Locks. *Polym. Chem.* **2018**, *9* (43), 5278–5285. https://doi.org/10.1039/c8py01209a.

49. Hu, Y.; Song, F.; Xu, Z.; Tu, Y.; Zhang, H.; Cheng, Q.; Lam, J. W. Y.; Ma, D.; Tang, B. Z. Circularly Polarized Luminescence from Chiral Conjugated Poly(Carbazole- Ran - Acridine)s with Aggregation-Induced Emission and Delayed Fluorescence . *ACS Appl. Polym. Mater.* **2019**, *1* (2), 221–229. https://doi.org/10.1021/acsapm.8b00118.

50. Dhbaibi, K.; Shen, C.; Jean, M.; Vanthuyne, N.; Roisnel, T.; Górecki, M.; Jamoussi, B.; Favereau, L.; Crassous, J. Chiral Diketopyrrolopyrrole-Helicene Polymer With Efficient Red Circularly Polarized Luminescence. *Front. Chem.* **2020**, *8* (April), 2–9. https://doi.org/10.3389/fchem.2020.00237.

51. Lee, S.; Kim, K. Y.; Jung, S. H.; Lee, J. H.; Yamada, M.; Sethy, R.; Kawai, T.; Jung, J. H. Finely Controlled Circularly Polarized Luminescence of a Mechano-Responsive Supramolecular Polymer. *Angew. Chemie - Int. Ed.* **2019**, *58* (52), 18878–18882. https://doi.org/10.1002/anie.201911380.

52. Sang, Y.; Han, J.; Zhao, T.; Duan, P.; Liu, M. Circularly Polarized Luminescence in Nanoassemblies: Generation, Amplification, and Application. *Adv. Mater.* **2019**, *1900110* (11), 1–33. https://doi.org/10.1002/adma.201900110.

Chapter 2

Novel Chiral Optical Properties of Ru(II) Complexes by Association with DNA

Novel Chiral Optical Properties of Ru(II) Complexes by Association with DNA

As described in previous chapter, Ru(II) complexes shows orange emission with relatively strong intensity and long emission lifetime due to ^{3}MLCT state. In addition, its electrochemical reactivity and electrochemical stability are expected to apply for opto-electrochemical devices such as OLEDs and ECLDs. Associations of DNA and Ru(II) complexes have been studied since the 1990s, and their structures and optical properties have been investigated.[1] Several reports demonstrated the application of DNA/Ru(bpy)$_3^{2+}$ (bpy = 2,2′-bipyridine) for the opto-electrochemical functional devices like OLED[2] and ECLD.[3] However, there have been only few reports that remarkably reflect the structural chirality of DNA as an optical property of association. Therefore, additional novel optical properties can be expected to appear by utilizing the structural chirality of DNA effectively.

This study focused on the chiral Ru(II) complexes (Δ-, Λ-Ru(phen)$_3^{2+}$; phen: 1,10-phenanthroline) as a material to build a complex with DNA. Δ-, Λ-Ru(phen)$_3^{2+}$ has an enantiomeric relationship due to its structure (Figure 2-1). Since DNA also has a very well-known right-handed double helix structure, it is conceivable that these components exhibit different binding form upon the interaction. Furthermore, it is expected that chiral optical properties such as CD and CPL will be induced by the difference in the interaction form with DNA. In this chapter, I will first introduce the interaction between DNA and Ru(bpy)$_3^{2+}$ which is most widely investigated Ru(II) complex. After that, the interaction between Δ-, Λ-Ru(phen)$_3^{2+}$ and DNA, and the specific changes in optical properties upon the interaction will be described.

Δ-Ru(phen)$_3^{2+}$ **Λ-Ru(phen)$_3^{2+}$**
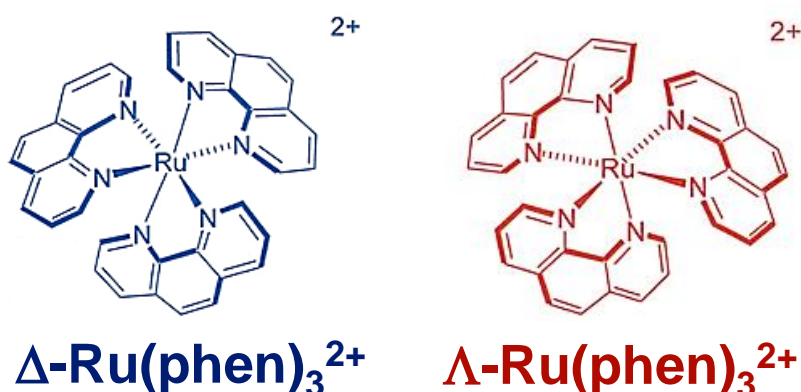
Figure 2-1.   Structure of Δ-Ru(phen)$_3^{2+}$ (left) and Λ-Ru(phen)$_3^{2+}$ (right).

Materials

All the chemicals were used as received.   Tris(2,2'-bipyridine)ruthenium(II) chloride was purchased from Tokyo Chemical Industry Co. Ltd., Japan. Δ-, Λ-tris(1,10-phenanthroline)ruthenium(II) chloride were provided by Tanaka Kikinzoku Kogyo K.K., Japan.   The sodium salts of DNA (base pairs: ca. 10,000) were provided by Nippon Chemical Feed Co., Ltd. (Japan).   They were marine-based salts that were first isolated from frozen salmon milt through a homogenization process followed by removal of proteins and impurities.   Sodium chloride was purchased from Tokyo Chemical Industry Co. Ltd., Japan.

Preparation of DNA/Ru(II) complex solutions

DNA and each Ru(II) complex (0.1 mM) were dissolved at a molar concentration of [DNA (phosphate group concentration)]:[Ru(II) complex] = 0:1 ~ 30:1 to prepare a DNA/Ru(II) complex aqueous solution.   In addition, DNA/Ru(phen)$_3^{2+}$/NaCl solutions were prepared by mixing DNA (2 mM), Δ- or Λ- Ru(phen)$_3^{2+}$, and NaCl (0, 30, …420 mM) in aqueous solution.

Photophysical measurements

Nitrogen-gas bubbling was conducted to remove oxygen from solutions before optical measurement.   UV-vis absorption spectra of the samples were measured using a spectrophotometer (JASCO, V-570).   Circular dichroism (CD) spectra of the DNA complex were measured using a CD spectrometer (JASCO, J-820).   Photoluminescence spectra were obtained using a spectrofluorometer (JASCO, FP-6600).   Excitation wavelength of the samples was 450 nm.   The emission lifetimes were determined by using a time-resolved fluorescence spectrometer (IBH 5000U-CS, HORIBA Jobin Yvon IBH Ltd., UK).

2.1 Emission enhancement of Ru(bpy)$_3$$^{2+}$ upon the interaction with DNA

Interaction between DNA and Ru(bpy)$_3$$^{2+}$

First, I introduce the interaction between DNA and Ru(bpy)$_3$$^{2+}$, which is most widely investigated opto-electric functional metal complex. The concentration of DNA was defined as the concentration of phosphate groups. It is known that cationic Ru(bpy)$_3$$^{2+}$ can interact with anionic phosphate groups of DNA through electrostatic interaction.[4-6] The emission intensity and lifetime of Ru(bpy)$_3$$^{2+}$ were enhanced corresponding to the increasing DNA concentration as shown in Fig. 2-2.

Figure 2-2. Emission spectra of the DNA/Ru(bpy)$_3$$^{2+}$ aqueous solution containing 0.1 mM Ru(bpy)$_3$$^{2+}$ as a function of DNA concentration (0–2 mM).

The emission intensity from ^{3}MLCT of Ru(bpy)$_3^{2+}$ at approximately 600 nm increased with the increasing DNA concentration. The emission enhancement saturated at a constant intensity when the DNA/Ru(bpy)$_3^{2+}$ molar ratio was more than 10:1 (Figure 2-3). This indicates averagely 5 base pairs of DNA bind with a Ru(bpy)$_3^{2+}$ molecule to form DNA/Ru(bpy)$_3^{2+}$ in a solution containing Ru(bpy)$_3^{2+}$ of 0.1 mmol/L. This enhancement of emission intensity was attributed to the decrease in non-emissive transitions (k_{nr}) due to the immobilization onto the DNA molecule. Namely, the vibrational deactivation by water and intramolecular vibration of Ru(bpy)$_3^{2+}$ were suppressed upon the association with DNA backbone.

Figure 2-3. Change in emission intensity associated with DNA concentration at approximately 600 nm from excited Ru(bpy)$_3^{2+}$ in aqueous solution containing DNA. The concentration of Ru(bpy)$_3^{2+}$ was fixed to be 0.1 mM.

2.2 Enantioselective emission enhancement of chiral Ru(II) complexes upon the interaction with DNA

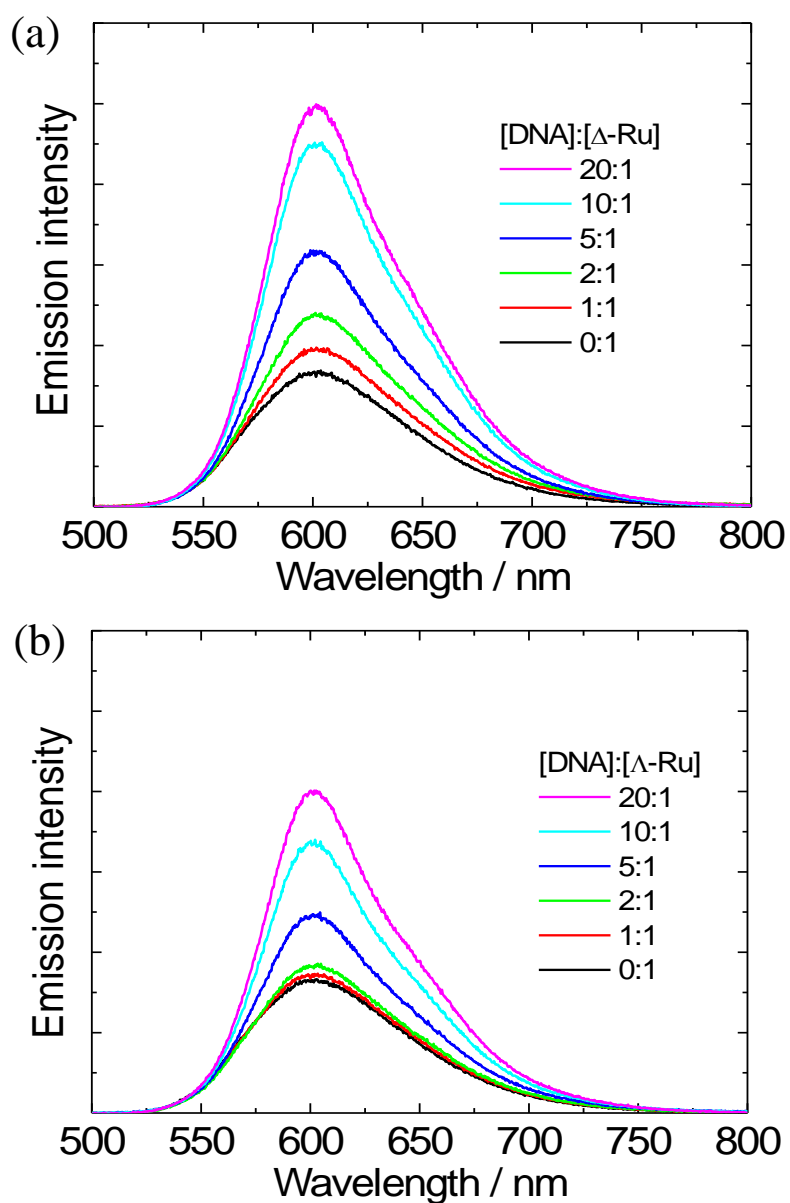Generally, it is known that chiral luminescent complexes have ability to exhibit chiral optical properties such as circular dichroism (CD) and circularly polarized luminescence (CPL) as a result of the structural chirality of the complex.[7,8] Thus, the DNA/chiral material complexes can be expected to show unique chiral optical properties reflecting the specific interaction due to the structural chirality of each compounds. Among them, this study focused on the interaction between chiral Δ- or Λ- Ru(phen)$_3^{2+}$ and DNA to prepare the novel photo-functional material. In this section, Δ- or Λ- Ru(phen)$_3^{2+}$ and DNA were associated with each other toward the preparation of novel photo-functional material.   These interaction modes were analyzed from various photophysical measurements and it was revealed that Δ- or Λ- Ru(phen)$_3^{2+}$/DNA complexes show enantioselective luminescent enhancement corresponding to each different interaction mode.

Emission enhancement of Δ- or Λ-Ru(phen)$_3^{2+}$ in the presence of DNA

Aqueous solutions of Δ- or Λ-Ru(phen)$_3^{2+}$ and DNA (purified from salmon testes provided by Piotrek Co., Ltd.) with various molar ratios were firstly prepared.   The overall concentration of DNA was defined as the phosphate concentration.   Next, optical properties (photoluminescence, absorption, circular dichroism, etc.) of the solutions were measured.   In order to investigate the change in luminescence properties of the Δ- and Λ-Ru(phen)$_3^{2+}$ in the presence of DNA, photoluminescence spectra of DNA/Ru(phen)$_3^{2+}$ in aqueous solutions were measured (Figure 2-4). The DNA-to-Ru(phen)$_3^{2+}$ ratio ([DNA]:[Ru(phen)$_3^{2+}$]) was varied from 0:1 to 30:1.   With excitation of the metal-to-ligand charge transfer (MLCT) absorption band of the Ru(phen)$_3^{2+}$ (450 nm), the complexes showed red luminescence at around 610 nm, which can be attributed to phosphorescence from the ^{3}MLCT state.[9,10]   When DNA was absent ([DNA]:[Ru(phen)$_3^{2+}$] = 0:1) in the solution, Δ- and Λ-Ru(phen)$_3^{2+}$ showed same shapes and intensities of the emission bands.   As the concentration of DNA was increased, the luminescence intensities for both Δ- and Λ-Ru(phen)$_3^{2+}$ increased whereas significant change of their spectral shapes were not observed.   This emission enhancement is attributed to immobilization of the Ru(phen)$_3^{2+}$ onto DNA structure.   The immobilization of the luminescent molecule induces suppression of emission quenching caused by intramolecular vibration and vibrational excitation of matrices.

Figure 2-4. Photo luminescence spectra of the DNA/Δ-Ru(II) (a) and DNA/Λ-Ru(II) (b) complex in aqueous solution with various [DNA]:[Ru(II)] ratios.   Concentration of Ru(phen)$_3{}^{2+}$ was set to 0.10 mmol/L.   Excitation wavelength was 450 nm.

Difference in extent of emission enhancement between Δ- form and Λ-form

Interestingly, the extent of emission enhancement was different between the Δ- and Λ-isomers. Figure 2-5 shows changes in the luminescence intensities of Δ- and Λ-Ru(phen)$_3^{2+}$ with various [DNA]/[Ru(phen)$_3^{2+}$] ratio. It was found that the luminescence enhancement of the Δ-form was greater than that of the Λ-form. The extent of enhancement were 3.1 times for Δ-form and 2.4 times for Λ-form compared to the Ru(phen)$_3^{2+}$ alone solution. Enantioselective enhancement in luminescence of Ru(phen)$_3^{2+}$ was demonstrated by interaction with DNA. This enantioselective property suggests that Δ- or Λ-Ru(phen)$_3^{2+}$ show different interactions with DNA.
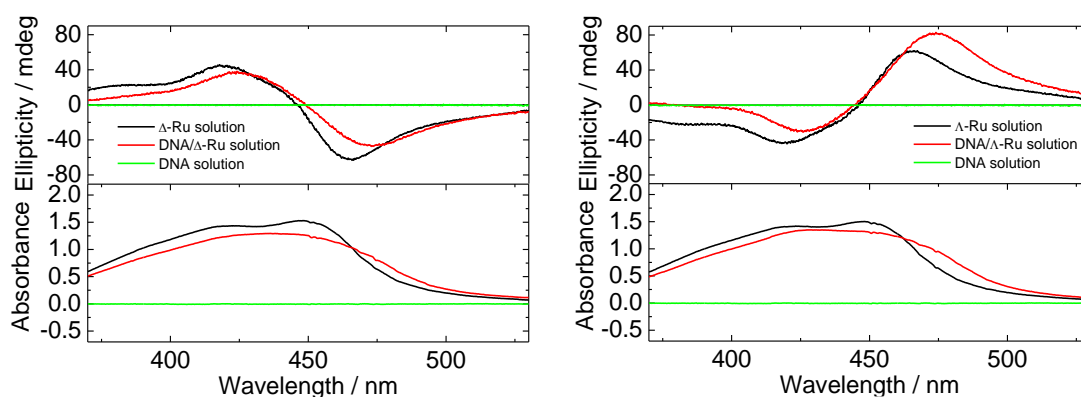

Figure 2-5. Change in the emission intensity of DNA/Δ-,Λ-Ru(II) complexes in aqueous solution with various [DNA]/[Ru(II)] concentration ratios.

2.3 Interaction mode between DNA and Δ- or Λ-Ru(phen)$_3^{2+}$

Structural change of Δ- or Λ-Ru(phen)$_3^{2+}$ upon the interaction with DNA

In order to discuss the interaction modes between these compounds, absorption and CD spectra of the DNA/Δ- or Λ-Ru(phen)$_3^{2+}$ solutions and DNA, Δ- Ru(phen)$_3^{2+}$ and Λ-Ru(phen)$_3^{2+}$ alone solution were measured (Figure 2-6). No absorption or CD signals attributable to DNA were observed in the 350–550 nm range. After association of Δ- and Λ-Ru(phen)$_3^{2+}$ with DNA, the absorption maxima of the MLCT bands (around 450 nm) of the Δ- and Λ-Ru(phen)$_3^{2+}$ were slightly red-shifted with increase in DNA content. In addition, decreases in absorbance of the MLCT band were observed. These behaviors suggest that Δ- and Λ-Ru(phen)$_3^{2+}$ are likely intercalated between base pairs in the DNA chains.[11-13] In the CD spectra, symmetric signals with exciton-splitting type of cotton effects were observed for both Δ- and Λ-Ru(phen)$_3^{2+}$ alone solution. In the case of DNA/Δ-Ru(phen)$_3^{2+}$, the CD signals of both the positive (at 420 nm) and negative (at 470 nm) bands are reduced upon the association with DNA. On the other hand, the signal of longer wavelength band increased for DNA/Λ-Ru(phen)$_3^{2+}$. From the results observed in the absorption and CD measurements, spatial and/or electronic structural changes are suggested for Δ- and Λ-Ru(phen)$_3^{2+}$ upon DNA association. The binding modes between DNA and Ru(phen)$_3^{2+}$ are distinct for the two enantiomers, as revealed by the comparative changes in the CD spectra.

Figure 2-6. CD and absorbance spectra of Δ-, Λ-Ru(phen)$_3^{2+}$, DNA and DNA/Δ-, Λ-Ru(phen)$_3^{2+}$ solution. Concentration of Ru(phen)$_3^{2+}$ was set to 0.10 mM. Optical path length: 1.0 cm.

Effect of cation exchange on emission intensity

Next, the influence of these binding modes on the emission properties of DNA/Ru(phen)$_3^{2+}$ was investigated. It has been shown previously that the main binding mode in forming complexes from DNA and cationic metal complexes is electrostatic interaction.[14,15] Since Ru(phen)$_3^{2+}$ is cationic, electrostatic interaction with the anionic phosphate group in DNA is expected as well as intercalation. In order to discuss the contribution of electrostatic interactions between DNA and Ru(phen)$_3^{2+}$, the change in luminescence intensities with addition of NaCl to the DNA/Ru(II) complex aqueous solutions were measured (Figure 2-7, emission intensity of Ru(II) complexes are normalized to 1). By addition of excess Na$^+$ ion into the DNA/(cationic Ru(II) complex) solutions, near quantitative disassociation of the Ru(II) complexes from DNA occurs because of cation exchange with Na$^+$.[16] Therefore, the contribution of electrostatic interactions to emission properties can be estimated by optical measurements in the presence of Na$^+$ ion. For the Ru(bpy)$_3^{2+}$, Δ-Ru(phen)$_3^{2+}$ and Λ-Ru(phen)$_3^{2+}$ solutions, intensities and shapes of the emission band did not change even after addition of excess Na$^+$ ions, indicating that Na$^+$ ions did not affect luminescence properties of the free Ru(II) complexes. In the case of Ru(bpy)$_3^{2+}$, which is known to bind to DNA by only electrostatic interactions,[17] luminescence intensity of DNA/Ru(bpy)$_3^{2+}$ reduced to that of free Ru(bpy)$_3^{2+}$ with increasing Na$^+$ ion. This result indicates that the enhancement of luminescence due to immobilization on DNA caused by electrostatic interaction was nearly quantitatively eliminated by an excess amount of Na$^+$ ions. This was because Ru(bpy)$_3^{2+}$ associated with DNA by electrostatic interaction were displaced with Na$^+$ ions. Similarly, a decrease in luminescence intensity of both Δ- and Λ-Ru(phen)$_3^{2+}$ were also observed with increasing Na$^+$ concentration. These results suggest that the Ru(phen)$_3^{2+}$ is associated with DNA through not only intercalation but also electrostatic interactions. However, even when Na$^+$ ion is added in excess, emission intensities of the DNA/Ru(phen)$_3^{2+}$ are still enhanced in comparison with those of Ru(phen)$_3^{2+}$ alone solution. These enduring emission enhancements indicate that intercalation remains even in existence of excess Na$^+$ ions. As expected from the red shift and hypochromic effect in absorption spectra of DNA/Ru(phen)$_3^{2+}$, Ru(phen)$_3^{2+}$ can intercalate between DNA base pairs. Concerning luminescence intensity in the presence of excess Na$^+$ ions, the DNA/Δ-Ru(phen)$_3^{2+}$ complex showed higher luminescence intensity than the DNA/Λ-Ru(phen)$_3^{2+}$ complex. Degree of emission enhancement by intercalation of Δ-enantiomer is thought to be larger than that of the Λ-enantiomer, implying enantioselective interaction between DNA and Ru(phen)$_3^{2+}$.
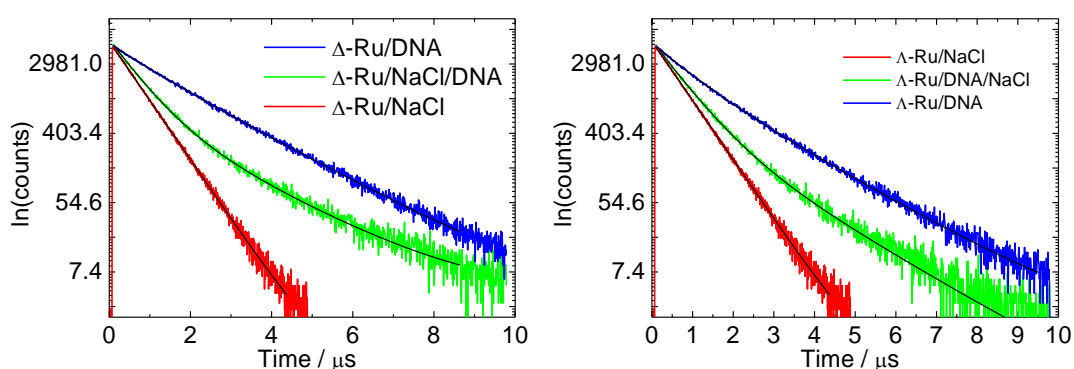
Figure 2-7. Normalized emission intensity of DNA/Ru complexes in aqueous solution with various NaCl concentrations. Concentration of Ru(phen)$_3{}^{2+}$ was set as 0.10 mM.

Emission lifetime measurements to reveal the binding mode between DNA and Ru(phen)$_3$$^{2+}$
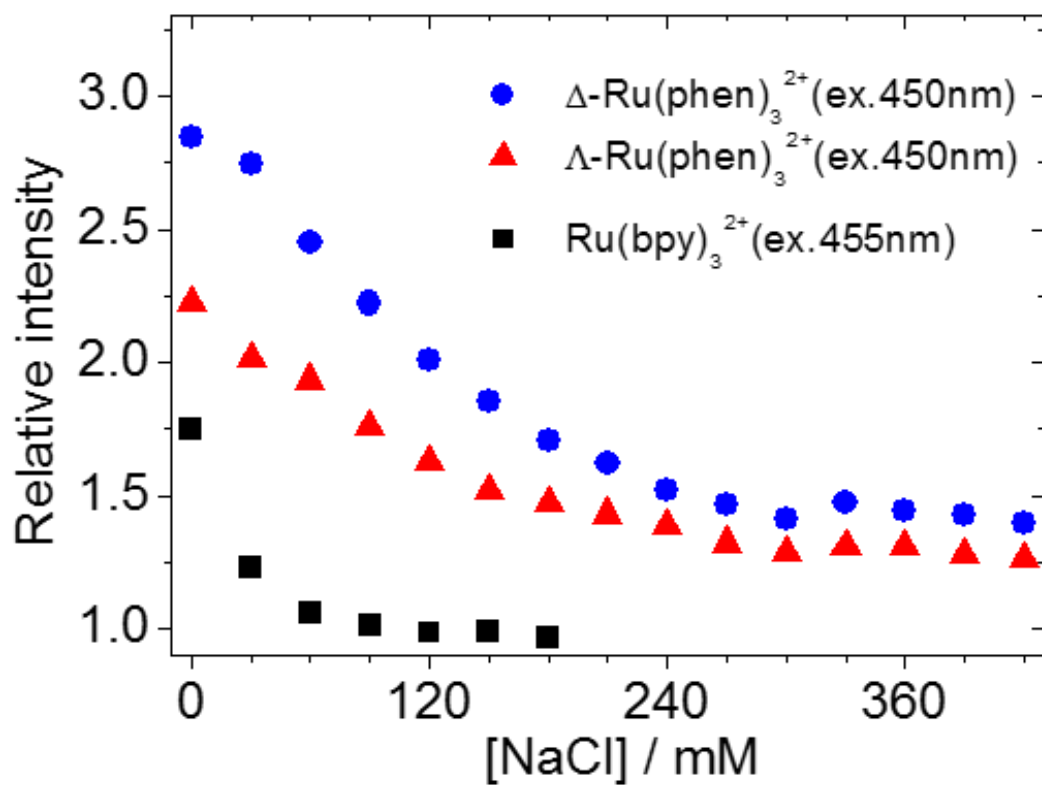
For detailed discussion of the binding behavior, luminescence lifetimes of Δ- and Λ-enantiomers were compared.   Table 2-1 shows luminescence lifetimes of Ru(phen)$_3$$^{2+}$ alone, DNA/Ru(phen)$_3$$^{2+}$ and DNA/Ru(phen)$_3$$^{2+}$ in the presence of excess Na$^+$ ions.   In the case of the Ru(phen)$_3$$^{2+}$ alone solution, the luminescence lifetimes of each enantiomer was found to be approximately 590 ns with a single component.   In the presence of DNA ([DNA]:[Ru(phen)$_3$$^{2+}$] = 30:1), emission decays of Δ- and Λ-Ru(phen)$_3$$^{2+}$ become longer. The increase in the decays is due to the suppression in vibrational deactivation of the ^{3}MLCT of Ru(phen)$_3$$^{2+}$ by immobilization onto DNA structure.   These decays consisted of two components (1500–1600 ns and 700–800 ns), clearly suggesting that DNA and Ru(phen)$_3$$^{2+}$ have two different binding forms.   Considering the changes of various photophysical properties, the major binding modes between DNA and Ru(phen)$_3$$^{2+}$ were intercalation and the electrostatic interaction.   Therefore, each component in the emission decay corresponds to either intercalation or electrostatic interaction.   In order to reveal the relationships between the emission decay components and the binding modes, electrostatic interaction was excluded by adding excess Na$^+$ ions into the DNA/Ru(phen)$_3$$^{2+}$ aqueous solution.   For the Δ- and Λ-Ru(phen)$_3$$^{2+}$ alone solutions, significant change in emission decay were not observed even after the addition of excess Na$^+$ ions.   For the DNA/Ru(phen)$_3$$^{2+}$ solution, the components with longer lifetimes (Δ-: 1620 ns, Λ-: 1520 ns) remained similar value.   However, the shorter lifetime components (Δ-: 826 ns, Λ-: 734 ns) decreased to the same value as Ru(phen)$_3$$^{2+}$ alone (~600 ns).   This indicates that the decay components with longer lifetime are due to the Ru(phen)$_3$$^{2+}$ intercalated to DNA and the shorter lifetime components are assignable to electrostatic interactions.   Then, the percentage of each lifetime component was calculated.   It was found that the percentage of the intercalated Ru(phen)$_3$$^{2+}$ accounted for approximately 90% for the Δ-isomer and 70% for the Λ-isomer in [DNA]:[Ru(phen)$_3$$^{2+}$] = 30:1 solution.

Various photophysical analyses indicated that Δ-Ru(phen)$_3$$^{2+}$ tends to intercalate into DNA more effectively than Λ-enantiomer, resulting in the enantioselective emission enhancement as shown in Figure 2-5.   Detailed investigation of this enantioselective interaction between Ru(phen)$_3$$^{2+}$ and DNA was conducted by NMR measurements and molecular modelings.[18-20]   According to the literature, Δ-Ru(phen)$_3$$^{2+}$ interacts to DNA only with minor distortions of the DNA structure, whereas Λ-Ru(phen)$_3$$^{2+}$ imposes stronger distortions to the DNA structure because of steric hinderance.   This kind of enantioselective avidity affected the luminescent properties of Ru(phen)$_3$$^{2+}$, such as luminescence intensities and lifetimes.

Figure 2-8.   Emission decay cuarves of Δ-, Λ-Ru(phen)$_3$$^{2+}$ solution, DNA/Δ-, Λ-Ru(phen)$_3$$^{2+}$ solution and DNA/Δ-, Λ-Ru(phen)$_3$$^{2+}$/NaCl solution.

Table 2-1.   Emission lifetimes of Δ-, Λ-Ru(phen)$_3$$^{2+}$ alone solution, DNA/Δ-, Λ-Ru(phen)$_3$$^{2+}$ solution and DNA/Δ-, Λ-Ru(phen)$_3$$^{2+}$/NaCl solution.

	Δ-form	Λ-form
Ru(phen)$_3$$^{2+}$	585 ns (100 %)	583 ns (100 %)
DNA/Ru(phen)$_3$$^{2+}$	1620 ns (87 %)	1520 ns (72 %)
	826 ns (13 %)	734 ns (28 %)
DNA/Ru(phen)$_3$$^{2+}$ +NaCl	1650 ns (36 %)	1450 ns (28 %)
	589 ns (64 %)	604 ns (13 %)

2.4 Summary of Chapter 2

In this chapter, chiral Ru(II) complexes (Δ-, Λ-Ru(phen)$_3{}^{2+}$) were associated with DNA toward the preparation of novel material showing chiral photo functions such as CD and CPL. Δ- and Λ-Ru(phen)$_3{}^{2+}$ formed associations with DNA thorough different interaction modes.   It was revealed that the interaction modes of these complexes were mainly intercalation into the base pairs of DNA.   From the results of various photophysical analyses, the strength and percentage of intercalation were higher in the case of Δ- form than that in Λ- form.   Corresponding to this difference in the interaction mode of Δ-, Λ-Ru(phen)$_3{}^{2+}$ and DNA, CD indicated obviously different change.   Such change in optical chirality is expected to apply for chemical sensors, bio-probes, and security systems.   As a result of different interaction with DNA, Δ- and Λ-Ru(phen)$_3{}^{2+}$ showed enantioselective emission enhancement.   The extent of emission enhancement of Δ-form (ca. 3times compared to original) was higher than that of Λ-form (2.5 times). This enantioselective emission enhancement is also suitable for various sensor systems.

However, although obvious chiral change in absorption and enantioselective emission enhancement were observed, significant CPL signal was not obtained from these complexes.   Thus, in order to obtain CPL from Ru(II) complex, it would be necessary to devise ways to further stimulate the electrical or magnetic environment that contributes to light emission.   Next chapter, energy transfer and following upconversion were applied to the Ru(II) complex based system toward the generation of CPL

References of Chapter 2

1. Friedman, A. E.; Barton, J. K.; Chambron, J. C.; Sauvage, J. P.; Turro, N. J.; Barton, J. K. Molecular "Light Switch" for DNA: $Ru(Bpy)_2(Dppz)^{2+}$. *J. Am. Chem. Soc.* **1990**, *112* (12), 4960–4962. https://doi.org/10.1021/ja00168a052.

2. Kobayashi, N.; Uemura, S.; Kusabuka, K.; Nakahira, T.; Takahashi, H. An Organic Red-Emitting Diode with a Water-Soluble DNA–Polyaniline Complex Containing $Ru(Bpy)_3^{2+}$. *J. Mater. Chem.* **2001**, *11* (7), 1766–1768. https://doi.org/10.1039/b102882k.

3. Tsuneyasu, S.; Takahashi, R.; Minami, H.; Nakamura, K.; Kobayashi, N. Ultrafast Response in AC-Driven Electrochemiluminescent Cell Using Electrochemically Active DNA/$Ru(Bpy)_3^{2+}$ Hybrid Film with Mesoscopic Structures. *Sci. Rep.* **2017**, *7* (1), 1–7. https://doi.org/10.1038/s41598-017-09123-2.

4. Li, G. Y.; Guan, R. L.; Ji, L. N.; Chao, H. DNA Condensation Induced by Metal Complexes. *Coord. Chem. Rev.* **2014**, *281*, 100–113. https://doi.org/10.1016/j.ccr.2014.09.005.

5. Yang, G.; Wu, J. Z.; Wang, L.; Ji, L. N.; Tian, X. Study of the Interaction between Novel Ruthenium(II)-Polypyridyl Complexes and Calf Thymus DNA. *J. Inorg. Biochem.* **1997**, *66* (2), 141–144. https://doi.org/10.1016/S0162-0134(96)00194-8.

6. N. Kobayashi and K. Nakamura, "Interelectrode stretched photoelectro- functional DNA nanowire. In: T. Ogawa, ed. Molecular architectonics: the third stage of single molecule electronics. Berlin, Germany, Springer, (2017), pp. 321-340.

7. Dai, L.; Lo, W. S.; Coates, I. D.; Pal, R.; Law, G. L. New Class of Bright and Highly Stable Chiral Cyclen Europium Complexes for Circularly Polarized Luminescence Applications. *Inorg. Chem.* **2016**, *55* (17), 9065–9070. https://doi.org/10.1021/acs.inorgchem.6b01546.

8. Yuasa, J.; Ohno, T.; Miyata, K.; Tsumatori, H.; Hasegawa, Y.; Kawai, T. Noncovalent Ligand-to-Ligand Interactions Alter Sense of Optical Chirality in Luminescent Tris(β-Diketonate) Lanthanide(III) Complexes Containing a Chiral Bis(Oxazolinyl) Pyridine Ligand. *J. Am. Chem. Soc.* **2011**, *133* (25), 9892–9902. https://doi.org/10.1021/ja201984u.

9. Hara, K.; Sugihara, H.; Singh, L. P.; Islam, A.; Katoh, R.; Yanagida, M.; Sayama, K.; Murata, S.; Arakawa, H. New Ru(II) Phenanthroline Complex Photosensitizers Having Different Number of Carboxyl Groups for Dye-Sensitized Solar Cells. *J. Photochem. Photobiol. A Chem.* **2001**, *145* (1–2), 117–122. https://doi.org/10.1016/S1010-6030(01)00570-6.

10. McGee, K. A.; Mann, K. R. Inefficient Crystal Packing in Chiral [Ru(Phen)3](PF 6)2 Enables Oxygen Molecule Quenching of the Solid-State MLCT Emission. *J. Am. Chem. Soc.* **2009**, *131* (5), 1896–1902. https://doi.org/10.1021/ja8075605.

11. Annaraj, J.; Srinivasan, S.; Ponvel, K. M.; Athappan, P. R. Mixed Ligand Copper(II) Complexes of Phenanthroline/Bipyridyl and Curcumin Diketimines as DNA Intercalators

and Their Electrochemical Behavior under Nafion® and Clay Modified Electrodes. *J. Inorg. Biochem.* **2005**, *99* (3), 669–676. https://doi.org/10.1016/j.jinorgbio.2004.11.018.

12. Ganeshpandian, M.; Loganathan, R.; Suresh, E.; Riyasdeen, A.; Akbarsha, M. A.; Palaniandavar, M. New Ruthenium(II) Arene Complexes of Anthracenyl-Appended Diazacycloalkanes: Effect of Ligand Intercalation and Hydrophobicity on DNA and Protein Binding and Cleavage and Cytotoxicity. *Dalt. Trans.* **2014**, *43* (3), 1203–1219. https://doi.org/10.1039/C3DT51641E.

13. Li, H.; Le, X. Y.; Pang, D. W.; Deng, H.; Xu, Z. H.; Lin, Z. H. DNA-Binding and Cleavage Studies of Novel Copper(II) Complex with L-Phenylalaninate and 1,4,8,9-Tetra-Aza-Triphenylene Ligands. *J. Inorg. Biochem.* **2005**, *99* (11), 2240–2247. https://doi.org/10.1016/j.jinorgbio.2005.08.005.

14. Zianna, A.; Psomas, G.; Hatzidimitriou, A.; Lalia-Kantouri, M. Ni(II) Complexes with 2,2-Dipyridylamine and Salicylaldehydes: Synthesis, Crystal Structure and Interaction with Calf-Thymus DNA and Albumins. *J. Inorg. Biochem.* **2016**, *163*, 131–142. https://doi.org/10.1016/j.jinorgbio.2016.07.003.

15. Li, G. Y.; Guan, R. L.; Ji, L. N.; Chao, H. DNA Condensation Induced by Metal Complexes. *Coord. Chem. Rev.* **2014**, *281*, 100–113. https://doi.org/10.1016/j.ccr.2014.09.005.

16. Su, L.; Sen, D.; Yu, H.-Z. Voltammetric Study of the Ion-Exchange Binding of Non-Electroactive Metal Cations to DNA-Modified Surfaces. *Analyst* **2006**, *131* (2), 317–322. https://doi.org/10.1039/B504580K.

17. Yang, G.; Wu, J. Z.; Wang, L.; Ji, L. N.; Tian, X. Study of the Interaction between Novel Ruthenium(II)-Polypyridyl Complexes and Calf Thymus DNA. *J. Inorg. Biochem.* **1997**, *66* (2), 141–144. https://doi.org/10.1016/S0162-0134(96)00194-8.

18. Eriksson, M.; Leijon, M.; Hiort, C.; Norden, B.; Graeslund, A. Binding of Δ- and Λ-[Ru(Phen)$_3$]$^{2+}$ to [d(CGCGATCGCG)]$_2$ Studied by NMR. *Biochemistry* **1994**, *33* (17), 5031–5040. https://doi.org/10.1021/bi00183a005.

19. Coggan, D. Z. M.; Haworth, I. S.; Bates, P. J.; Robinson, A.; Rodger, A. DNA Binding of Ruthenium Tris(1,10-Phenanthroline): Evidence for the Dependence of Binding Mode on Metal Complex Concentration. *Inorg. Chem.* **1999**, *38* (20), 4486–4497. https://doi.org/10.1021/ic990654c.

20. Barton, J. K.; Goldberg, J. M.; Kumar, C. V.; Turro, N. J. Binding Modes and Base Specificity of Tris(Phenanthroline)Ruthenium(II) Enantiomers with Nucleic Acids: Tuning the Stereoselectivity. *J. Am. Chem. Soc.* **1986**, *108* (8), 2081–2088. https://doi.org/10.1021/ja00268a057.

Chapter 3

Electrochemically triggered upconverted luminescence with Ru(bpy)$_3{}^{2+}$ toward the enhancement of luminescent chirality

Electrochemically triggered upconverted luminescence with Ru(bpy)$_3^{2+}$ toward the enhancement of luminescent chirality

In previous chapter, chiral Ru(II) complexes were associated with DNA toward the preparation of novel material showing chiral photo functions such as CD and CPL. However, CPL was still not obtained from these materials. Therefore, I attempted an approach to obtain circularly polarized light by affecting the electrical or magnetic environment by energy transfer between the Ru(II) complex and other molecules. In recent years, it has been reported that CPL with a high degree of circularly polarization appears when the luminescent molecules excited by a process such as energy transfer or upconversion instead of directly excitation.[1,2] Thus, this study focused on the triplet–triplet energy transfer (TTET) and subsequent triplet–triplet annihilation upconversion (TTA-UC) based on the Ru(II) complex. It is known that Ru(II) complexes have ability to cause high efficient TTET between triplet states of other molecules due to its high stability of ^{3}MLCT.[3,4] TTET from Ru(bpy)$_3^{2+}$ to anthracene derivative (9,10-diphenylanthracene: DPA) and subsequent TTA-UC has also been reported.[5-7] It is assume that Ru(II) complex-based material may exhibit CPL by utilizing TTET and TTA-UC. At present, most of the research for TTET and TTA-UC of Ru(II) complex are utilizing the photo excitation as a trigger.[8-11] If the electrochemical function of the Ru(II) complex as described in Chapter 1 can be applied to these system, it will be of great value to not only the luminescent materials, but also the medical and energy fields.

In this section, photo-electrochemical properties of Ru(bpy)$_3^{2+}$/DPA mixed solutions were investigated toward the fabrication of electrochemical device showing CPL. As a result, the electrochemically triggered upconverted luminescence through TTET and subsequent TTA-UC was firstly observed.

3.1 Investigation of Photophysical Interaction Between Ru(bpy)$_3^{2+}$ and 9,10-diphenylanthracene (DPA)

Reagents

All the chemicals were commercially available and used as received. Tris(2,2'-bipyridine)ruthenium(II) bis(hexafluorophosphate) was purchased from Tokyo Chemical Industry Co. Ltd., Japan, and used as an orange electrochemiluminescent material. 9,10-Diphenylanthracene was purchased from Tokyo Chemical Industry Co. Ltd., Japan, and used as a blue electrochemiluminescent material. Tetra-n-butyl ammonium perchlorate (TBAP) was purchased from Kanto Chemical Co. Japan and used as the supporting electrolyte. Propylene carbonate (PC) was purchased from Tokyo Chemical Industry Co. Ltd., Japan, and used as the solvent for the ECL electrolyte solution. Toluene was purchased from Sigma-Aldrich Co., USA, and used as the solvent for the ECL electrolyte solution. In order to prepare the ECL electrolyte solution, Ru(bpy)$_3^{2+}$ and DPA were used at various concentrations with 100 mmol L^{-1} TBAP dissolved in PC/toluene (volume ratio = 1:1).

Fabrication of the ECL device

The ECL devices were fabricated by sandwiching ECL solutions between pairs of indium-tin oxide (ITO) electrodes, with inter-electrode distances kept at 300 mm by silicone spacers. The effective electrode area of the ECL devices was 1.0×1.0 cm^2. The ECL devices were fabricated in a glove box filled with Ar atmosphere.

Electrochemical Measurements

Cyclic voltammograms (CVs) were acquired using an ALS440 A (CH Instruments, Inc., USA) equipped with a computer. For the analysis of redox properties of ECL materials, a three-electrode cell was fabricated with indium tin oxide (ITO) as the working electrode, a Pt disk ($\phi = 3$ mm) as the counter electrode, and an Ag/Ag$^+$ electrode as the reference electrode.

Measurements of ECL properties

A function generator (SG-4115, Iwatsu Electric Co., Ltd, Japan) and an electrical amplifier (NF 4010, NF Techno Commerce Co., Ltd, Japan) were utilized to apply AC voltages to the ECL devices. A photonic multichannel analyzer (PMA C10027, Hamamatsu Photonics, Japan) was employed to obtain ECL spectra. All experiments were conducted in a glove box filled with Ar atmosphere.


Measurements of optical properties

Nitrogen-gas bubbling was conducted to remove oxygen from solutions before optical measurement. Photoluminescence spectra of $Ru(bpy)_3^{2+}$/DPA solutions were measured with an excitation wavelength of 532 nm (Nd: YAG, 2ω, 10 mW) using a photonic multichannel analyzer (PMA C10027, Hamamatsu Photonics, Japan). The emission lifetimes were obtained by using a time-resolved fluorescence spectrometer (IBH 5000U-CS, HORIBA Jobin Yvon IBH Ltd., UK). These measurements were carried out under ambient conditions (temperature: 25 C; humidity: 50–60%; oxygen concentration: 20%).

3.2 Electrochemical response of $Ru(bpy)_3^{2+}$ and DPA

**CV curves of $Ru(bpy)_3^{2+}$ or DPA alone solution**

First, the CVs were measured for the $Ru(bpy)_3^{2+}$ and DPA solutions to clarify their electrochemical redox properties (Figure 3-1). For the $Ru(bpy)_3^{2+}$ alone solution, three reversible peaks assignable to the reduction of $Ru(bpy)_3^{2+}$ were observed at -2.0 V, -2.2 V, and -2.5 V (vs. Ag/Ag$^+$). In addition, a reversible oxidation peak was also observed at 0.7 V in the positive potential region. The energy gap for $Ru(bpy)_3^{2+}$ derived from the onset potentials was 2.3 eV. In the DPA alone solution similarly, reversible peaks assignable to redox reactions were observed (oxidation: 0.7 V, reduction: -2.7 V), and the energy gap was 2.8 eV. This indicates that both $Ru(bpy)_3^{2+}$ and DPA have stable redox reactivity in the electrolyte solutions. In addition, the energy gap of DPA is larger than that of $Ru(bpy)_3^{2+}$.
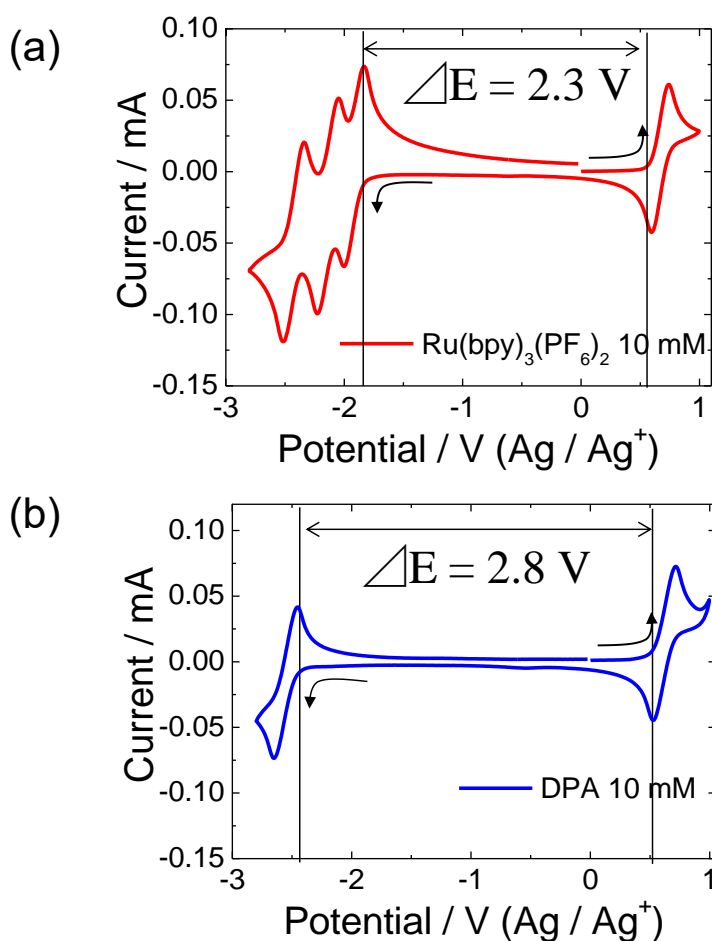
Figure 3-1. CV curves of 3-electrode cells containing (a) $Ru(bpy)_3^{2+}$ and (b) DPA in PC/toluene. Scan rate were set to be 50 mV/s.

CV curves of Ru(bpy)$_3^{2+}$/DPA mixed solutions

Figure 3-2 shows the CV curves of the Ru(bpy)$_3^{2+}$/DPA mixed solutions with various concentrations of Ru(bpy)$_3^{2+}$.   The current peaks assignable to redox of Ru (bpy)$_3^{2+}$ increased as the concentration of Ru(bpy)$_3^{2+}$ increased without a significant change in the shapes.   Additionally, even in the mixed solutions, the current peaks due to the reverse reaction from oxidized or reduced species of DPA to neutral state were observed.   This indicates that the electron transfer from the redox species of DPA to Ru(bpy)$_3^{2+}$ hardly occur with this concentration ratios.   Significant change was not observed in the redox potentials of Ru(bpy)$_3^{2+}$ and DPA, suggesting that there is no obvious interaction in the ground state between these molecules.   Therefore, it was revealed that DPA and Ru(bpy)$_3^{2+}$ can show ECL because of their stable redox reactions even in mixed solutions.
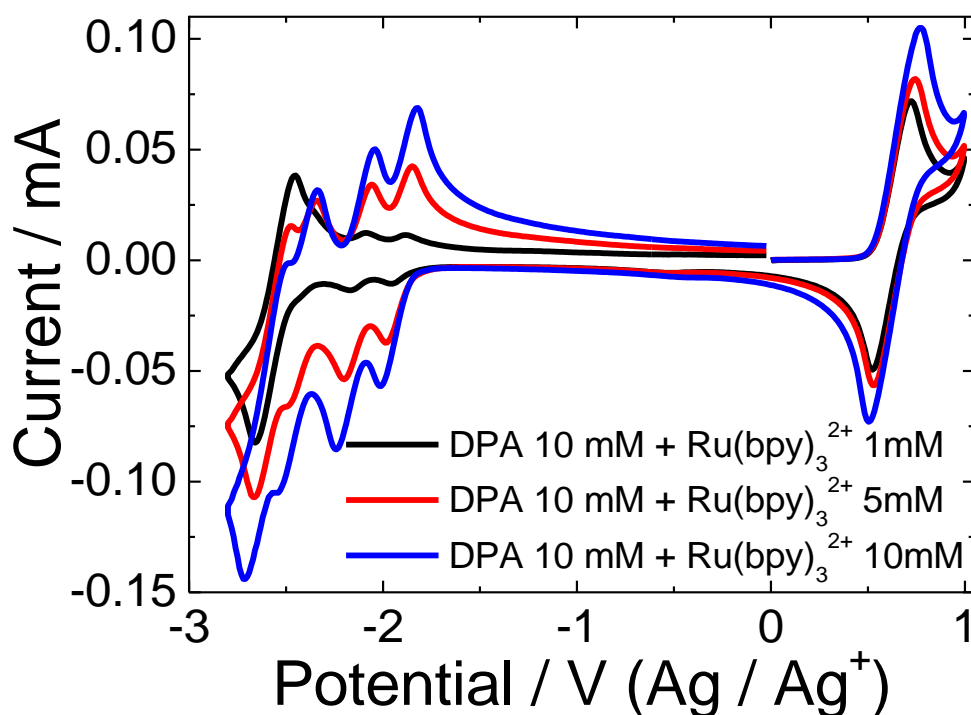

Figure 3-2.   CV curves of 3-electrode cells with various concentration ratios of Ru(bpy)$_3^{2+}$/DPA in PC/toluene.   Scan rate were set to be 50 mV/s.

3.3 Photophysical interaction between Ru(bpy)$_3^{2+}$ and DPA

Triplet-triplet energy transfer (TTET) from Ru(bpy)$_3^{2+}$ to DPA

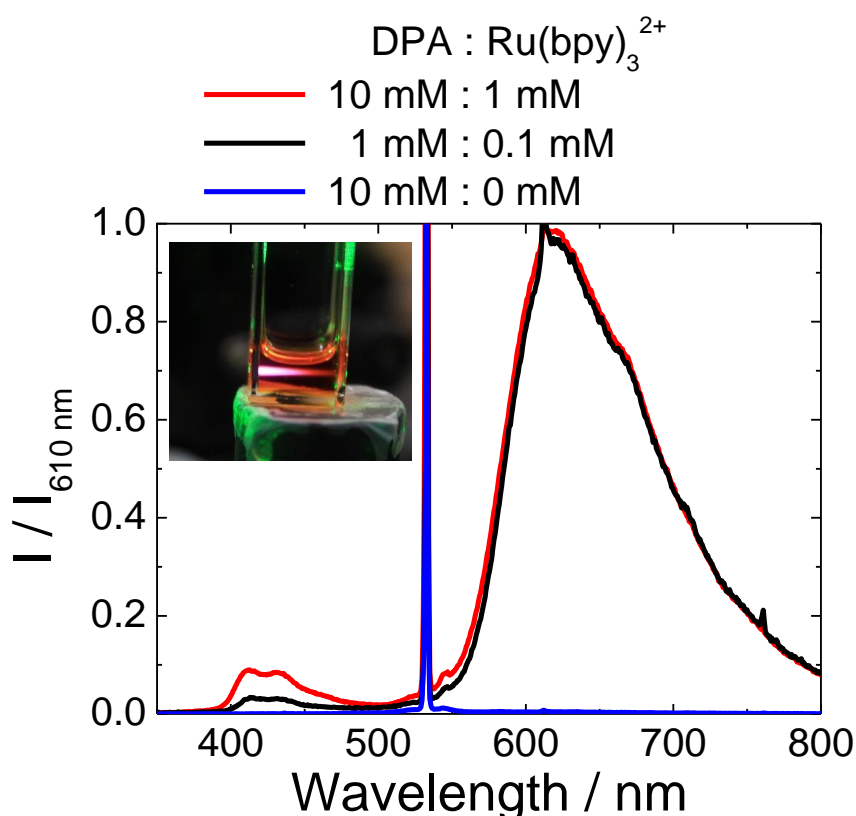In order to discuss the TTET and subsequent TTA-UC between Ru(bpy)$_3^{2+}$ and DPA under photoexcitation, the emission lifetimes and the luminescence spectra of Ru(bpy)$_3^{2+}$/DPA mixed solutions were measured. Figure 3-3 shows emission decay curves of electrolyte solutions containing Ru(bpy)$_3^{2+}$ or Ru(bpy)$_3^{2+}$/DPA. The emission decay rate became higher in the presence of DPA compared to the Ru(bpy)$_3^{2+}$ alone solution. The emission lifetime of the Ru(bpy)$_3^{2+}$ alone solution was calculated to be 490 ns. For the Ru(bpy)$_3^{2+}$/DPA mixed solutions, it was calculated to be 340 ns for 1 mM DPA, 110 ns for 5 mM DPA, and 85 ns for 10 mM DPA. This indicates that DPA behaves as a quencher of Ru(bpy)$_3^{2+}$. Namely, TTET from Ru(bpy)$_3^{2+}$ to DPA occurred. The Stern–Volmer quenching constant (K$_{SV}$) was calculated to be 482 M^{-1} and this value was consistent with reported quenching constants for Ru(bpy)$_3^{2+}$ and DPA system.[12] These behaviors suggested that TTET occurs more efficiently as the concentration of DPA increases, i.e. the intermolecular distances for species in the solution become shorter.
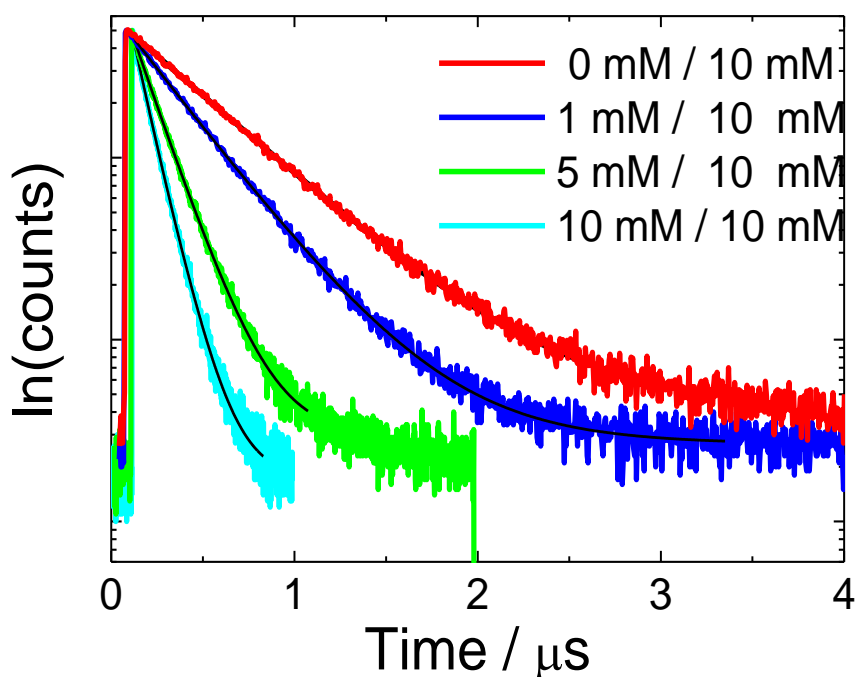
Figure 3-3. Emission decay of Ru(bpy)$_3^{2+}$ in PC/toluene solution containing Ru(bpy)$_3^{2+}$ (10 mM) and DPA (0–10 mM).

Upconverted luminescence from DPA due to the photophysical interaction with Ru(bpy)$_3$$^{2+}$

 Next, emission spectra of the mixture solutions upon the excitation of Ru(bpy)$_3$$^{2+}$ by green laser (Nd: YAG, 2ω, 532 nm, 10 mW) were observed to investigate the TTA-UC luminescence from DPA subsequent by TTET from photo-excited Ru(bpy)$_3$$^{2+}$ (Figure 3-4).   From the DPA alone solution, emission was not observed since DPA has no absorption band at 532 nm.[13]   On the other hand, not only orange emission from Ru(bpy)$_3$$^{2+}$ but also blue emission from DPA were observed in the case of Ru(bpy)$_3$$^{2+}$/DPA mixed solution ([DPA]:[Ru(bpy)$_3$$^{2+}$] = 10 mM:1 mM).   These results obviously indicates TTET from Ru(bpy)$_3$$^{2+}$ to DPA and following TTA-UC between triplet states of DPA. Further, in the case of dilute solution ([DPA]:[Ru(bpy)$_3$$^{2+}$] = 1 mM:0.1 mM), the emission intensity ratio of the blue emission to the orange emission (I_{DPA}/I_{Ru}) was smaller than that in relatively concentrated solution ([DPA]:[Ru(bpy)$_3$$^{2+}$] = 10 mM:1 mM).   This indicates that the TTET efficiency is influenced by the intermolecular distances in the solution, as theoretically considered.

**Figure 3-4.**   Photoluminescence spectra of DPA (blue) and Ru(bpy)$_3$$^{2+}$/DPA in PC/toluene. Excitation wavelength was 532 nm.

3.4 Electrochemically triggered upconverted luminescence

ECL from Ru(bpy)$_3^{2+}$ or DPA single device

Based on the achievement of TTA-UC in Ru(bpy)$_3^{2+}$/DPA system with photoexcitation, ECL devices consist of electrolyte solutions containing DPA and/or Ru(bpy)$_3^{2+}$ were prepared and their ECL spectra and electrode potentials under the AC voltage application were obtained. Figure 3-5 shows the ECL spectra from devices consist of DPA or Ru(bpy)$_3^{2+}$ alone solution. Since the energy gap between the HOMO and LUMO of DPA is 2.8 eV (Figure 3-1b), the ECL device consist of DPA alone solution did not emit light under $\pm$2.5 V AC whereas it showed blue ECL upon a voltage application of $\pm$ 3.3 V. For the Ru(bpy)$_3^{2+}$ alone solution-based ECL device, orange ECL was obtained upon the application of both $\pm$2.5 V and $\pm$3.3 V. This is attributed to the energy gap of Ru(bpy)$_3^{2+}$ (2.3 eV) is smaller than that of DPA (Figure 3-1a).

(a) DPA 10 mM   (b) Ru(bpy)$_3^{2+}$
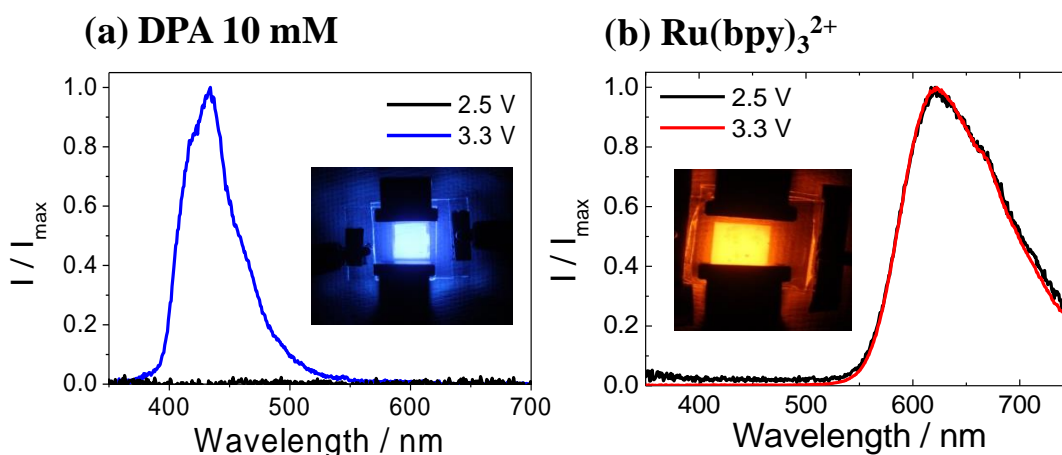
Figure 3-5. ECL spectra of 2-electrode devices containing (a) DPA or (b) Ru(bpy)$_3^{2+}$ solution under the application of an AC voltage (50 Hz).

Upconverted ECL from Ru(bpy)$_3^{2+}$/DPA mixed device

The ECL spectra and photograph of the Ru(bpy)$_3^{2+}$/DPA mixed device were shown in Figure 3-6. ECL from both Ru(bpy)$_3^{2+}$ and DPA were observed upon the AC voltage application. Interestingly, blue emission from DPA was observed even under the application of ±2.5 V, which did not induce ECL with a DPA alone solution. As a result of the mixture of blue and orange luminescence, the device emitted magenta light. These results demonstrated that it is possible to generate blue ECL from DPA with low-voltage application in the presence of Ru(bpy)$_3^{2+}$.
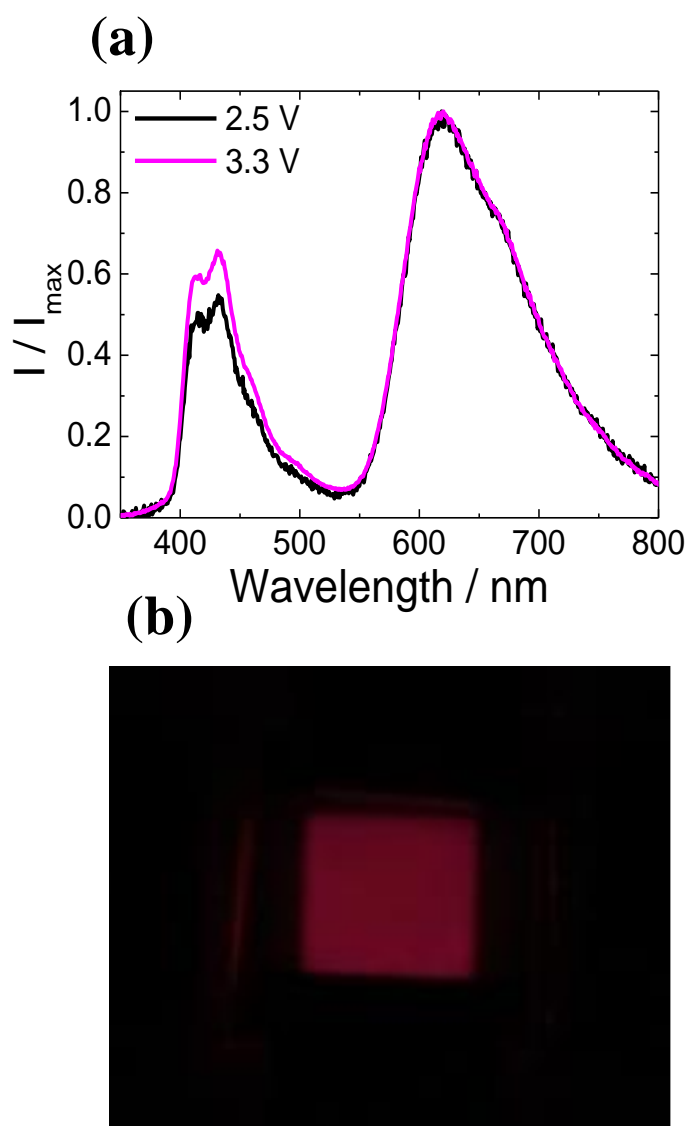
Figure 3-6. (a) ECL spectra of 2-electrode devices containing Ru(bpy)$_3^{2+}$/DPA solution ([Ru(bpy)$_3^{2+}$]/[DPA] = 5 mM/10 mM) under the application of an AC voltage (50 Hz). (b) Photograph of light-emitting 2-electrode ECL device.

Electrode potential of Ru(bpy)$_3$$^{2+}$/DPA device

In order to discuss the mechanism of low voltage generation of blue ECL in this device, electrode potential of Ru(bpy)$_3$$^{2+}$/DPA mixed solution-based device was measured under application of AC voltage (Figure 3-7). In both cases of AC ±2.5 V and AC ±3.3 V, although electrode potential reached the reduction onset potential of the Ru(bpy)$_3$$^{2+}$ (ca. −1.8 V) at the negative voltage, it did not reach that of DPA (ca. −2.4 V). Therefore, it was estimated that the DPA-derived blue ECL was generated without causing electrochemical reduction of DPA in this Ru(bpy)$_3$$^{2+}$/DPA ECL device.
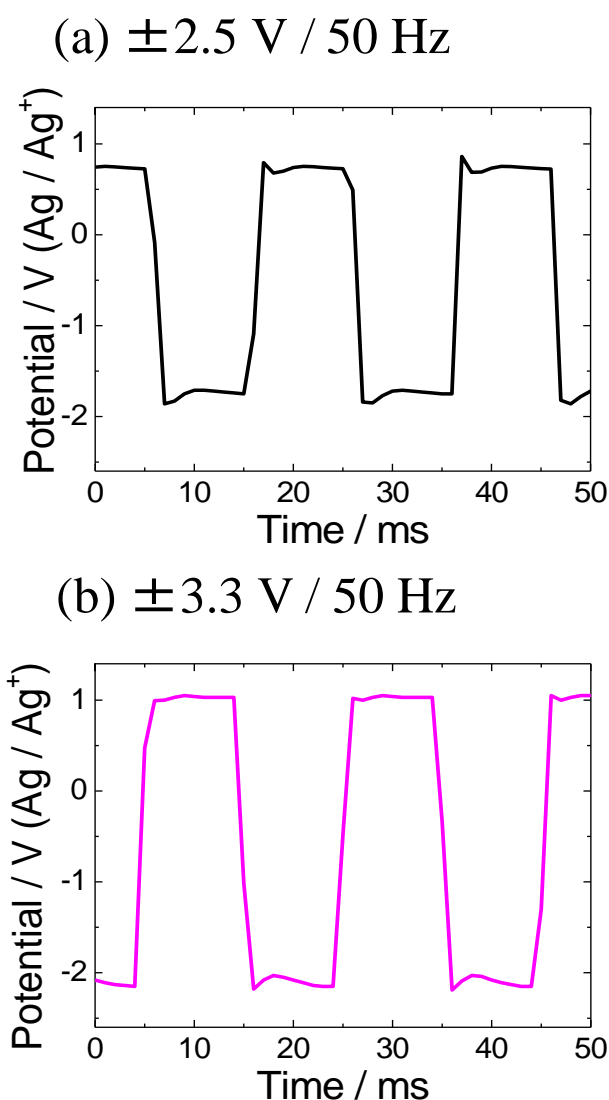
(a) ±2.5 V / 50 Hz

(b) ±3.3 V / 50 Hz

Figure 3-7.   Electrode potential of 2-electrode ECL device consist of Ru(bpy)$_3$$^{2+}$/DPA solution upon the application of (a) 2.5 V/50 Hz AC and (b) 3.3 V /50 Hz AC.

Upconverted ECL under the controlled electrode potential

In addition, a three-electrode ECL device was constructed and the ECL spectrum was measured under applying rectangular voltage of -2.1 V and $+0.8$ V (vs. Ag/Ag$^+$) at which the electrochemical reduction of DPA should not occur (Figure 3-8).　 As a result, blue ECL from DPA was generated even at a voltage at which reduced species of DPA was not generated.　 Since only excited species of Ru(bpy)$_3$$^{2+}$ can be electrochemically formed under such conditions, it is estimated that this blue ECL is generated through TTA-UC subsequent by TTET from the excited state of Ru(bpy)$_3$$^{2+}$ to DPA molecule.

Figure 3-8.　ECL spectrum of 3-electrode device containing Ru(bpy)$_3$$^{2+}$/DPA solution upon the application of $+0.8$ V/-2.1 V and 50 Hz AC.
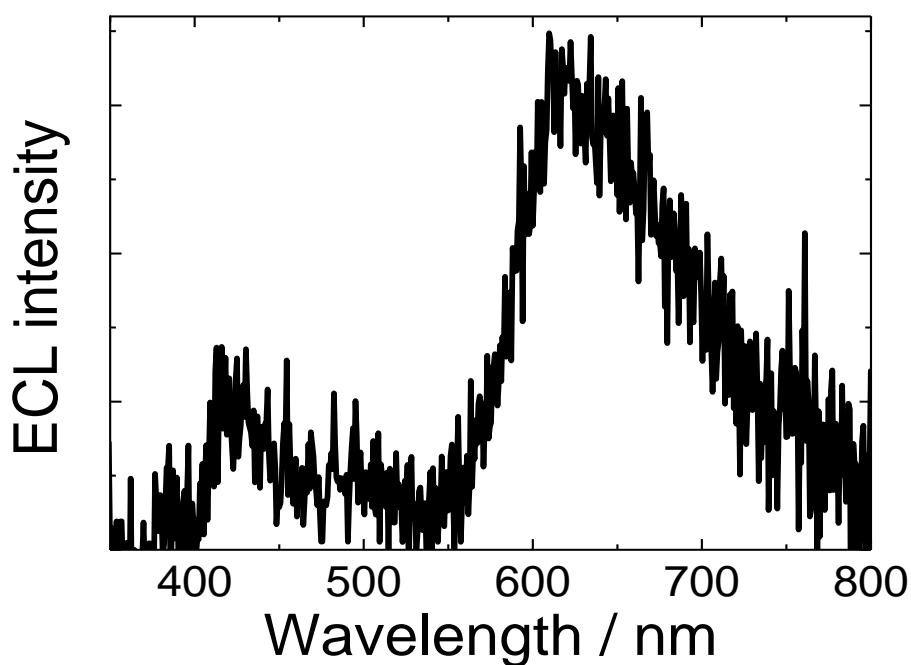
The mechanism of upconverted ECL

The proposed mechanism of blue luminescence in the $Ru(bpy)_3^{2+}$/DPA ECL device upon the application of ± 2.5 V was shown in Figure 3-9. First, $Ru(bpy)_3^{2+}$ are oxidized and reduced electrochemically near the electrode. Then, TTET occur from the ^{3}MLCT excited state of $Ru(bpy)_3^{2+}$ generated by electron transfer reaction, to the DPA molecule, resulting in the generation of the T_1 state. Finally, an S_1 state of DPA was formed due to the TTA-UC reaction between DPA molecules in T_1 states, leading to the expression of blue luminescence from the S_1 state. Hence, blue ECL though TTET and subsequent TTA-UC was successfully achieved from the $Ru(bpy)_3^{2+}$/DPA composite ECL device.
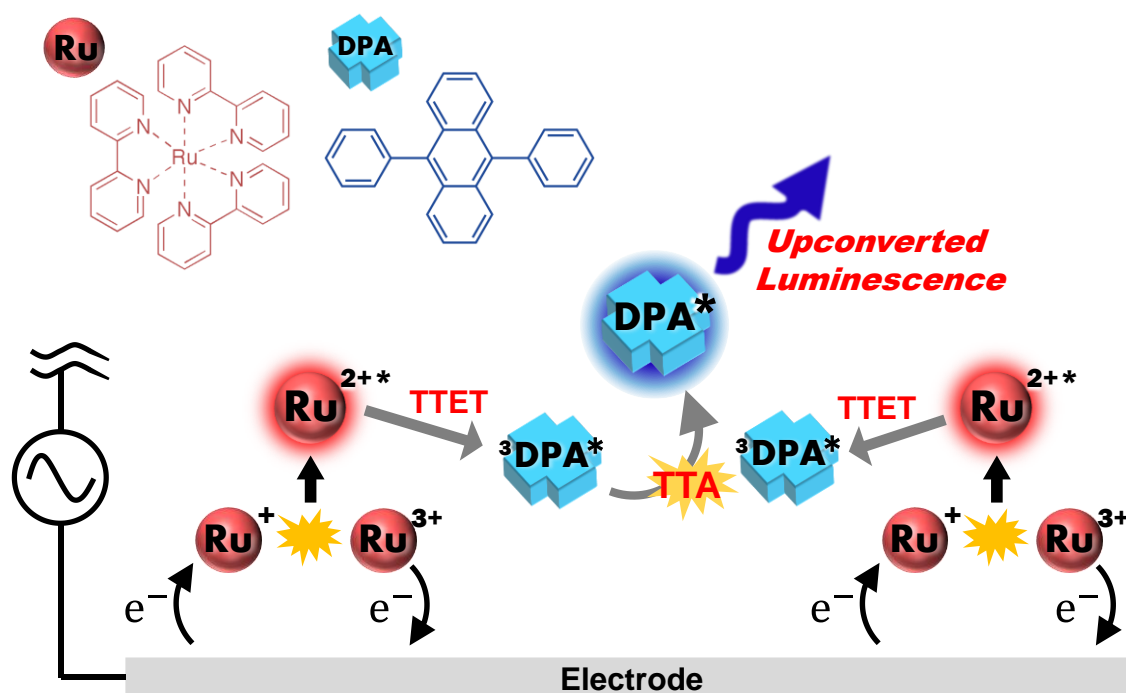
Figure3-9. Schematic description of the mechanism of blue luminescence from the 2-electrode device with the $Ru(bpy)_3^{2+}$/DPA mixed solution.

3.5 Summary of Chapter 3

In this chapter, $Ru(bpy)_3^{2+}$ and DPA were mixed in electrolyte solution and their photo-electrochemical properties were investigated toward the achievement of CPL with high dissymmetry. Triggered by the electrochemical excitation of $Ru(bpy)_3^{2+}$ TTET from $Ru(bpy)_3^{2+}$ to DPA and subsequent TTA-UC between the triplet states of DPA occurred. As a result, blue luminescence from DPA molecule was observed upon the application of AC voltage with lower voltage which is not able to generate redox spices of DPA. Such electrochemically upconverted luminescence could be useful for further development of ECL devices in terms of low voltage application and multicolor luminescence device.

However, CPL from Ru(II) complex-based systems has not yet been obtained. Considering this, while the Ru (II) complex exhibits strong light emission due to a large electric dipole moment (μ), it is difficult to give a large circular polarization degree to the light emission. Theoretically, luminescent dissymmetry (g_{lum}) can be defined as $g_{lum} = 4\ (|m|/|\mu|) \cdot \cos \tau$, where m and μ are the magnetic and electric dipole transition moments, respectively, and τ is the angle between them.[35] From this relation as well, it is considered difficult to obtain highly dissymmetry CPL from Ru(II) complex having large μ. Therefore I focused on Eu(III) complexes having small μ for luminescent material to show CPL. From next chapter, this study focus on the DNA/Eu(III) complex system to achieve both strong emission and CPL with high dissymmetry.

References of Chapter 3

1   Han, J.; Duan, P.; Li, X.; Liu, M. Amplification of Circularly Polarized Luminescence through Triplet-Triplet Annihilation-Based Photon Upconversion. *J. Am. Chem. Soc.* **2017**, *139* (29), 9783–9786. https://doi.org/10.1021/jacs.7b04611.

2   Yang, D.; Duan, P.; Zhang, L.; Liu, M. Chirality and Energy Transfer Amplified Circularly Polarized Luminescence in Composite Nanohelix. *Nat. Commun.* **2017**, *8* (11), 1–9. https://doi.org/10.1038/ncomms15727.

3   Sun, Y.; Collins, S. N.; Joyce, L. E.; Turro, C. Unusual Photophysical Properties of a Ruthenium(II) Complex Related to $[Ru(Bpy)_2(Dppz)]^{2+}$. *Inorg. Chem.* **2010**, *49* (9), 4257–4262. https://doi.org/10.1021/ic9025365.

4   Abrahamsson, M.; Jäger, M.; Kumar, R. J.; Österman, T.; Persson, P.; Becker, H. C.; Johansson, O.; Hammarström, L. Bistridentate Ruthenium(II)Polypyridyl-Type Complexes with Microsecond 3MLCT State Lifetimes: Sensitizers for Rod-like Molecular Arrays. *J. Am. Chem. Soc.* **2008**, *130* (46), 15533–15542. https://doi.org/10.1021/ja804890k.

5   Boutin, P. C.; Ghiggino, K. P.; Kelly, T. L.; Steer, R. P. Photon Upconversion by Triplet-Triplet Annihilation in $Ru(Bpy)_3$- and DPA-Functionalized Polymers. *J. Phys. Chem. Lett.* **2013**, *4* (23), 4113–4118. https://doi.org/10.1021/jz402311j.

6   Fujimoto, K.; Kawai, K.; Masuda, S.; Mori, T.; Aizawa, T.; Inuzuka, T.; Karatsu, T.; Sakamoto, M.; Yagai, S.; Sengoku, T.; Takahashi, M.; Yoda, H. Triplet-Triplet Annihilation-Based Upconversion Sensitized by a Reverse Micellar Assembly of Amphiphilic Ruthenium Complexes. *Langmuir* **2019**, *35* (30), 9740–9746. https://doi.org/10.1021/acs.langmuir.9b01433.

7   Wilke, B. M.; Castellano, F. N. Photochemical Upconversion: A Physical or Inorganic Chemistry Experiment for Undergraduates Using a Conventional Fluorimeter. *J. Chem. Educ.* **2013**, *90* (6), 786–789. https://doi.org/10.1021/ed300142z.

8   Fukuzaki, A.; Kawai, H.; Sano, T.; Takehara, K.; Nagamura, T. Efficient Upconversion by Highly Water-Soluble Cationic Sensitizer and Emitter in Aqueous Solutions with DNA. *ACS Biomater. Sci. Eng.* **2017**, *3* (8), 1809–1814. https://doi.org/10.1021/acsbiomaterials.7b00238.

9   Chen, Q.; Liu, Y.; Guo, X.; Peng, J.; Garakyaraghi, S.; Papa, C. M.; Castellano, F. N.; Zhao, D.; Ma, Y. Energy Transfer Dynamics in Triplet-Triplet Annihilation Upconversion Using a Bichromophoric Heavy-Atom-Free Sensitizer. *J. Phys. Chem. A* **2018**, *122* (33), 6673–6682. https://doi.org/10.1021/acs.jpca.8b05901.

10 Fan, C.; Wu, W.; Chruma, J. J.; Zhao, J.; Yang, C. Enhanced Triplet-Triplet Energy Transfer and Upconversion Fluorescence through Host-Guest Complexation. *J. Am. Chem. Soc.* **2016**, *138* (47), 15405–15412. https://doi.org/10.1021/jacs.6b07946.

11 Kerzig, C.; Wenger, O. S. Sensitized Triplet-Triplet Annihilation Upconversion in Water and Its Application to Photochemical Transformations. *Chem. Sci.* **2018**, *9* (32), 6670–6678. https://doi.org/10.1039/c8sc01829d.

12 Xu, K.; Zhao, J.; Moore, E. G. Photo-Induced Electron Transfer in a Diamino-Substituted Ru(Bpy)$_3$[PF$_6$]$_2$ Complex and Its Application as a Triplet Photosensitizer for Nitric Oxide (NO)-Activated Triplet-Triplet Annihilation Upconversion. *Photochem. Photobiol. Sci.* **2016**, *15* (8), 995–1005. https://doi.org/10.1039/c6pp00153j.

13 Tsuneyasu, S.; Ichikawa, T.; Nakamura, K.; Kobayashi, N. Electrochemical Stability of Diphenylanthracene and Its Effect on Alternating-Current-Driven Blue-Light Electrochemiluminescence Properties. *ChemElectroChem* **2017**, *4* (7), 1731–1735. https://doi.org/10.1002/celc.201600896.

14 Zhou, Y.; Ayad, S.; Ruchlin, C.; Posey, V.; Hill, S. P.; Wu, Q.; Hanson, K. Examining the Role of Acceptor Molecule Structure in Self-Assembled Bilayers: Surface Loading, Stability, Energy Transfer, and Upconverted Emission. *Phys. Chem. Chem. Phys.* **2018**, *20* (31), 20513–20524. https://doi.org/10.1039/c8cp03628d.

Chapter 4

Induced Circularly Polarized Luminescence from Achiral Eu(III) Complex by Associating with DNA-CTMA

Induced Circularly Polarized Luminescence from Achiral Eu(III) Complex by Associating with DNA-CTMA

So far, I focused on the Ru(II) complexes toward the achievement of brilliant CPL because it have possible application as novel electrochemical luminescent devices due to its excellent photophysical properties and electrochemical properties. However, it was difficult to obtain CPL from Ru(II) complex-based systems. Typically, chiral organic luminophores and transition metal complexes display a strong luminescence; however, the degree of polarization of the luminescence is considerably lower. The parameter g_{lum} is generally used as a dissymmetry ratio of the emission and is defined as $g_{lum} = 2(I_L - I_R)/(I_L + I_R)$, where I_L (I_R) is the intensity of left (right) circularly polarized luminescence. Theoretically, g_{lum} can be defined as $g_{lum} = 4 (|m|/|\mu|) \cdot \cos \tau$, where m and μ are the magnetic and electric dipole transition moments, respectively, and τ is the angle between them.[1] Thus, luminophores which have a large μ owing to the allowed π-π* transition maintain a low g_{lum} while showing a high luminescence quantum yield.

In order to prepare the novel material showing CPL, Eu(III) complexes were utilized from this section. As described in Chapter 1, lanthanide complexes including Eu(III) complex show the luminescence with high color purity and long emission lifetime due to f-f transition.[2] Since the f-f transition is originally forbidden, the electric dipole moment (μ) of Eu(III) complex become low. Therefore, it is expected that Eu(III) complex-based materials exhibit luminescence with large g_{lum}. Aiming to develop improved DNA-based photo-functional materials with Eu(III) complex, it is necessary to fabricate DNA/Eu(III) complex. Since DNA is soluble only in water whereas Eu(D-facam)$_3$ is insoluble in water, DNA is modified with CTMA (cetyltrimethylammonium chloride), which is one of the most typical surfactants utilized for biomolecules.[3-6] Today, various optoelectronic devices utilizing this DNA-surfactant complex, such as optical amplifiers,[7-10] organic light emitting diodes (OLEDs),[11-13] photo-detectors,[14] and organic transistors[15-16] have reported.

In this section, it was aimed to express CPL by changing the ligand field around Eu(III) ion due to the helical structure of DNA by combining the achiral Eu(III) complex (Eu(tta)$_3$(H$_2$O)$_2$) with DNA-CTMA.

4.1 Interaction mode between Eu(tta)$_3$(H$_2$O)$_2$ and DNA

4.1.1 Association of luminescent Eu(tta)$_3$(H$_2$O)$_2$ with DNA

Materials

The sodium salts of DNA (base pairs: ca. 10,000) were provided by Nippon Chemical Feed Co., Ltd. (Japan). They were marine-based salts that were first isolated from frozen salmon milt through a homogenization process followed by removal of proteins and impurities. Tris(2-thenoyltrifluoroacetonato)europium(III) [Eu(tta)$_3$(H$_2$O)$_2$], cetyltrimethylammonium chloride (CTMA) with the purity of 98%, and butanol were purchased from Tokyo Chemical Industry Co., Ltd. (Japan) Poly(methylmethacrylate) (PMMA, Mw: ca. 350,000) was also purchased from Sigma-Aldrich (United States). These materials were used without further purification.

Preparation of DNA-CTMA complex

Preparation of DNA-CTMA was accomplished by precipitating the DNA with a cationic surfactant complex of CTMA in water through an ion exchange reaction which replaced the sodium cation of the DNA. The DNA complex with CTMA (DNA-CTMA) was prepared by adding 10 mmol/L of DNA (concentration of the phosphate group) aqueous solution to 10 mmol/L of the CTMA solution. The precipitate was filtered and thoroughly washed with ultrapure water and then dried in vacuo. The resulting DNA-CTMA became water insoluble and more mechanically stable due to the long alkyl chain of the CTMA. By forming the CTMA complex, DNA-CTMA could be dissolved in solvents more compatible with device fabrication, such as chloroform, ethanol, methanol, butanol, or a chloroform/alcohol blend.

Preparation of DNA-CTMA/Eu(tta)$_3$(H$_2$O)$_2$ films

Butanol solution containing Eu(tta)$_3$(H$_2$O)$_2$ (1 mmol/L) were added to the butanol solution containing DNA-CTMA. The concentration ratios of the DNA-CTMA to Eu(tta)$_3$(H$_2$O)$_2$ were varied by changing DNA-CTMA concentration (defined as concentration of phosphate group) in the solution. The DNA-CTMA/Eu(tta)$_3$(H$_2$O)$_2$ films were prepared by casting method on quartz substrates. The weight percentage of the Eu(tta)$_3$(H$_2$O)$_2$ in the DNA-CTMA film were varied in the 6wt% to 38wt% range.

The PMMA films containing the Eu(tta)$_3$(H$_2$O)$_2$ with various weight percentage were also prepared for comparison.

Photophysical measurements

UV-vis absorption spectra of the samples were measured using a spectrophotometer (JASCO, V-570).   Circular dichroism (CD) spectra of the DNA complex were measured using a CD spectrometer (JASCO, J-820).   Photoluminescence spectra were obtained using a spectrofluorometer (JASCO, FP-6600).   Excitation wavelength of the samples was 337 nm.   Emission quantum yields of the films were determined by standard procedures with an integral sphere (JASCO ILF-533, diameter 10 cm) mounted on a spectrofluorometer (JASCO FP-6600).   The emission lifetimes were determined by using a N$_2$ laser with a 337-nm wavelength and 4-ns pulse width (Spectra-Physics, VSL337) and a photomultiplier (Hamamatsu Photonics, H10721-20MOD, response time 0.8 ns).   Samples were excited by nanosecond pulse of N$_2$ laser (337 nm).   Emission from the sample was guided to the photomultiplier through a sharp-cut filter.   Emission decays were monitored with a digital oscilloscope (Sony Tektronix, TDS3052, 500 MHz) synchronized to single-pulse excitation.

CPL spectra of the DNA complex films were measured according to previously reported system.[17]   The excitation light with the wavelength of 375 nm was irradiated to the film samples from the same-side to the detection in the epi-illumination con-figuration.   In order to maintain circularly polarized component in the emission, the dichroic filter was precisely settled to be 45° against the optical path.   The retardation of the emitted light was controlled by a photo-elastic modulator (Hinds, PEM-90) that was modulated with the frequency of 50 kHz.   For analyzing CPL signal, the circularly polarized component was converted to the linearly polarized light by passing through the linearly polarized cubic prism (200,000:1).   Then the linearly polarized light was detected a photomultiplier tube (Hamamatsu, H7732-10).   The AC component of the PMT output with frequency of 50 kHz was analyzed by a lock-in amplifier (EG&G, Model 7265), which can be modulated by the reference frequency signal from the PEM. A PC system controls a monochromator and the PEM for the appropriate detection wavelength.

4.1.2 Interaction mode between Eu(tta)$_3$(H$_2$O)$_2$ and DNA

Absorbance change of Eu(tta)$_3$(H$_2$O)$_2$ in the presence of DNA

 UV-visible absorption spectra of the DNA-CTMA/Eu(tta)$_3$(H$_2$O)$_2$ in butanol with various ratios of [DNA-CTMA]:[Eu(tta)$_3$(H$_2$O)$_2$] are shown in Figure 4-1.   The concentration of the Eu(tta)$_3$(H$_2$O)$_2$ was set to constant value of 0.01 mmol/L.   The concentration of the DNA-CTMA was defined as the concentration of phosphate groups in DNA main chain.   The absorption bands at around 340 nm were assignable to π-π* transition of the tta ligands.   The absorption bands of DNA base pairs (210nm and 260 nm) were increased with increase in DNA content.   The absorbance of the DNA base pairs exhibited almost liner increase with DNA-CTMA concentration.   Close up view of the absorption bands of the tta ligand are shown in Figure 4-1b.   When DNA-CTMA was absent in the Eu(tta)$_3$(H$_2$O)$_2$ solution ([DNA-CTMA]:[Eu(tta)$_3$(H$_2$O)$_2$] = 0:1), the absorption maximum of the tta ligands was observed at 340 nm.   The absorption maximum became slightly red-shifted with increasing the DNA concentration, resulting absorption maximum at 343 nm.   On the other hand, the absorbance corresponding to tta also decreased by addition of DNA-CTMA.   These phenomena such as the reduction in the UV/visible absorbance of the molecules, as well as a red shift in the absorbance maximum indicate that the Eu(III) complex was likely intercalated or semi-intercalated into the DNA-CTMA.[18-19]
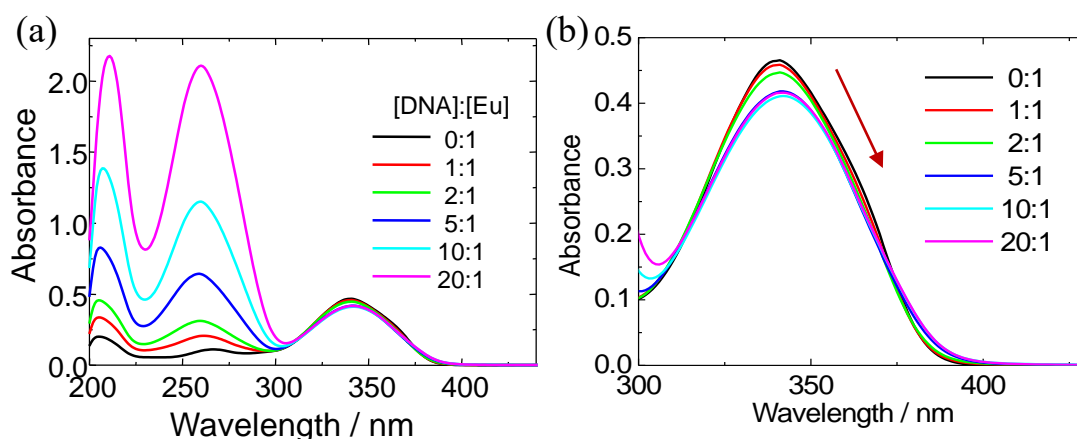
Figure 4-1. (a) Absorption spectra of DNA-CTMA/Eu(tta)$_3$(H$_2$O)$_2$ in butanol and (b) an expanded view of the 300–400 nm region. The [DNA-CTMA] to [Eu(tta)$_3$(H$_2$O)$_2$] ratio ranged from 0:1 to 20:1.

Change in structural chirality of Eu(tta)₃(H₂O)₂

In order to discuss the detailed interaction mode between DNA-CTMA and Eu(tta)$_3$(H$_2$O)$_2$, CD spectra measurements of the DNA-CTMA and DNA-CTMA/Eu(tta)$_3$(H$_2$O)$_2$ in the film state were carried out.   Fig. 4-2 shows the CD spectra of the DNA-CTMA film, DNA-CTMA/Eu(tta)$_3$(H$_2$O)$_2$ film and differential spectra of two spectra.   Molar composition of the film was [DNA-CTMA]:[Eu(tta)$_3$(H$_2$O)$_2$] = 5:1 (i.e. 19 wt% Eu(III) complex).   In the UV region, a positive Cotton effect at 280 nm and two negative Cotton effects at 250 and 225 nm were observed, which were similar to CD signals of A-form DNA rather than B-form DNA.   On the other hand, negative Cotton effect corresponding to the absorption of tta ligand was observed at around 340 nm on CD spectra of the DNA-CTMA/Eu(tta)$_3$(H$_2$O)$_2$ film and differential spectrum.   The appearance of the CD signal from the tta absorption indicate that the electron transition of tta ligand was affected by chiral condition of the DNA-CTMA matrix, suggesting interaction between DNA backbone and Eu(tta)$_3$(H$_2$O)$_2$ as predicted by changes of absorption spectra.
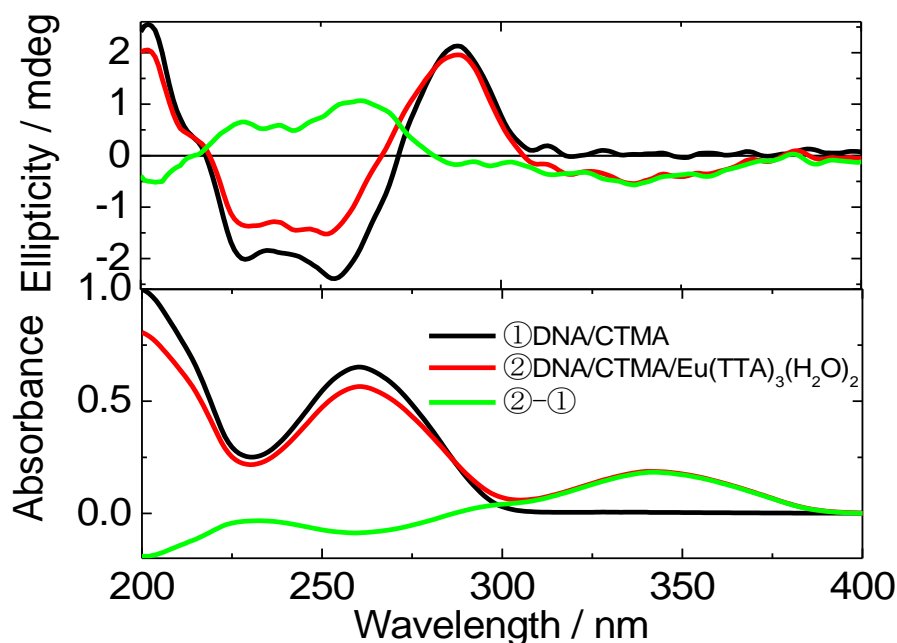

Figure 4-2. Absorption (top) and CD (bottom) spectra of DNA-CTMA film, DNA-CTMA/Eu(tta)$_3$(H$_2$O)$_2$ film, and differential spectra.   ([DNA-CTMA]:[Eu(tta)$_3$(H$_2$O)$_2$] = 5:1, i.e. 19wt% of Eu(III) complex).

4.2 Emission Enhancement by the Immobilization onto DNA structure

Photoluminescence properties of the DNA-CTMA/Eu(tta)$_3$(H$_2$O)$_2$ film

  Photoluminescence properties of the DNA-CTMA/Eu(tta)$_3$(H$_2$O)$_2$ films were investigated to discuss the influence of the interaction between DNA-CTMA and Eu(III) complex on the luminescence properties.   Fig. 4-3 shows the emission spectra of the Eu(tta)$_3$(H$_2$O)$_2$ in DNA-CTMA film or PMMA film under 337 nm excitation.   The contents of the Eu(tta)$_3$(H$_2$O)$_2$ in both films were 19 wt%   (i.e.   [DNA-CTMA]:[Eu(tta)$_3$(H$_2$O)$_2$]=5:1).   From both films, sharp red emission bands of excited Eu(III) were observed at 590, 615, and 650 nm under excitation of the tta ligand.   These emission bands are attributed to the f-f transitions of $^5D_0 \rightarrow$ ^7F_J (J = 1, 2, and 3, respectively) in the excited Eu(III) ion.   Photo-excitation of the tta ligand, leading to generation of its S$_1$ state and the S$_1$ state subsequently decays to a T$_1$ state through intersystem crossing (ISC).   Finally, The T$_1$ state leads to the generation of the emissive excited state of 4f orbital in the central Eu(III) ion through excitation energy transfer.   The absorbance of both the DNA-CTMA/Eu(tta)$_3$(H$_2$O)$_2$ film and the PMMA/Eu(tta)$_3$(H$_2$O)$_2$ film was almost same at the excitation wavelength (Fig 4-3a inset).   Nevertheless, the emission intensity of the
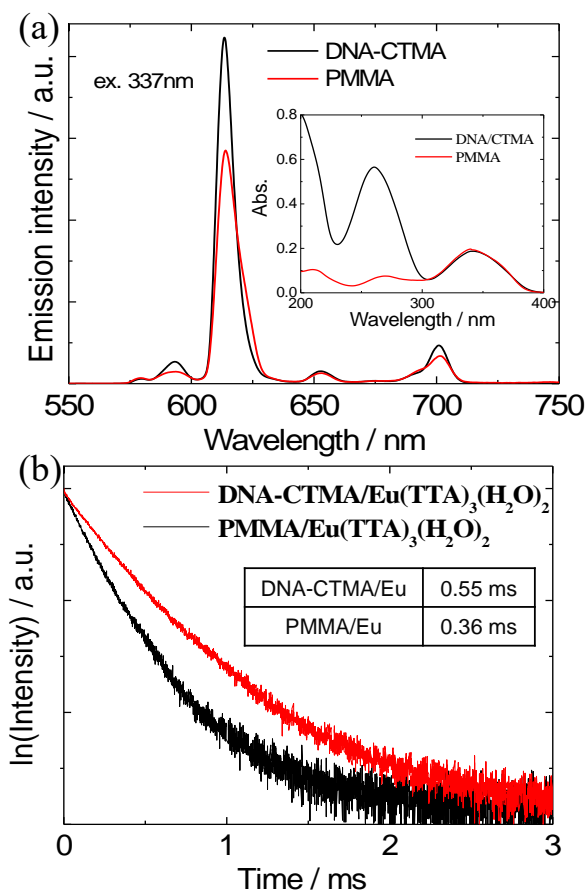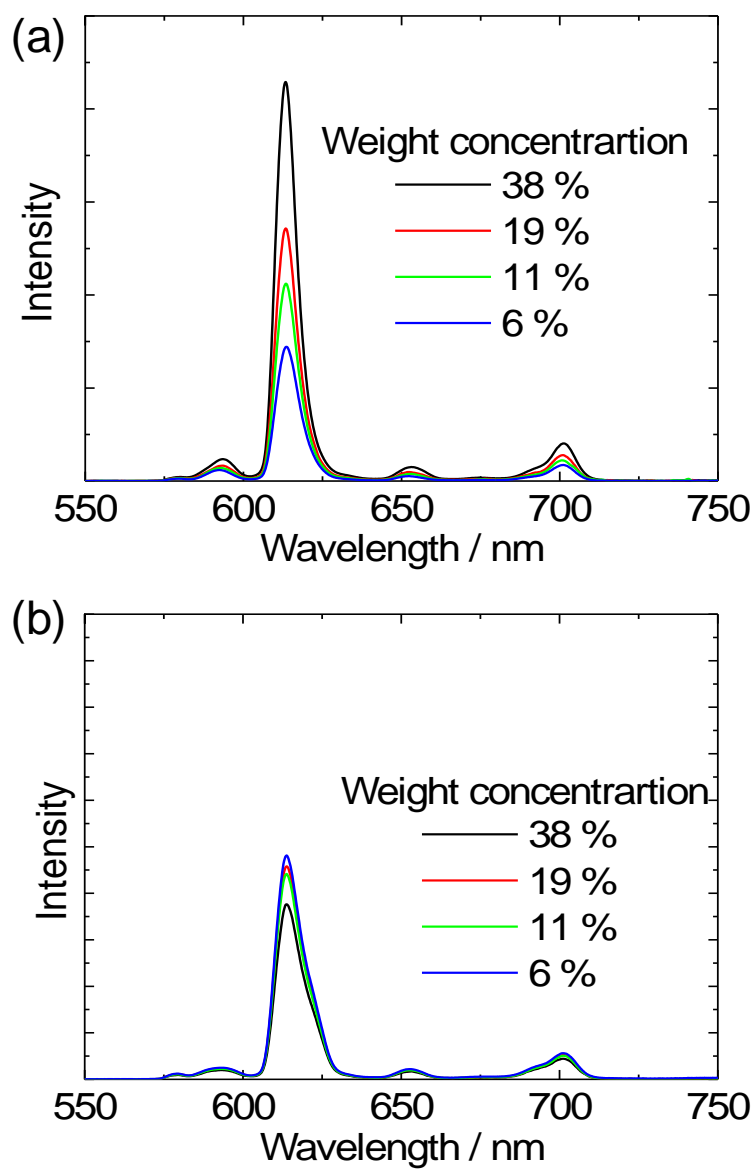

Figure 4-3. (a) Photoluminescence spectra of the Eu(tta)$_3$(H$_2$O)$_2$ complex in DNA-CTMA (red) or PMMA (black) films. Excitation wavelength is 337 nm. The inset shows the absorption spectra of the films. (b) Emission decay curves of the Eu(tta)$_3$(H$_2$O)$_2$ complex in DNA-CTMA (red) or PMMA (black) films. The emission was obtained at 615 nm.

63

DNA-CTMA/Eu(tta)$_3$(H$_2$O)$_2$ film was higher than that of the PMMA/Eu(tta)$_3$(H$_2$O)$_2$ film, indicating that the emission quantum yield of the Eu(III) complex was enhanced in DNA-CTMA matrix.　The emission decay curves of the DNA-CTMA/Eu(tta)$_3$(H$_2$O)$_2$ films and the PMMA/Eu(tta)$_3$(H$_2$O)$_2$ film were shown in Fig. 4-3b.

**Emission enhancement of Eu(tta)$_3$(H$_2$O)$_2$ upon the interaction with DNA-CTMA**

　Emission spectra of the DNA-CTMA/Eu(tta)$_3$(H$_2$O)$_2$ film and the PMMA/Eu(tta)$_3$(H$_2$O)$_2$ film with various contents of Eu(III) complex were measured. Fig. 4-4a shows emission spectra of the DNA-CTMA/Eu(tta)$_3$(H$_2$O)$_2$ films with various contents of Eu(III) complex in the DNA-CTMA.　The Eu(tta)$_3$(H$_2$O)$_2$ contents of 6, 11, 19, and 38 wt% were correspond to the molar compositions of [DNA-CTMA]:[Eu(tta)$_3$(H$_2$O)$_2$]=20:1, 10:1, 5:1, and 2:1, respectively.　The emission intensity of the DNA-CTMA/Eu(tta)$_3$(H$_2$O)$_2$ films were enlarged with increasing the content of the Eu(tta)$_3$(H$_2$O)$_2$, whereas those of the PMMA/Eu(tta)$_3$(H$_2$O)$_2$ (Fig. 4-4b) were slightly decreased with increasing the content of the Eu(tta)$_3$(H$_2$O)$_2$.　Generally, the emission intensities from luminophore tend to saturate and decrease in the higher concentration region because of the various kinds of concentration quenching, as shown in PMMA/Eu(tta)$_3$(H$_2$O)$_2$ film.　However, the emission intensities from the DNA-CTMA/Eu(tta)$_3$(H$_2$O)$_2$ films were still increasing at extremely high concentration region of [DNA-CTMA]:[Eu(tta)$_3$(H$_2$O)$_2$]=2:1 (i.e. 38wt% of Eu(III) complex).　This significantly indicates that the DNA-CTMA matrix suppressed the concentration quenching of the emission from Eu(III) unlike with conventional polymer matrix.　The enhancement of the emission intensity and the suppression of concentration quenching caused by DNA association were reported by using various kinds of organic and inorganic compounds, such as ethidium bromide [(3,8-diamino-5-ethyl-6-phenyl phenanthridinium bromide)],[20,21] tris(bipyridine)ruthenium(II) complexes,[22] etc.　In these systems, the association between luminescent compounds and DNA-CTMA could play a protective role, leading to suppression of vibrational quenching and aggregation of luminescent compounds.　In this cases, the vibrational quenching and aggregation quenching of Eu(tta)$_3$(H$_2$O)$_2$ complex would be also suppressed in DNA-CTMA matrix by interacting with DNA-CTMA as mentioned in former section, resulting in large enhancement of its emission in accordance with concentration of the Eu(III) complex.

64

Figure 4-4. Photoluminescence spectra of the Eu(tta)$_3$(H$_2$O)$_2$ complex in DNA-CTMA (a) or PMMA (b).   The weight percentage of the Eu(tta)$_3$(H$_2$O)$_2$ are varied in the 6wt% to 38wt% range.   Excitation wavelength is 337 nm.

Enhancement of the emission quantum yields

In order to analyse the detailed photophysical properties, emission quantum yields of these films were measured. Fig. 4-5 shows the emission quantum yields of DNA-CTMA/Eu(tta)$_3$(H$_2$O)$_2$ films and PMMA/Eu(tta)$_3$(H$_2$O)$_2$ film with various contents of Eu(tta)$_3$(H$_2$O)$_2$ complex. The emission quantum yields of the Eu(tta)$_3$(H$_2$O)$_2$ in PMMA films were approximately 40% and slightly decreased with increasing the Eu(III) contents. Interestingly, the emission quantum yields of the DNA-CTMA/Eu(tta)$_3$(H$_2$O)$_2$ films depended on the ratio of DNA-CTMA and Eu(tta)$_3$(H$_2$O)$_2$ (DNA-CTMA:Eu(tta)$_3$(H$_2$O)$_2$). When the concentration of Eu(tta)$_3$(H$_2$O)$_2$ was lower ([DNA-CTMA]:[Eu(tta)$_3$(H$_2$O)$_2$)]=20:1), the emission quantum yield was approximately 20% which was lower value than that of in the PMMA film. Then, the quantum yields of the films enhanced with increasing in the contents of the Eu(tta)$_3$(H$_2$O)$_2$, reaching to over 60% at the ratio of [DNA-CTMA]:[Eu(tta)$_3$(H$_2$O)$_2$)]=2:1. This indicated that the coordination environment of the Eu(III) complexes changed with the ratio of DNA-CTMA and Eu(tta)$_3$(H$_2$O)$_2$.
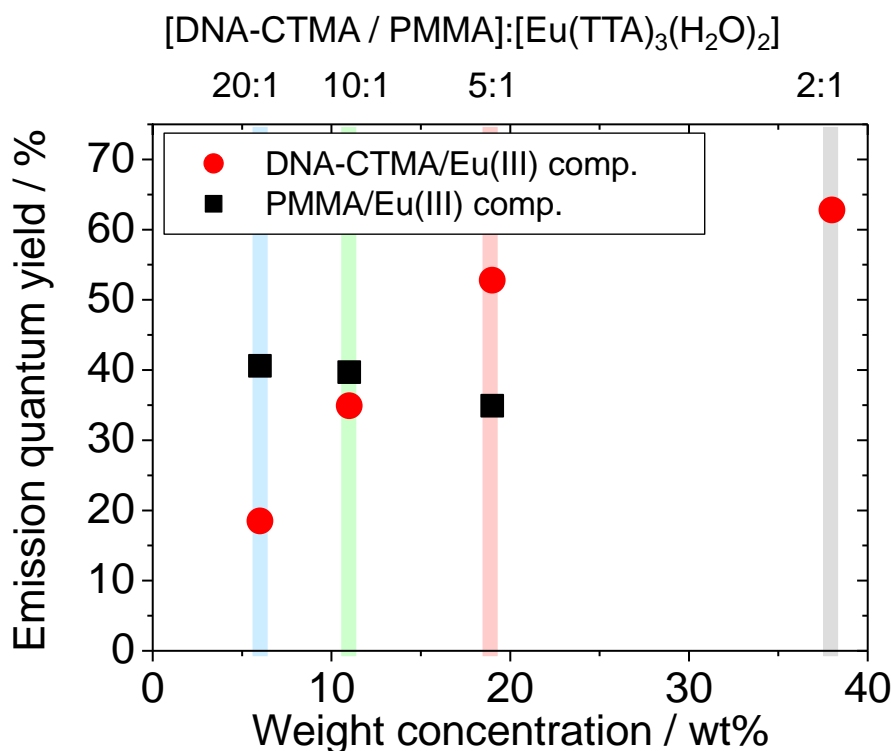
Figure 4-5. Emission quantum yields of DNA–CTMA/Eu(tta)$_3$(H$_2$O)$_2$ films (red circles) and PMMA/Eu(tta)$_3$(H$_2$O)$_2$ films (black squares) as functions of the Eu(III)-complex content.

Symmetry analysis of Eu(tta)$_3$(H$_2$O)$_2$

For the discussion of the coordination environment of the Eu(III) complex from emission spectra, relative intensities (I_{rel}) of the $^5D_0{\rightarrow}^7F_2$ transition (612 nm) to $^5D_0{\rightarrow}^7F_1$ transition (590 nm) were analysed.   For lanthanoid complexes, it is known that the emission peaks corresponding to the $^5D_0{\rightarrow}^7F_1$ transition is derived from the magnetic dipole (MD) moment, and its intensity is not easily perturbed by the ligand field.   In contrast, the emission peak near 613 nm due to the $^5D_0{\rightarrow}^7F_2$ transition is derived from the electric dipole (ED) moment, and its intensity can significantly change under the influence of the ligand field.   Therefore, the symmetry of Eu(tta)$_3$(H$_2$O)$_2$ can be estimated from the ratio of emission intensities derived from the MD moment (I_{MD}) and ED moment (I_{ED}).   The emission spectra of the Eu(tta)$_3$(H$_2$O)$_2$ in the DNA-CTMA films, which was normalized by $^5D_0{\rightarrow}^7F_1$ transition, are shown in Fig. 4-6a.   The I_{rel} values deceased from 18.2 ([DNA-CTMA]:[Eu(tta)$_3$(H$_2$O)$_2$)] = 2:1) to 9.8 ([DNA-CTMA]:[Eu(tta)$_3$(H$_2$O)$_2$)] = 50:1) with increasing of DNA-CTMA content, indicating that the coordination structure of the Eu(III) complex became more symmetric environment (Figure 4-6b).   Whereas, the I_{rel} values of PMMA/Eu(tta)$_3$(H$_2$O)$_2$ films were keeping almost constant value of 19.5.   This change of the coordination structures of the Eu(III) complex thought to induce enhancement of the emission quantum yields.
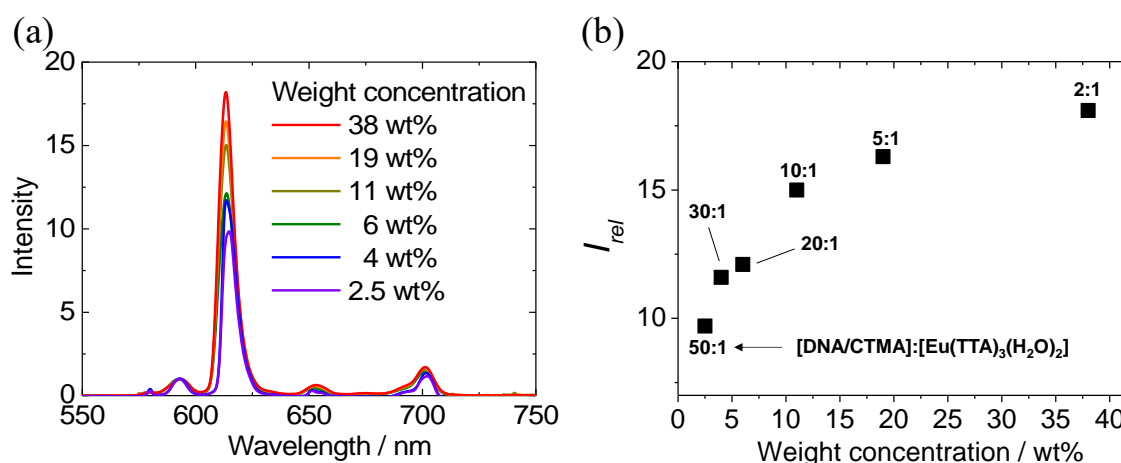
Figure 4-6. Emission spectra of Eu(tta)$_3$(H$_2$O)$_2$ in DNA-CTMA films normalized against the $^5D_0 \rightarrow {}^7F_1$ transition (590 nm) and (bottom) I_{rel} values (relative intensities of the $^5D_0 \rightarrow {}^7F_2$ transition (612 nm) to the $^5D_0 \rightarrow {}^7F_1$ transition (590 nm)) as functions of the Eu(III)-complex content. The weight percentage of Eu(tta)$_3$(H$_2$O)$_2$ ranged between 2.5 and 38 wt%. Excitation wavelength is 337 nm.

Change in Emission Lifetime

The emission lifetimes of the films were also determined from emission decay curves under excitation by nanosecond N_2 laser (Fig. 4-7). The emission lifetimes of the PMMA/Eu(tta)$_3$(H$_2$O)$_2$ films were approximately 340 μs. On the other hand, longer emission lifetimes of the Eu(III) complexes were observed in DNA-CTMA films. The emission lifetimes increased up to 500 μs by incorporating with DNA-CTMA matrix. These longer emission lifetimes would be due to the immobilization of Eu(III) complex in the DNA-CTMA, leading to suppression of vibrational and concentration quenching of the excited states of the Eu(III) complex. In addition, Eu(III) complexes with highly symmetrical structure are known to show low values of radiative rate constants, resulting in longer emission lifetimes.[23] As indicated above, coordination environments of the Eu(tta)$_3$(H$_2$O)$_2$ changed to more symmetrical structures by interaction with DNA-CTMA molecules. The change of coordination environments would be also contributing to longer emission lifetimes of the DNA-CTMA/Eu(tta)$_3$(H$_2$O)$_2$ film.
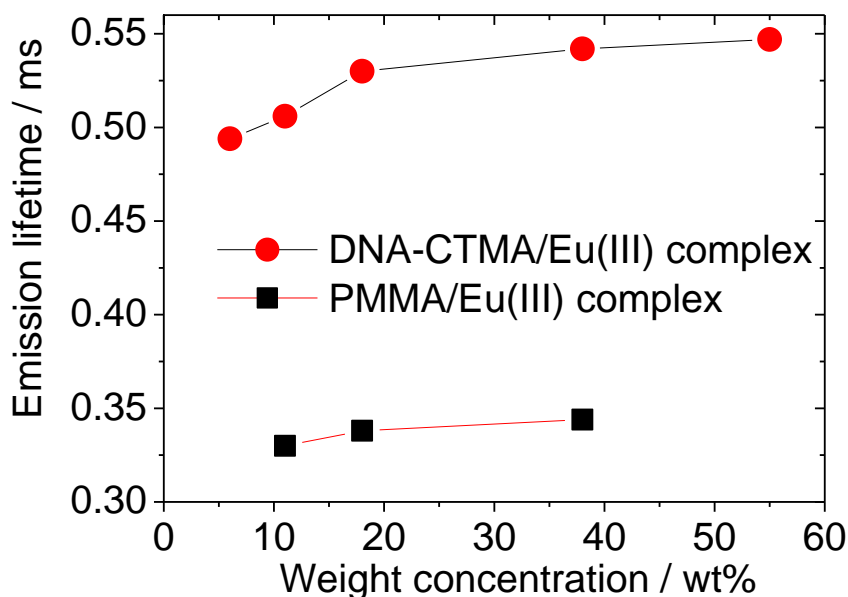

Figure 4-7. Emission lifetimes of the DNA-CTMA/Eu(tta)$_3$(H$_2$O)$_2$ films (red circles) and PMMA/Eu(tta)$_3$(H$_2$O)$_2$ films (black squares) as functions of the Eu(tta)$_3$(H$_2$O)$_2$ to DNA-CTMA ratio determined from emission decay curves following excitation by a nanosecond N_2 laser.

4.3. Circularly Polarized Luminescence Induced by DNA

The photophysical analyses of the DNA-CTMA/Eu(tta)$_3$(H$_2$O)$_2$ film suggested that the interaction between the Eu(III) complex and the DNA-CTMA enhanced its emission properties by suppression of vibrational quenching and aggregation quenching. In order to investigate the optical chirality in the photoluminescence, circularly polarized luminescence (CPL) was measured. CPL is defined as the differential emission of right- and left-handed circularly polarized light. CPL has attracted considerable interest in because of its capacity to investigate chiral structures in the excited state. The CPL materials also have potential applications in chemical sensors, biological probes, and three-dimensional displays. The CPL spectra of these films are shown in Figure 4-8. The Eu(tta)$_3$(H$_2$O)$_2$ in PMMA matrix did not show any CPL signal at the region of $^5D_0 \rightarrow$ ^7F_J bands (J = 1, 2, and 3, respectively). On the other hand, the positive CPL signals were observed at the emission bands of 590 nm and 612 nm ($^5D_0 \rightarrow {}^7F_1$ and $^5D_0 \rightarrow {}^7F_2$ band, respectively). Although dissymmetry factor (g_{lum}) of the CPL signals were relatively low (less than 0.01) in comparison with Eu(III) complex having chiral ligands, the appearance of the CPL signals were clearly indicating that the association of Eu(III) complex with DNA-CTMA induced the chirality of the emission from Eu(III) complexes.
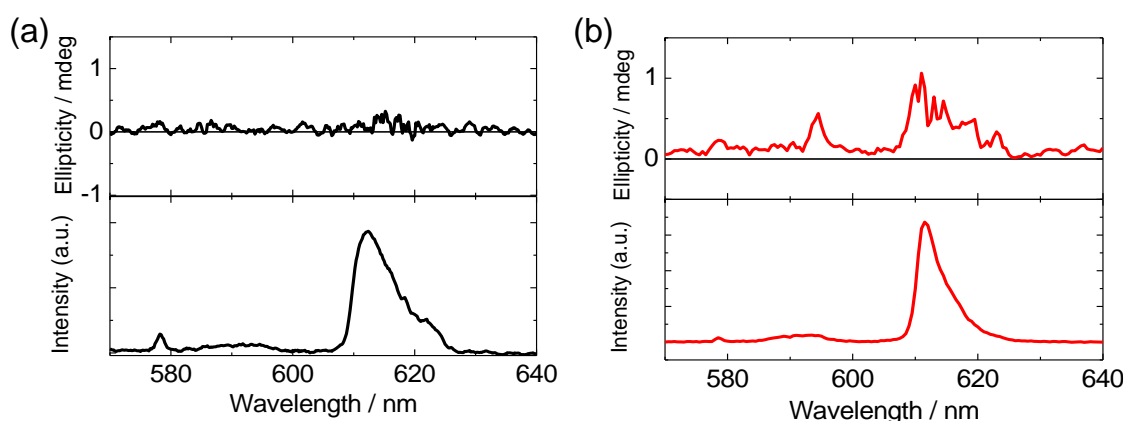
Figure 4-8. CPL spectra (top) and corresponding photoluminescence spectra (bottom) of (a) Eu(tta)$_3$(H$_2$O)$_2$ in the PMMA matrix and (b) Eu(tta)$_3$(H$_2$O)$_2$ in the DNA–CTMA matrix ([DNA–CTMA] : [Eu(tta)$_3$(H$_2$O)$_2$] = 5:1; i.e., 19 wt% of the Eu(III) complex).

4.4 Summary of Chapter 4

In this section, achiral Eu(III) complex (Eu(tta)$_3$(H$_2$O)$_2$) was associated with DNA-CTMA and their luminescent properties were investigated. When Eu(tta)$_3$(H$_2$O)$_2$ was incorporated in PMMA film which has no chiral structure, red emission with no luminescent dissymmetry was observed corresponding to the achiral Eu(tta)$_3$(H$_2$O)$_2$. When Eu(tta)$_3$(H$_2$O)$_2$ was associated with DNA-CTMA which have structural chirality assignable to the helical structure of DNA, induced CD signal was observed indicating the coordination structure of Eu(tta)$_3$(H$_2$O)$_2$ changed. As a result of association with DNA-CTMA, the emission intensity of Eu(tta)$_3$(H$_2$O)$_2$ was enhanced by ca. 3 times compared to in PMMA film. In addition, induced CPL was observed only from DNA-CTMA/ Eu(tta)$_3$(H$_2$O)$_2$ film. Like this, it was demonstrated that Eu(III) complex can exhibit CPL by associating with DNA corresponding the change in its coordination structure. Such induced CPL is suitable for the fields of chemical sensing, bio sensing, security systems etc.

However, the luminescent dissymmetry of DNA-CTMA/Eu(tta)$_3$(H$_2$O)$_2$ film was relatively low (less than 0.01) and its emission intensity was not strong even after the luminescence was enhanced. In order to develop DNA-based materials that express novel function to a practical level, it is indispensable to achieve both strong emission intensity and high circularly polarization of luminescence. To achieve these properties simultaneously, the Eu (III) complex having chiral ligands was introduced with the aim of increasing the change in coordination structure.

In next chapter, chiral Eu(III) complex (Eu(*D*-facam)$_3$) was associated with DNA toward the development of luminescent material indicate both strong emission and high luminescent dissymmetry.

References of Chapter 4

1. Richardson, F. S. Selection Rules for Lanthanide Optical Activity. *Inorg. Chem.* **1980**, *19* (9), 2806–2812. https://doi.org/10.1021/ic50211a063.

2. Eliseeva, S. V.; Bünzli, J. C. G. Lanthanide Luminescence for Functional Materials and Bio-Sciences. *Chem. Soc. Rev.* **2010**, *39* (1), 189–227. https://doi.org/10.1039/b905604c.

3. Grote, J. G.; Diggs, D. E.; Nelson, R. L.; Zetts, J. S.; Hopkins, F. K.; Ogata, N.; Hagen, J. A.; Heckman, E.; Yaney, P. P.; Stone, M. O.; Dalton, L. R. DNA Photonics [Deoxyribonucleic Acid]. *Mol. Cryst. Liq. Cryst.* **2005**, *426*, 3–17. https://doi.org/10.1080/15421400590890615.

4. Steckl, A. J. DNA – a New Material For. *Nat. Photonics* **2007**, *1* (1), 3–5. https://doi.org/10.1038/nphoton.2006.56.

5. Tanaka, K.; Okahata, Y. A DNA-Lipid Complex in Organic Media and Formation of an Aligned Cast Film. *J. Am. Chem. Soc.* **1996**, *118* (44), 10679–10683. https://doi.org/10.1021/ja9617855.

6. Liu, K.; Zheng, L.; Ma, C.; Göstl, R.; Herrmann, A. DNA-Surfactant Complexes: Self-Assembly Properties and Applications. *Chem. Soc. Rev.* **2017**, *46* (16), 5147–5172. https://doi.org/10.1039/c7cs00165g.

7. Kawabe, Y.; Wang, L.; Horinouchi, S.; Ogata, N. Amplified Spontaneous Emission from Fluorescent-Dye-Doped DNA-Surfactant Complex Films. *Adv. Mater.* **2000**, *12* (17), 1281–1283. https://doi.org/10.1002/1521-4095(200009)12:17<1281::AID-ADMA1281>3.0.CO;2-0.

8. Suzuki, T.; Kawabe, Y. Light Amplification in DNA-Surfactant Complex Films Stained by Hemicyanine Dye with Immersion Method. *Opt. Mater. Express* **2014**, *4* (7), 1411. https://doi.org/10.1364/ome.4.001411.

9. Mysliwiec, J.; Sznitko, L.; Sobolewska, A.; Bartkiewicz, S.; Miniewicz, A. Lasing Effect in a Hybrid Dye-Doped Biopolymer and Photochromic Polymer System. *Appl. Phys. Lett.* **2010**, *96* (14), 94–97. https://doi.org/10.1063/1.3377912.

10. Massin, J.; Parola, S.; Andraud, C.; Kajzar, F.; Rau, I. Enhanced Fluorescence of Isophorone Derivatives in DNA Based Materials. *Opt. Mater. (Amst).* **2013**, *35* (10), 1810–1816. https://doi.org/10.1016/j.optmat.2013.04.021.

11. Hagen, J. A.; Li, W.; Steckl, A. J.; Grote, J. G. Enhanced Emission Efficiency in Organic Light-Emitting Diodes Using Deoxyribonucleic Acid Complex as an Electron Blocking Layer. *Appl. Phys. Lett.* **2006**, *88* (17), 1–4. https://doi.org/10.1063/1.2197973.

12. Kobayashi, N.; Uemura, S.; Kusabuka, K.; Nakahira, T.; Takahashi, H. An Organic Red-Emitting Diode with a Water-Soluble DNA–Polyaniline Complex Containing Ru(Bpy)$_3^{2+}$. *J. Mater. Chem.* **2001**, *11* (7), 1766–1768. https://doi.org/10.1039/b102882k.

13. Nakamura, K.; Ishikawa, T.; Nishioka, D.; Ushikubo, T.; Kobayashi, N. Color-Tunable Multilayer Organic Light Emitting Diode Composed of DNA Complex and Tris(8-

Hydroxyquinolinato)Aluminum. *Appl. Phys. Lett.* **2010**, *97* (19), 2008–2011. https://doi.org/10.1063/1.3512861.

14. Steckl, A. J.; Spaeth, H.; You, H.; Gomez, E.; Grote, J. DNA as an Optical Material. *Opt. Photonics News* **2011**, *22* (7), 34. https://doi.org/10.1364/opn.22.7.000034.

15. Yumusak, C.; Singh, T. B.; Sariciftci, N. S.; Grote, J. G. Bio-Organic Field Effect Transistors Based on Crosslinked Deoxyribonucleic Acid (DNA) Gate Dielectric. *Appl. Phys. Lett.* **2009**, *95* (26). https://doi.org/10.1063/1.3278592.

16. Yukimoto, T.; Uemura, S.; Kamata, T.; Nakamura, K.; Kobayashi, N. Non-Volatile Transistor Memory Fabricated Using DNA and Eliminating Influence of Mobile Ions on Electric Properties. *J. Mater. Chem.* **2011**, *21* (39), 15575. https://doi.org/10.1039/c1jm12229k.

17. Tsumatori, H.; Nakashima, T.; Kawai, T. Observation of Chiral Aggregate Growth of Perylene Derivative in Opaque Solution by Circularly Polarized Luminescence. *Org. Lett.* **2010**, *12* (10), 2362–2365. https://doi.org/10.1021/ol100701w.

18. Aslanoglu, M. Electrochemical and Spectroscopic Studies of the Interaction of Proflavine with DNA. *Anal. Sci.* **2006**, *22* (3), 439–443. https://doi.org/10.2116/analsci.22.439.

19. Annaraj, J.; Srinivasan, S.; Ponvel, K. M.; Athappan, P. R. Mixed Ligand Copper(II) Complexes of Phenanthroline/Bipyridyl and Curcumin Diketimines as DNA Intercalators and Their Electrochemical Behavior under Nafion® and Clay Modified Electrodes. *J. Inorg. Biochem.* **2005**, *99* (3), 669–676. https://doi.org/10.1016/j.jinorgbio.2004.11.018.

20. Olmsted, J.; Kearns, D. R. Mechanism of Ethidium Bromide Fluorescence Enhancement on Binding to Nucleic Acids. *Biochemistry* **1977**, *16* (16), 3647–3654. https://doi.org/10.1021/bi00635a022.

21. Lepecq, J. B.; Paoletti, C. A Fluorescent Complex between Ethidium Bromide and Nucleic Acids. Physical-Chemical Characterization. *J. Mol. Biol.* **1967**, *27* (1), 87–106. https://doi.org/10.1016/0022-2836(67)90353-1.

22. Pyle, A. M.; Rehmann, J. P.; Meshoyrer, R.; Turro, N. J.; Barton, J. K.; Kumar, C. V. Mixed-Ligand Complexes of Ruthenium(II): Factors Governing Binding to DNA. *J. Am. Chem. Soc.* **1989**, *111* (8), 3051–3058. https://doi.org/10.1021/ja00190a046.

23. Nakamura, K.; Hasegawa, Y.; Kawai, H.; Yasuda, N.; Kanehisa, N.; Kai, Y.; Nagamura, T.; Yanagida, S.; Wada, Y. Enhanced Lasing Properties of Dissymmetric Eu(III) Complex with Bidentate Phosphine Ligands. *J. Phys. Chem. A* **2007**, *111* (16), 3029–3037. https://doi.org/10.1021/jp067672h.

Chapter 5

Dramatic Enhancement of Both Emission Intensity and Circularly Polarization of Luminescence by Introduction of Chiral Ligand Into the DNA-CTMA/Eu(III) Complex

Dramatic Enhancement of Both Emission Intensity and Circularly Polarization of Luminescence by Introduction of Chiral Ligand Into the DNA-CTMA/Eu(III) Complex

In the previous chaper, instead of the Ru(II) complex, which does not easily express CPL due to a high electronic transition moment (μ), an Eu(III) complex that emits light with a small μ due to its f-f transition was introduced.   DNA-CTMA/Eu(tta)$_3$(H$_2$O)$_2$ film expressed induced CPL due to structural change of coordination structure around Eu(III) ion caused by interaction with DNA, whereas PMMA/Eu(tta)$_3$(H$_2$O)$_2$ did not show significant CPL signal.   However, the luminescent dissymmetry of DNA-CTMA/Eu(tta)$_3$(H$_2$O)$_2$ film was relatively low (less than 0.01) and its emission intensity was not strong as practical level.   In this section, Eu(III) complex having chiral ligands (Eu(D-facam)$_3$)[1,2] was adopted to induce more efficient change in coordination structure around Eu(III) ion upon the interaction with DNA.   Interestingly, higher luminescence intensity and higher $|g_{lum}|$ of CPL from the Eu(D-facam)$_3$ compared with the conventional polymer were achieved upon the interaction with DNA.

5.1 Effect of alkyl ammonium salts on the luminescent properties of Eu(D-facam)$_3$

In Chapter 4, luminescence enhancement and induced CPL were observed by associating the achiral Eu(III) complex with DNA-CTMA.   It was concluded that this improved luminescence was due to the immobilization and structural changes of the Eu(III) complex upon the interaction with DNA.   On the other hand, it has been reported that the Eu(III) complexes changes its luminescence properties with also respect to additives such as ions.   Therefore, first, in order to independently examine the effects of DNA and its surfactant CTMA on luminescence, the effects of additives were examined for Eu(tta)$_3$(H$_2$O)$_2$ used in the previous section and Eu(D-facam)$_3$.

As mentioned before, since DNA is soluble only in water whereas Eu(III) complexes are not soluble in water, it is difficult to investigate the influence of natural DNA on the luminescence of Eu(III) complexes.   The effect of additives were investigated by mixing Eu(III) complexes and additives in 1-butanol.   If the Eu(III) complexes shows different luminescence changes respect to each additives, it will be applied not only as a simple luminescent material but also as a chemical sensors.

5.1.1 Emission properties of Eu(III) complexes in the presence of additives

First, changes in the luminescent properties of the Eu(III) complexes in the presence of CTMA were investigated. Figure 5-1 shows emission spectra of (a) Eu(tta)$_3$(H$_2$O)$_2$ and (b) Eu(*D*-facam)$_3$ in 1-butanol solution with various concentration of CTMA. In the case of Eu(tta)$_3$(H$_2$O)$_2$, significant change in intensities and shapes of spectra were not observed, indicating the improvement of luminescent properties of Eu(tta)$_3$(H$_2$O)$_2$ upon the interaction with DNA-CTMA (described in Chapter 4) was attributed to DNA, not CTMA. In contrast, in the case of Eu(*D*-facam)$_3$, the intensities and shapes of spectra obviously changed upon the addition of CTMA. Therefore, the effects of various additives on the luminescence of Eu(*D*-facam)$_3$ were investigated before constructing a novel photo-functional material by combining DNA-CTMA and Eu(*D*-facam)$_3$.
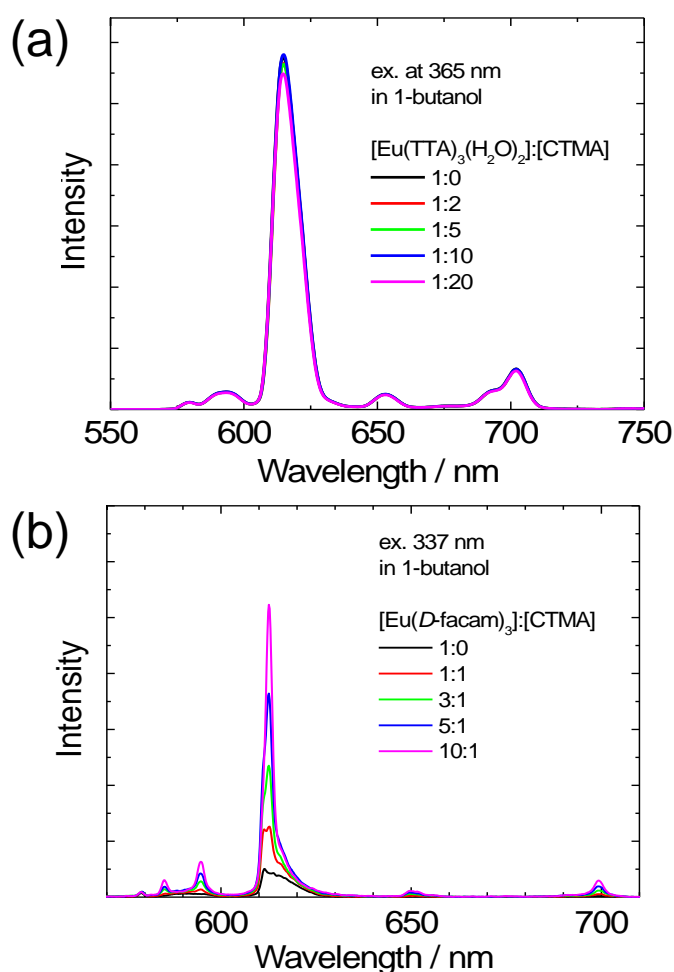
Figure 5-1. Emission spectra of (a) Eu(tta)$_3$(H$_2$O)$_2$ and (b) Eu(*D*-facam)$_3$ in 1-butanol solution with various concentration of CTMA.

To reveal which part of CTMA influenced to the emission properties of Eu(*D*-facam)$_3$, the luminescence change of the Eu(*D*-facam)$_3$ was investigated when cetyl alcohol, which is the main hydrophobic part of CTMA, and tetramethylammonium chloride, which is the cation site, were added to the solution. Obvious change in emission intensity was not observed when cetyl alcohol was added to the Eu(*D*-facam)$_3$ solution (red plots). On the other hand, dramatic emission enhancement was observed upon the addition of tetramethylammonium chloride (blue plots). Therefore, it is assumed that the improvement of luminescence of Eu(*D*-facam)$_3$ by CTMA was mainly attributed to the alkylammonium site in the CTMA.
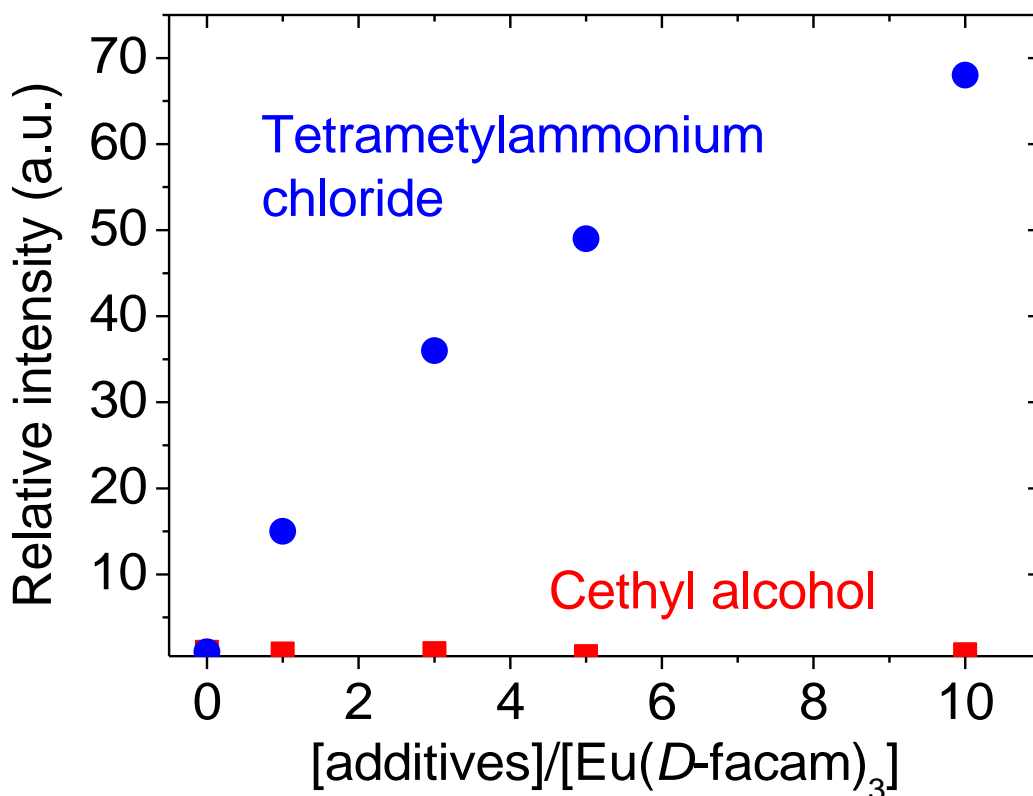
Figure 5-2. Change in emission intensity of Eu(*D*-facam)$_3$ at 613 nm ($^5D_0 \rightarrow ^7F_2$) by addition of tetramethylammonium (blue plots) and cethylalcohol (red plots).

5.1.2 Investigation of emission properties of Eu(*D*-facam)$_3$ with alkylammonium ions in 1-butanol

It was revealed that addition of tetramethylammonium chloride can improve the emission properties of Eu(*D*-facam)$_3$. Thus, the influence of addition of various alkylammonium salts on the emission properties of Eu(*D*-facam)$_3$ were investigated in 1-butanol.

Reagents

All the chemicals were commercially available and used as received. Europium tris[3-(trifluoromethylhydroxymethylene)-(+)-camphorate] (Eu(*D*-facam)$_3$) was purchased from Sigma-Aldrich, Japan. Ammonium salts [tetramethylammonium chloride (TBACl), tetraethylammonium chloride (TEACl), tetrabutylammonium chloride (TBACl), and tetrapropylammonium chloride (TPACl)] were purchased from Tokyo Chemical Industry Co. Ltd., Japan. 1-Butanol and 1-butanol-d_1 were purchased from Tokyo Chemical Industry Co. Ltd., Japan and used as the solvent.

Preparation of Eu(*D*-facam)$_3$/alkylammonium solutions

Eu(*D*-facam)$_3$/alkylammonium solutions were prepared by mixing Eu(*D*-facam)$_3$ and each alkylammonium salt (TMACl, TEACl, TBACl, and TPACl) in 1-butanol or 1-butanol-d_1. The molar ratios of Eu(*D*-facam)$_3$ and alkylammonium salts ([Eu(*D*-facam)$_3$]:[alkylammonium salt]) were 1:0, 1:1, 1:3, 1:5, and 1:10. The concentration of Eu(*D*-facam)$_3$ was fixed at 0.1 mmol/L.

Measurements of optical properties

Oxygen in the Eu(D-facam)$_3$/alkylammonium solutions were removed by bubbling nitrogen gas before optical measurements. Absorbance and CD spectra of Eu(D-facam)$_3$/TMACl were acquired using a photonic multichannel analyzer (J-1100, JASCO Corporation, Japan). Electrospray ionization-mass spectrometry (ESI-MS) spectra were recorded using Exactive (Thermo Fisher Scientific, United States). FT-IR spectra of Eu(D-facam)$_3$/TMACl were acquired using an FTIR 680 spectrophotometer, JASCO Corporation, Japan. Photoluminescence spectra were acquired using a spectrofluorometer (FP-6600, JASCO Corporation, Japan). Emission quantum yields were calculated from the data obtained from an absolute PL quantum yield spectrometer (Quantaurus-QY C11347-01, Hamamatsu photonics K. K., Japan). The emission lifetimes were determined using a time-resolved fluorescence spectrometer (Quantaurus-Tau C11367-21, Hamamatsu photonics K. K., Japan). CPL measurements were conducted using the previously reported system.[3] This system consists of the following components: 375 nm LED (M365L2, Thorlabs Japan Inc., Japan), LED driver (DC2100, Thorlabs Japan Inc., Japan), photoelastic modulator (PEM-90, Hinds instruments, Inc. United States), photomultiplier tube (H7732-10, Hamamatsu photonics K. K., Japan), linearly polarized cubic prism (200,000:1), photomultiplier tube (H7732-10, Hamamatsu photonics K. K., Japan), and dual phase DSP lock-in amplifier (7265, Signal Recovery Ltd., United Kingdom). The appropriate detection wavelength of the monochromator and the PEM was controlled by a PC.

5.1.3 Drastic emission enhancement of Eu(D-facam)$_3$ with short alkylammonium salts

Emission change of Eu(D-facam)$_3$ upon the addition of tetramethylammonium salt
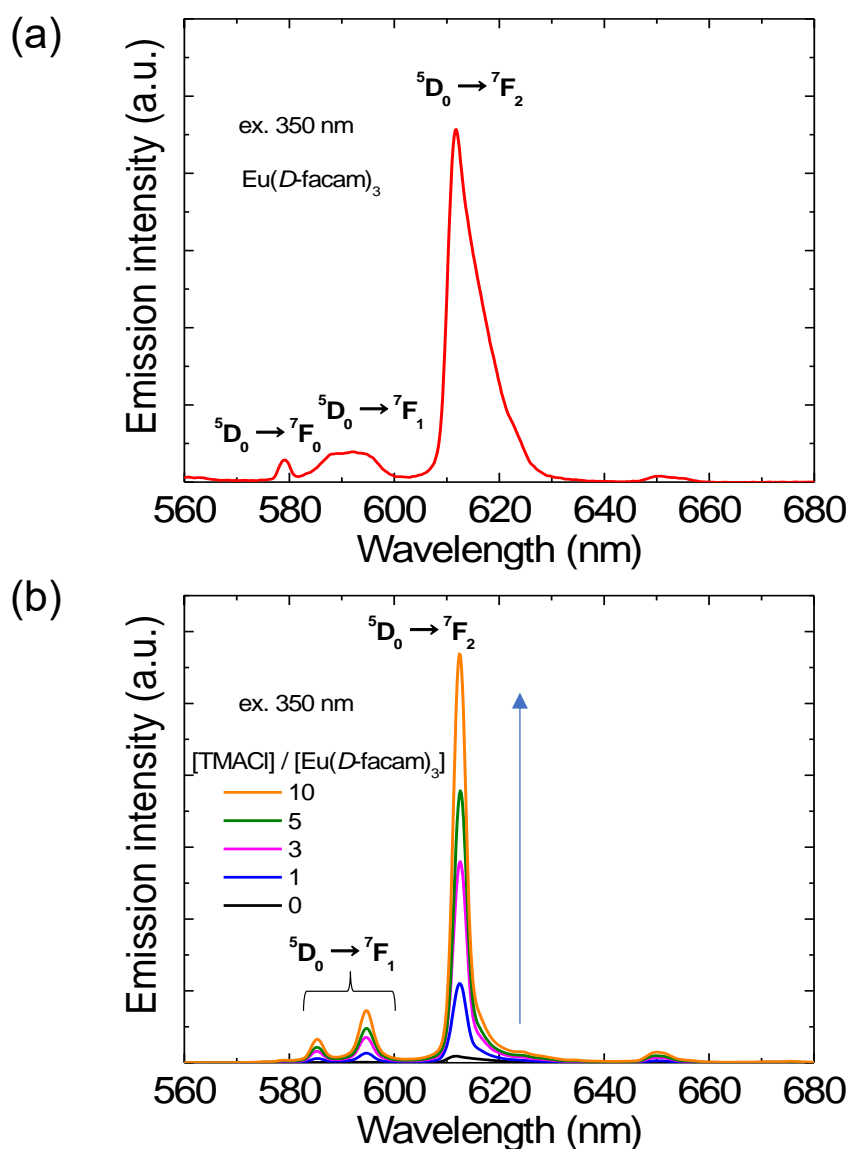
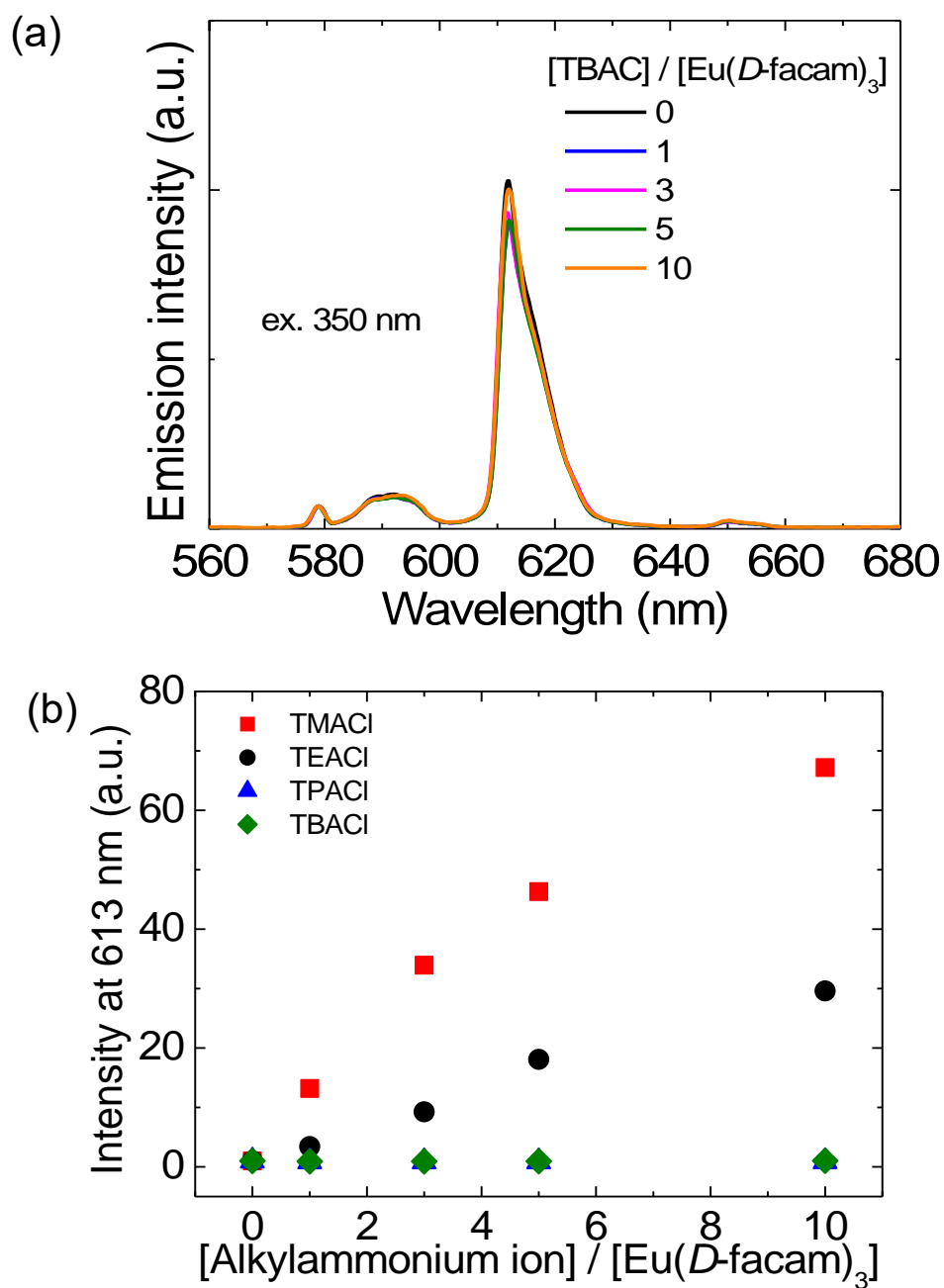**Figure 5-3.** (a) Emission spectrum of Eu(D-facam)$_3$ in 1-butanol.　(b) Emission spectra of Eu(D-facam)$_3$/TMACl solutions at various [Eu(D-facam)$_3$]:[TMACl] ratios upon excitation at 350 nm.　Concentration of Eu(D-facam)$_3$ was fixed at 0.2 mmol/L. Excitation wavelength was 350 nm.

First, the effect of TMACl, which has four methyl groups, on the luminescent properties of europium tris[3-(trifluoromethylhydroxymethylene)-(+)-camphorate] (Eu(D-facam)$_3$) was investigated. The emission spectra of Eu(D-facam)$_3$ in the presence of various concentrations of TMACl (i.e., at different Eu(D-facam)$_3$/TMACl concentration ratios) were acquired (Figure 5-3). In the absence of TMACl, the emission spectrum of Eu(D-facam)$_3$ had sharp peaks at 579, 590, and 613 nm corresponding to the $^5D_0 \rightarrow {}^7F_0$, $^5D_0 \rightarrow {}^7F_1$, and $^5D_0 \rightarrow {}^7F_2$ transitions, respectively, in Eu(III).[4] The emission intensity increased with increasing concentrations of TMACl. In addition, the emission peak corresponding to the $^5D_0 \rightarrow {}^7F_1$ transition split into two peaks (585 nm and 595 nm), indicating that TMACl significantly affected the crystal field of around Eu(III) ion.

When [Eu(D-facam)$_3$]:[TMACl] = 1:10, the emission intensity at 613 nm corresponding to the $^5D_0 \rightarrow {}^7F_2$ transition was ~70 times higher compared to the emission intensity of Eu(D-facam)$_3$ alone. This indicates the existence of interactions between Eu(D-facam)$_3$ and TMACl.

Influence of various alkylammonium ions

To verify if the emission enhancement of Eu(D-facam)$_3$ depends on the alkyl chain length of the ammonium salt, emission spectra of Eu(D-facam)$_3$ were acquired in the presence of ammonium salts with different alkyl chain lengths (Figure 5-4). No remarkable increase in the emission intensity was observed when TPACl or TBACl was added to the Eu(D-facam)$_3$ solution. Interestingly, the emission intensity increased with increasing concentrations of alkyl ammonium salts with shorter chain lengths, i.e., TEACl and TMACl. At a molar concentration ratio of [Eu(D-facam)$_3$]:[alkylammonium salt] = 1:10, a 30-fold and 70-fold enhancement in the emission intensity at 613 nm were observed for Eu(D-facam)$_3$/TEACl and Eu(D-facam)$_3$/TMACl, respectively, compared to the emission intensity of Eu(D-facam)$_3$ alone. Thus, the extent of enhancement of the Eu(D-facam)$_3$ emission intensity was significantly affected by the alkyl chain length in the ammonium salts.

Figure 5-4. (a) Emission spectra of Eu(*D*-facam)₃/TBACl solutions at various [Eu(*D*-facam)₃]:[TBACl] ratios. (b) Change in the emission intensity of Eu(*D*-facam)₃ at 613 nm with increasing concentrations of various alkylammonium salts.

5.1.4 Structural change of Eu(*D*-facam)₃ upon the interaction with tetramethylammonium

Symmetry of Eu(*D*-facam)₃ in the presence of TMACl

In the lanthanoid complex such as Eu(*D*-facam)₃, it is known that the emission peak near 595 nm caused by $^5D_0 \rightarrow ^7F_1$ is derived from a magnetic dipole (MD) moment, and its intensity is not easily affected by the ligand field.   On the other hand, the emission peak near 612 nm caused by $^5D_0 \rightarrow ^7F_2$ is derived from the electric dipole (ED) moment, and its intensity changes greatly under the influence of the ligand field.   Therefore, the symmetric property of Eu(*D*-facam)₃ can be estimated from the ratio of emission intensity derived from MD moment (I_{MD}) and ED moment (I_{ED}).[5]   Figure 5-5 shows the change in the emission ratio ($I_{rel} = I_{ED}/I_{MD}$) with increasing TMACl or TBACl concentration. Since the value of I_{rel} decreased with increasing TMACl concentration, it was indicated that the coordination structure around Eu(III) ion in Eu(*D*-facam)₃ was changed to be higher symmetry by addition of TMACl.   Thus, the change of symmetry around Eu(III) ion given by I_{rel} value clearly suggested that Eu(*D*-facam)₃ and TMACl interact each other, lead to great emission enhancement as shown in Figure 5-3.   Whereas, addition of TBACl did not change the emission intensity and I_{rel} value of Eu(*D*-facam)₃, indicating there is no significant interaction between these compounds.
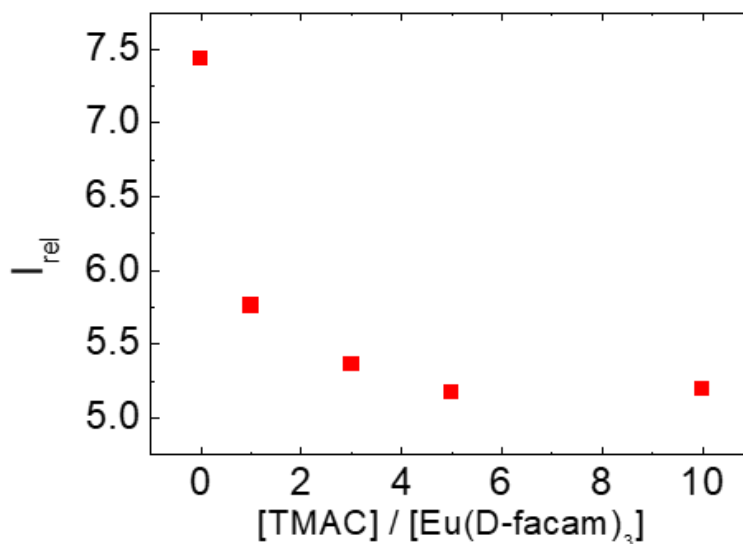
Figure 5-5. Change in I_{rel} (= I_{MD}/I_{ED}) of Eu(*D*-facam)₃/TMACl solution with increasing TMACl concentration.

Change in absorption and circular dichroism

Then, structural information of the Eu(*D*-facam)₃/TMACl and Eu(*D*-facam)₃/TBACl solutions were investigated. Figure 5-6 shows absorption and circular dichroism (CD) spectra of Eu(*D*-facam)₃/TMACl and Eu(*D*-facam)₃/TBACl solutions. These solutions showed absorption band at around 310 nm due to π-π* transition of the *D*-facam ligands.[6] There was no significant change in absorption of the ligand in both solutions by addition of TMACl or TBACl. For CD spectra, although there is no obvious change in the CD signal corresponding to the ligand absorption by addition of TBACl, peak of the CD signal changed to be longer wavelength with increasing in TMACl concentration. This result suggests the structural change of Eu(*D*-facam)₃ in the presence of TMACl.
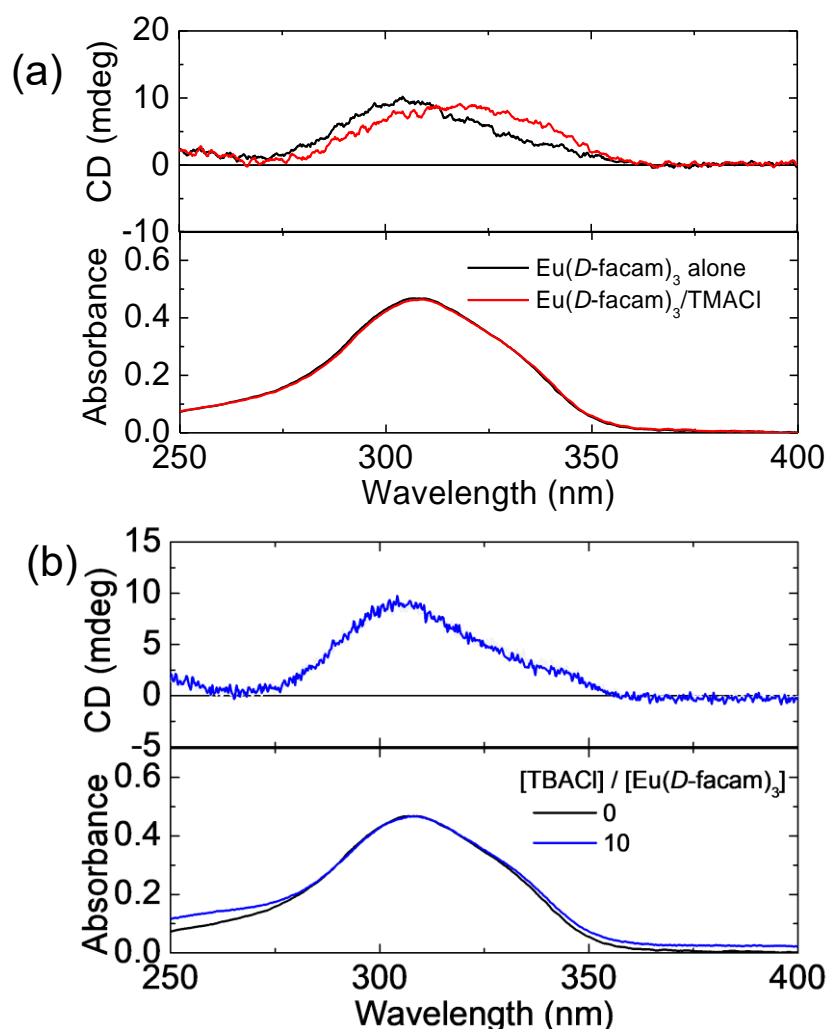
Figure 5-6. Absorbance (bottom) and CD (top) spectra of Eu(*D*-facam)₃/TMACl (a) and Eu(*D*-facam)₃/TBACl (b) solutions. The concentration of Eu(*D*-facam)₃ was fixed 0.1 mmol/L. Length of light path was set to 1 mm.

Change in the vibrational structure

In the FT-IR spectrum of Eu(*D*-facam)₃, two peaks due to stretching vibration of conjugated bonds (C=C=C) in *β*-diketonate was observed at 1500-1600 cm⁻¹ (Figure 5-7).[7]   These peaks turned into one broad peak around 1500 cm⁻¹ by addition of TMACl. Thus, it can be considered that the length and/or angle of these bonds were changed in the presence of TMACl.
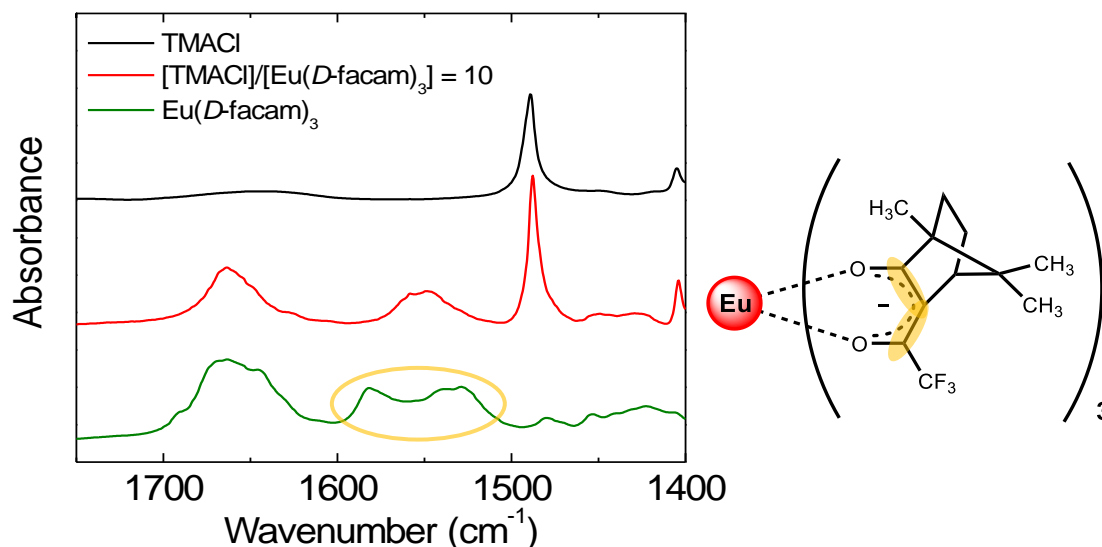
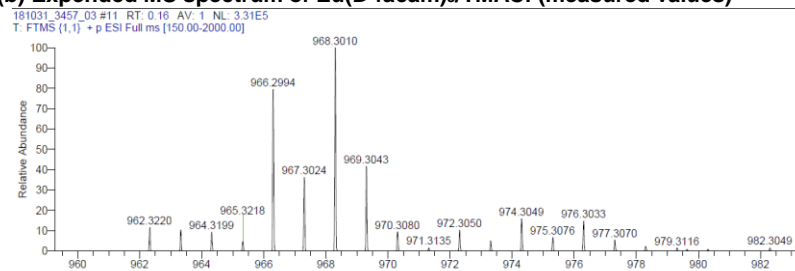**Figure 5-7.** FT-IR spectra of Eu(*D*-facam)₃ and TMACl and Eu(*D*-facam)₃/TMACl.

ESI-MS analysis

In order to reveal association of Eu(*D*-facam)₃ and alkyl ammonium ions, SPI-MS measurements were carried out (Figure 5-8~5-10).   In case of Eu(*D*-facam)₃/TMACl solution, m/z peaks corresponding to [Eu(*D*-facam)₃·TMA]⁺ and [Eu(*D*-facam)₃·2TMA·Cl]⁺ were observed.   This result suggested that Eu(*D*-facam)₃ and TMA⁺ formed associated structure in 1-butanol solutions as indicated by CD measurement.   On the other hands, any m/z peaks due to association of Eu(*D*-facam)₃ and TBA⁺ was not observed in Eu(*D*-facam)₃/TBACl solution.   Thus, no significant change of absorption, CD and luminescent spectra of Eu(*D*-facam)₃/TBACl solution discussed above was supported by the MS measurement.   Therefore, it could be thought that Eu(*D*-facam)₃ interacts with TMA⁺ and leads to change the coordination structure and symmetry of Eu(*D*-facam)₃.   From these results, Eu(*D*-facam)₃ and TMACl having shorter alkyl chain can interact each other to change symmetrical structure of Eu(III) ion, leading to remarkable emission enhancement over 70 times larger.
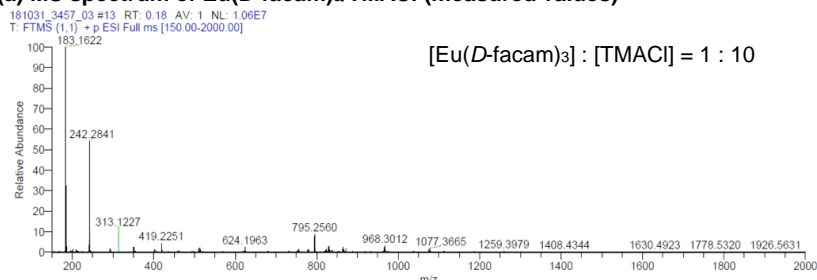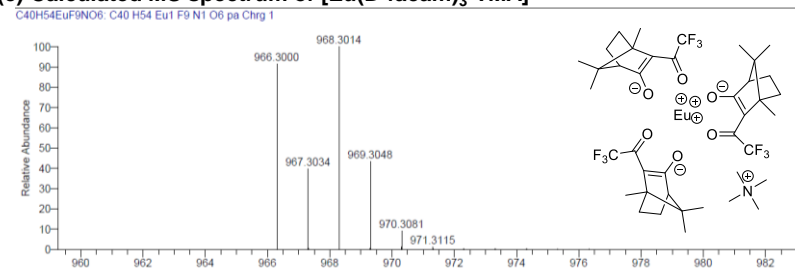
Figure 5-8. MS spectra of Eu(*D*-facam)₃/TMACl (a, b, d) and calculated MS spectrum of [Eu(D-facam)₃·TMA]⁺ (c) and [Eu(D-facam)₃·2TMA·Cl]⁺ (e).

85

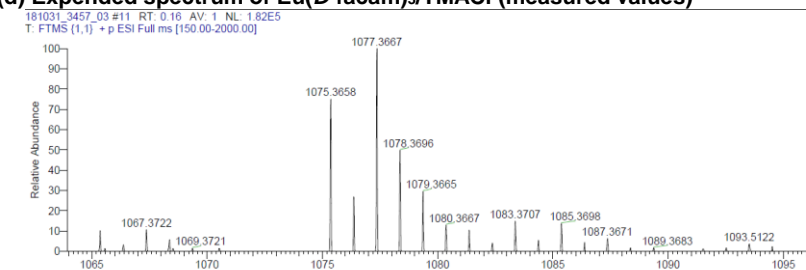**(a) Expended MS spectrum of Eu(*D*-facam)₃/TBACl (measured values)**

(b) Calculated MS spectrum of [Eu(*D*-facam)₃·Cl]⁻
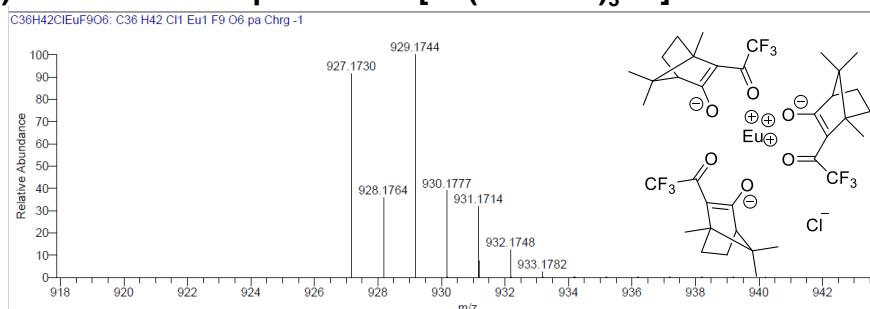
(c) Expended MS spectrum of Eu(*D*-facam)₃/TBACl (measured values)

(d) Calculated MS spectrum of [Eu(*D*-facam)₄]⁻

Figure 5-9. MS spectra of Eu(*D*-facam)₃/TBACl (a, c) and calculated MS spectrum of Eu(*D*-facam)₃·Cl]⁻ (b) and [Eu(*D*-facam)₄]⁻ (d).

(a) Expended MS spectrum of Eu(*D*-facam)₃/TBACl (measured values)
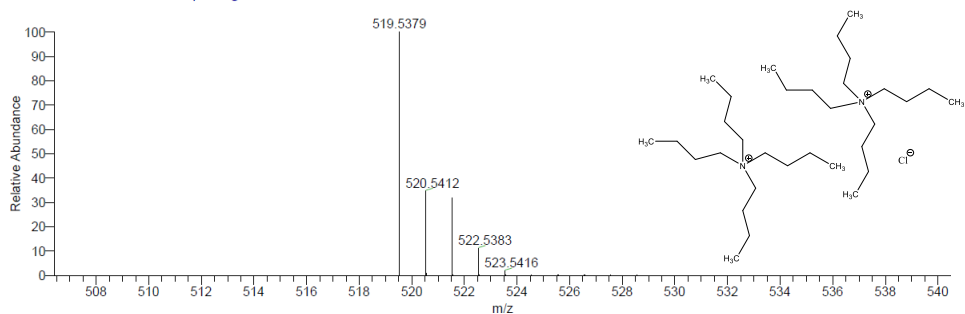
(b) Calculated MS spectrum of [2TBA·Cl] ⁺

(c) Expended MS spectrum of Eu(*D*-facam)₃/TBACl (measured values)

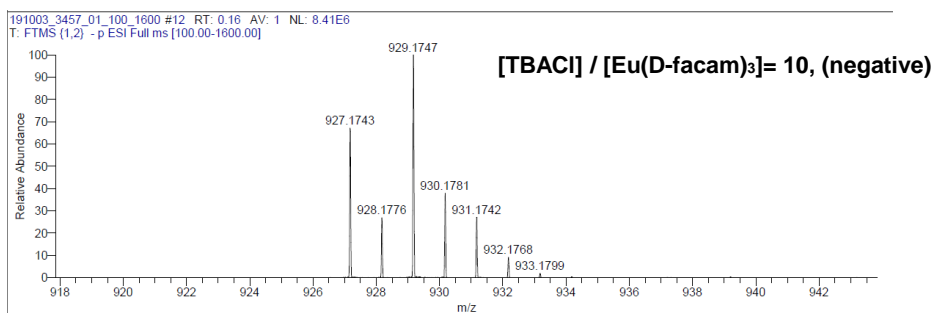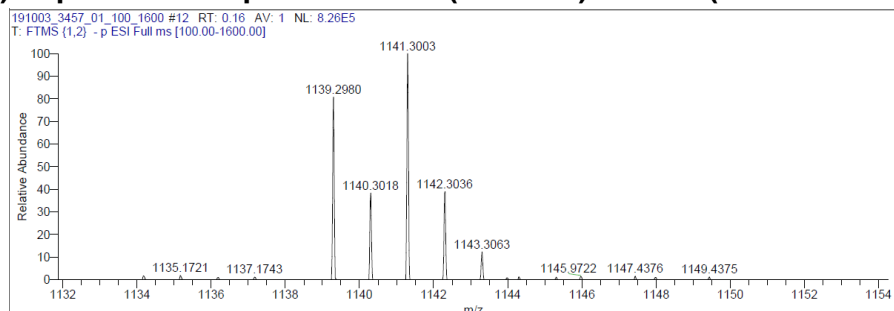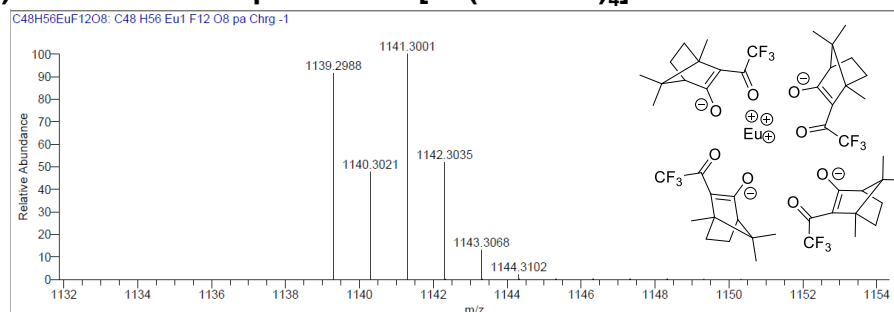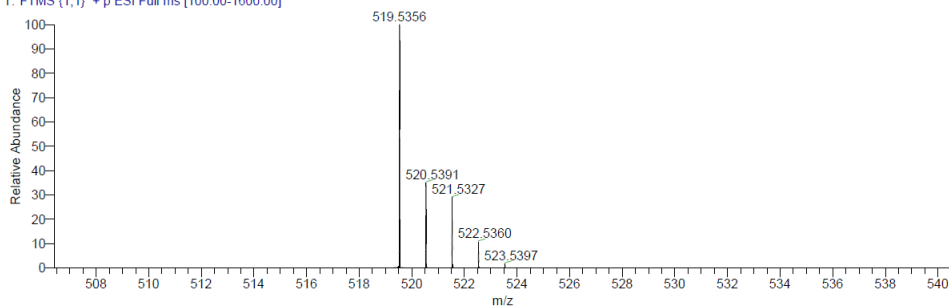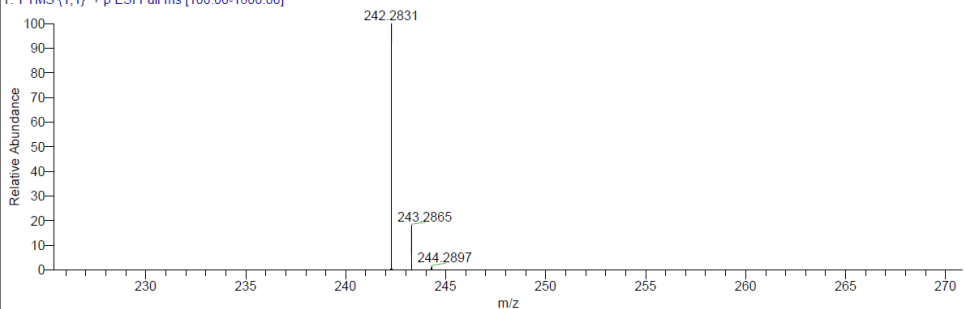**(d) Calculated MS spectrum of [TBA]⁺**
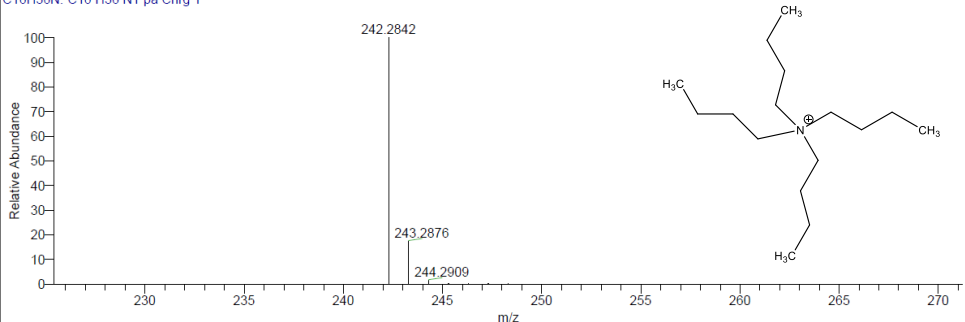
Figure 5-10. MS spectra of Eu(*D*-facam)₃/TBACl (a, c) and calculated MS spectrum of [2TBA·Cl]⁺ (b) and [TBA]⁺ (d).

87

Influence of -OH vibrational quenching

In general, it is known that Eu(III) ion with high symmetrical structure hardly show strong emission because the high symmetry of Eu(III) ion leads to smaller radiative rate.[8]　Thus, this great enhancement of emission of the Eu(D-facam)$_3$ with higher symmetry evident from various photophysical analyses seems to contradict to general phenomena on the Eu(III) complexes.
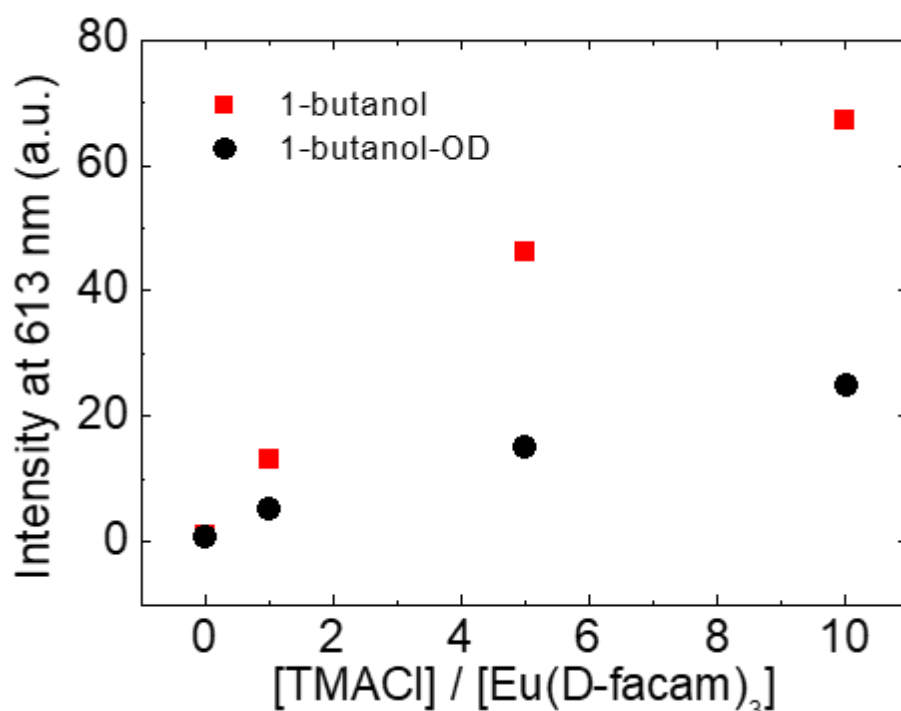
Figure 5-11. Change in emission intensity (613 nm) of Eu(D-facam)$_3$ upon the addition of TMACl in 1-butanol or 1-butanol-d_1. The intensities of Eu(D-facam)$_3$ alone in 1-butanol and 1-butanol-d_1 were normalized to 1.

In order to clarify the mechanism of the emission enhancement, vibrational quenching of excited states of the Eu(D-facam)$_3$ was focused.[9]　Influence of the vibrational quenching due to -OH groups in 1-butanol used as a solvent was investigated by comparing change in emission intensity of Eu(D-facam)$_3$ by addition of TMACl in 1-butanol with that in 1-butanol-d_1.　Figure 5-11 shows the changes in emission intensity of Eu(D-facam)$_3$ in 1-butanol and 1-butanol-d_1 by addition of TMACl.　The intensity of Eu(D-facam)$_3$-singly dissolved solution in 1-butanol and 1-butanol-d_1 were normalized to be 1 respectively. It was revealed that the degree of emission enhancement of Eu(D-facam)$_3$ caused by

88

addition of TMACl in 1-butanol was greater than that in 1-butanol-d_1.   The enhancement degree when the [Eu(D-facam)$_3$]:[TMACl] = 1:10 concentration ratio were 70 times in 1-butanol and 25 times in 1-butanol-d_1 comparing to the Eu(D-facam)$_3$ singly dissolved solutions.   The emission enhancement by TMACl was greater in 1-butanol containing -OH group than that in 1-butanol-d_1 without -OH group.   This result indicates that the interaction with TMACl suppresses quenching emission of Eu(D-facam)$_3$ due to vibrational deactivation of -OH groups.   However, since 25 times emission enhancement of Eu(D-facam)$_3$ by TMACl was observed in 1-butanol-d_1, it would be sufficiently considered to have effects of suppressing molecular vibrations, vibrational excitation of matrices and reverse energy transfer from Eu(III) ion to ligands besides suppression of quenching by -OH group.   Therefore, it was aimed to elucidate the factors that contribute to the emission enhancement of Eu(D-facam)$_3$.

Calculation of photophysical parameters

  To elucidate the factors that contribute to the emission enhancement of Eu(D-facam)$_3$, total quantum yields (Φ_{tot}) and luminescence lifetimes (τ) of Eu(D-facam)$_3$/TMACl solutions with various concentration ratio were measured.   The emission decay curves are shown in Figure 5-12.   In solution of Eu(D-facam)$_3$ alone, two components of emission lifetime were observed.   The shorter component was ca. 30 μs (70 %) and longer one was ca. 220 μs (30 %) for the Eu(D-facam)$_3$ alone solution.   The existence of multi components in the Eu(D-facam)$_3$ alone solution suggested presence of different states of the complex.   For example, number of coordinated waters may affect emission lifetime of complexes.   By addition of TMACl, the shorter lifetime component disappeared and decay curves of almost single component with life time of ~250 μs were observed.   This result indicated that interaction between TMACl and Eu(D-facam)$_3$ eliminated lower emissive state (shorter lifetime state) of Eu(D-facam)$_3$.   Also, radiative rates of Eu(III) ions (k_r) were calculated by using:

$$k_r = A_{MD,0} \times n^3 \times \left(\frac{I_{tot}}{I_{MD}}\right)$$

where $A_{MD,0}$ is the spontaneous emission coefficient of $^5D_0 \rightarrow {}^7F_1$ (=14.65 sec^{-1}), n is the refractive index of the medium (= 1.399 in 1-buthanol) and I_{tot}/I_{MD} is the ratio of the integrated total radiation from the $^5D_0 \rightarrow {}^7F_j$ (j = 0-6) to the area of the $^5D_0 \rightarrow {}^7F_1$ transition.[5,10]   Averaged lifetime was adopted to calculate photophysical parameters of Eu(D-facam)$_3$ alone solution.   The non-radiative rate (k_{nr}) can be calculated from:

$$\tau = \frac{1}{k_r + k_{nr}} \quad , \quad k_{nr} = \frac{1}{\tau} - k_r$$

and the intrinsic quantum yield (Φ_{Ln}) and the efficiency of the sensitization of the lanthanide luminescence by the ligand (η_{sens}) can be calculated from the relation[11]:

$$\Phi_{Ln} = \frac{k_r}{k_r + k_{nr}} \quad , \quad \eta_{sens} = \frac{\Phi_{tot}}{\Phi_{Ln}}$$

These photo-physical parameters are showed in Table 1.   It was revealed that k_r decrease from 329 s^{-1} to 263 s^{-1} with increasing the concentration of TMACl.   In other words, the light emission probability from the excited state decreases with the addition of TMACl, which is consistent with structural change around Eu(III) ion to higher symmetry as discussed above.   On the other hands, decreasing of the k_{nr} and improvement of the η_{sens} were observed with increasing in TMACl concentration.   The k_{nr} value without TMACl was found to be ca. 10000 s^{-1}, whereas, the k_{nr} decreased to be 3800 s^{-1} by addition of TMACl.   This decrease of k_{nr} clearly indicates suppression of vibrational deactivation of excited states of Eu(III) ion.   From the comparison of solvent dependence (1-butanol and 1-butanol-d_1), the vibrational quenching was mainly caused by -OH groups.   This decrease of k_{nr} contributes to improve of the intrinsic quantum yield (Φ_{Ln}); the calculated Φ_{Ln} increased ca. 2.1 times by addition of TMACl (from 3.15 % to 6.54 %).   Here, it should be noted that the increase of η_{sens} by interaction with TMACl was greatly large, more than 30 times compared to the original.   It is considered that such significant improvement of η_{sens} mainly contributes to the 70 times emission enhancement of the Eu(D-facam)$_3$ as shown in Figure 5-3.
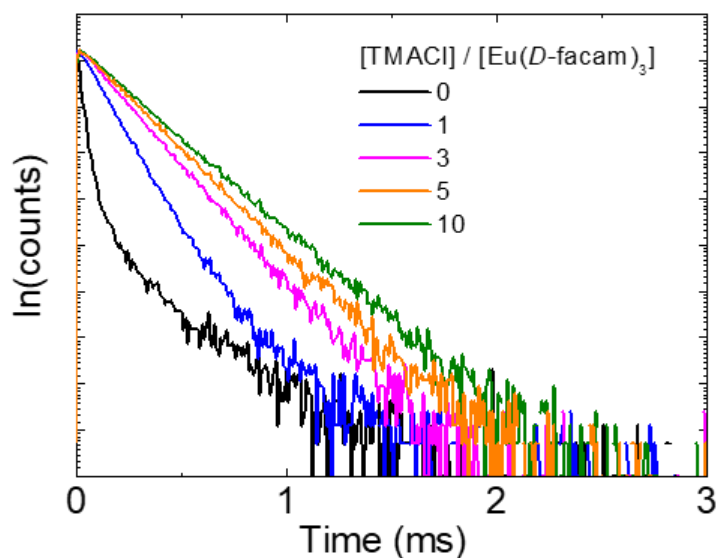
Figure 5-12. Emission decay curves of Eu(D-facam)$_3$/TMACl solutions with various concentration ratio. Excitation wavelength was 405 nm and emission were detected at 613 nm.

**Table 5-1** Luminescence lifetimes (τ), intrinsic quantum yields of Eu(III) ion (Φ_{Ln}), total quantum yields (Φ_{tot}), efficiencies of sensitization (η_{sens}), radiative rates (k_r), non-radiative rates (k_{nr}), and ratio of emission intensity in MD moment and ED moment (I_{rel}) of Eu(D-facam)$_3$ alone and Eu(D-facam)$_3$/TMACl solutions of various concentration ratios.

$\dfrac{[TMACl]}{[Eu(D\text{–}facam)_3]}$	I_{rel}	τ (µs)	Φ_{Ln} (%)	Φ_{tot} (%)	k_r (s^{-1})	k_{nr} (s^{-1})	η_{sens} (%)
0	7.4	95.8	3.15	0.0074	329	10110	0.24
1	5.8	130.7	3.80	0.12	291	7360	3.2
5	5.2	222.3	6.09	0.31	274	4224	5.1
10	5.2	248.6	6.54	0.55	263	3759	8.4

It is known that the η_{sens} of lanthanide complexes are greatly affected by the relationship between the T$_1$ level of the ligands and the receiving 4f level of the central metal ion. The adequate energy gap between the T$_1$ level and the 4f level encourages the energy transfer from the ligands to the metal ion. However, the close match between the T$_1$ level and the 4f level should be avoided because it induces back energy transfer from the metal ion to the ligands.[11]

In order to investigate the change of the T$_1$ level of the ligands in Eu(D-facam)$_3$ by the addition of TMACl, the phosphorescence measurements of the Eu(D-facam)$_3$/TMACl solutions with various TMACl concentration were conducted at 77 K (Figure 5-13).[12] Broad phosphorescent bands due to the D-facam were observed at around 400-500 nm from Eu(D-facam)$_3$/TMACl solutions, and their intensity decreased corresponding to the increase of TMACl concentration. In case of [Eu(D-facam)$_3$]:[TMACl] = 1:10, phosphorescence from the D-facam was almost quenched (Figure 5-13a). This result indicates that addition of TMACl improved the efficiency of energy transfer (η_{sens}) from D-facam to Eu(III) ion in Eu(D-facam)$_3$; the improved energy transfer efficiently deactivated T$_1$ state of the D-facam, resulting in quenching of the phosphorescence.

On the other hands, the shapes and onset wavelength of the phosphorescence spectra were not changed by TMACl (Figure 5-13b), indicating that the T$_1$ level of the D-facam was not influenced. This result suggested that the improvement of η_{sens} was caused by factors other than change in the T$_1$ level of ligands. From the Table 1, non-radiative
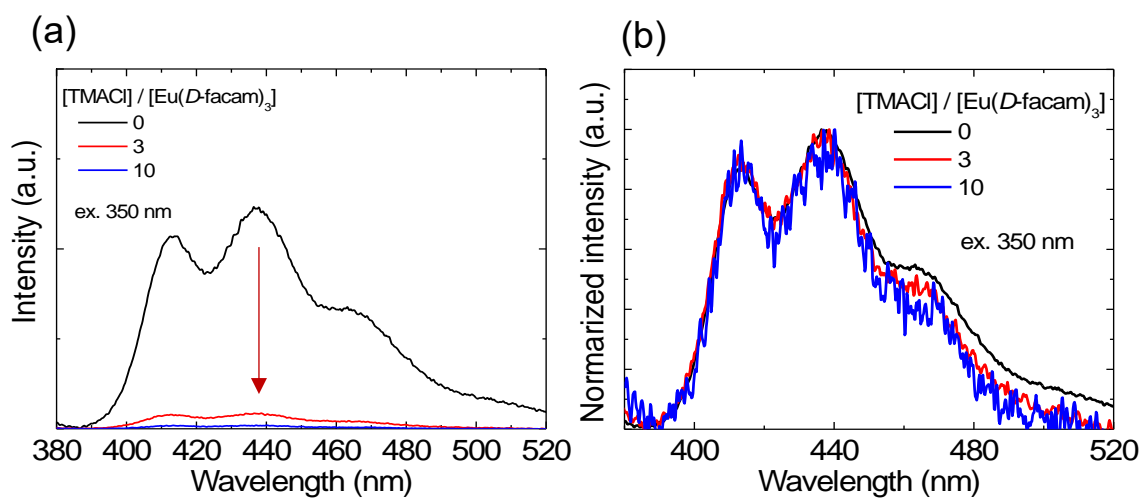
Figure 5-13. Phosphorescence spectra of Eu(D-facam)$_3$ solutions in the presence of various concentrations of TMACl at 77 K (b: normalized spectra).

deactivation of excited state of Eu(III) ion such as vibrational quenching was suppressed by addition of TMACl (decrease of k_{nr}). Suppression of the vibrational quenching would prolong lifetime of T$_1$ state of the ligand, leading to increase of energy transfer efficiency from ligand to Eu(III) ion.   In addition, the changes in the distance between Eu(III) and ligands and the angle between them, as evident from the CD spectra, IR spectra, and I_{rel} values, would also contributed to the significant improvement in η_{sens}.

5.1.5 Change in the optical chirality of Eu(*D*-facam)₃ due to the structural change

The circularly polarized luminescence (CPL) from the Eu(*D*-facam)₃ in the presence of TMACl was investigated because CPL of lanthanide complexes are significantly affected by the coordination structure and crystal fields around the metal ion.[13]   CPL intensity is defined as the difference between the intensity of left-handed CPL and right-handed CPL ($I_{CPL} = I_L - I_R$).   The degree of chiral dissymmetry in luminescence is quantified with using the anisotropy factor (g_{lum}) of CPL, which is given as $g_{lum} = 2(I_L - I_R)/(I_L + I_R)$.[14] Figure 5-14 shows g_{lum} spectra of the Eu(*D*-facam)₃/TMACl solutions with various concentration ratio.   The Eu(*D*-facam)₃ singly dissolved solution did not show significant CPL signal from 580 nm to 630 nm in 1-butanol.   After the addition of TMACl, Eu(*D*-facam)₃ showed negative and positive CPL signal at around 598 nm ($^5D_0 \rightarrow {}^7F_1$) and 613 nm ($^5D_0 \rightarrow {}^7F_2$), respectively.   In the [Eu(*D*-facam)₃]:[TMACl] = 1:10 concentration ratio, the g_{lum} was calculated to −0.69 at 598 nm and −0.09 at 613 nm. From the CD measurements and luminescent analyses, coordination structure of Eu(*D*-facam)₃ was suggested to be transformed by association with TMA⁺, leading to great enhancement of luminescent properties as discussed above.   In the same way as the specific enhancement of luminescence, the CPL properties of Eu(*D*-facam)₃ would be improved by TMA⁺.
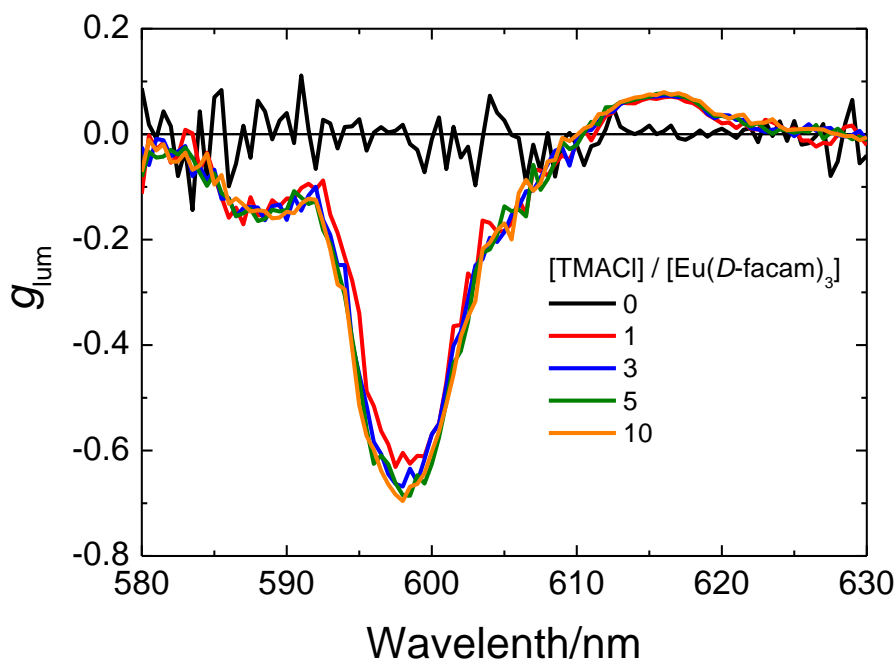
Figure 5-14. CPL spectra of Eu(*D*-facam)₃ alone and Eu(*D*-facam)₃/TMACl solution with various concentration ratios.

To summarize so far, the influence of additives on the photophysical properties of Eu(D-facam)$_3$ in 1-butanol were precisely investigated. Drastic enhancements in emission (70-fold) and dissymmetry factor of CPL (-0.69) were observed upon interaction with TMACl. Various photophysical analyses suggested that the emission enhancement was mainly due to an increased sensitization (high η_{sens}) from ligands to Eu(III) ion by the suppression of reverse energy transfer. These phenomena are primarily driven by the transformation of the coordination structure of Eu(D-facam)$_3$ upon association with TMACl. It is believed that such enhancement in the optical properties of Eu(III) complexes in alcohol can aid in the development of not only luminescent devices, nanodevices and catalysts but also applications related to biological fields.

5.2 Brilliant CPL from DNA-CTMA/Eu(*D*-facam)₃ film

The chiral Eu(*D*-facam)₃ showed a high degree of circular polarization with dramatically enhanced luminescence when additives, especially short alkylammonium ion salt like TMACl and TEACl, were added.   This novel luminescence was attributed to the structural change of Eu(*D*-facam)₃ upon the association with additives.   On the other hand, as described in Chapter 4, association with DNA can lead to further improvement in luminescence through immobilization in its structure and contribution of helical structure.   In addition, fabrication of novel photo-functional films will open up the possibilities of application to various fields.

Therefore, DNA-CTMA/Eu(*D*-facam)₃ films were fabricated and their luminescent properties were investigated toward the further improved photo-functional material.

5.2.1 Introduction of Chiral Eu(*D*-facam)₃ into DNA-based system

Reagents

All chemicals were commercially available and used as received. Europium tris[3-(trifluoromethylhydroxymethylene)-(+)-camphorate] (Eu(*D*-facam)₃), (+)-3-(trifluoroacetyl)camphor, and poly(methylmethacrylate) (PMMA, Mw: ~350,000) were purchased from Sigma-Aldrich (USA). Gadolinium(III) acetate hydrate was purchased from FUJIFILM Wako Pure Chemical Corporation (Japan). The sodium salts of DNA (base pairs: ca. 10,000) were provided by Nippon Chemical Feed Co., Ltd. (Japan). These were marine-based salts that were first isolated from frozen salmon milt through a homogenization process followed by removal of proteins and impurities. Cetyltrimethylammonium chloride (CTMA, 98% purity) and 1-butanol were purchased from Tokyo Chemical Industry Co., Ltd (Japan).

Preparation of the DNA-CTMA complex

DNA-CTMA was prepared by precipitating DNA with a cationic surfactant complex of CTMA in water through an ion exchange reaction that replaced the sodium cations of the DNA.   The DNA complex with CTMA (DNA-CTMA) was prepared by the addition of a 10 mM aqueous solution of DNA (based on the concentration of the phosphate groups) to a 10 mM CTMA solution.   The precipitate was filtered and thoroughly washed with

ultrapure water and then dried in vacuo.　The resulting DNA-CTMA was more water insoluble and more mechanically stable than the DNA itself due to the long alkyl chain of the CTMA.　Through the formation of the CTMA complex, DNA-CTMA was soluble in solvents more compatible with device fabrication, such as chloroform, ethanol, methanol, butanol, or a chloroform/alcohol blend.

Preparation of DNA-CTMA/Eu(*D*-facam)₃ films

DNA-CTMA/Eu(*D*-facam)$_3$ solutions were prepared by dissolving DNA-CTMA and Eu(*D*-facam)$_3$ in 1-butanol. The concentration of DNA-CTMA and Eu(*D*-facam)$_3$ were set to 0.1-1.0 mmol/L and 0.1 mmol/L, respectively. The concentration ratio of DNA-CTMA to Eu(*D*-facam)$_3$ was varied by changing the DNA-CTMA concentration (based on the concentration of the phosphate groups) in solution. The DNA-CTMA/Eu(*D*-facam)$_3$ films were prepared by casting 200 μL of these solutions onto quartz substrates (2×2 cm^2). The weight percentages of Eu(*D*-facam)$_3$ in the DNA-CTMA films ranged between 12 and 58 wt%. A PMMA film containing Eu(*D*-facam)$_3$ (12 wt%) was also prepared for comparison.

Measurements of the optical properties

The absorbance and CD spectra of the DNA-CTMA/Eu(*D*-facam)$_3$ and PMMA/Eu(*D*-facam)$_3$ films were acquired using a photonic multichannel analyzer (J-1100, JASCO Corporation, Japan). The emission spectra were acquired using a spectrofluorometer (FP-6600, JASCO Corporation, Japan). The emission quantum yields were calculated from the data obtained from an absolute PL quantum yield spectrometer (Quantaurus-QY C11347-01, Hamamatsu photonics K. K., Japan). The emission lifetimes were determined using a time-resolved fluorescence spectrometer (Quantaurus-Tau C11367-21, Hamamatsu photonics K. K., Japan). CPL measurements were conducted using a previously reported system,[1,2] which consisted of the following components: 375 nm LED (M365L2, Thorlabs Japan Inc., Japan), LED driver (DC2100, Thorlabs Japan Inc., Japan), photoelastic modulator (PEM-90, Hinds instruments, Inc. United States), photomultiplier tube (H7732-10, Hamamatsu photonics K. K., Japan), linearly polarized cubic prism (200,000:1), photomultiplier tube (H7732-10, Hamamatsu photonics K. K., Japan), and dual phase DSP lock-in amplifier (7265, Signal Recovery Ltd., United Kingdom). The appropriate detection wavelength of the monochromator and PEM was controlled by a PC.

5.2.2 Interaction Between the Chiral Eu(*D*-facam)₃ and DNA-CTMA

Change in absorbance and CD spectrum in the DNA film

  First, I introduced Eu(*D*-facam)₃ into DNA structure to analyze their optical properties. As described in Chapter 4, DNA is soluble only in water, while Eu(*D*-facam)₃ is insoluble in water.   Therefore, DNA was modified with CTMA, which is one of the most typical surfactants utilized for biomolecules.   By utilizing DNA-CTMA, the DNA-CTMA/Eu(*D*-facam)₃ films were successfully prepared.   The absorption and CD spectra of the DNA-CTMA/Eu(*D*-facam)₃ films with various molar ratios of Eu(*D*-facam)₃:DNA-CTMA are shown in Figure 5-15.   The optical analysis of a PMMA/Eu(*D*-facam)₃ film was also carried out for comparison.   PMMA has no structural chirality whereas DNA has a well-known axisymmetric helical structure.[15] For the PMMA/Eu(*D*-facam)₃ film, an absorption band due to the π-π* transition of the β-diketonate[6] in the ligand (*D*-facam) was observed around 305 nm.   On the other hand, the absorption peaks of the DNA-CTMA/Eu(*D*-facam)₃ films were red-shifted by about 10 nm compared to that of the PMMA/Eu(*D*-facam)₃ film, suggesting an interaction between DNA and Eu(*D*-facam)₃.   It is possible that Eu(*D*-facam)₃ electrostatically approach the anionic phosphate groups in the DNA backbone, and such absorption change suggests the intercalation or semi-intercalation between base pairs subsequent by electrostatic interaction.[16,17]   The CD spectrum indicates ellipticity which is proportional to the difference in absorbance of right- and left-circularly polarized light at each wavelength.   Therefore, CD spectrum reveals the structural chirality of the molecules corresponding to its absorption.   In the PMMA/Eu(*D*-facam)₃ film, a positive Cotton effect corresponding to the absorption band of *D*-facam was observed.   This was attributed to the fact that the *D*-facam ligand of Eu(*D*-facam)₃ possesses a chiral structure. For the DNA-CTMA/Eu(*D*-facam)₃ films, typical exciton-splitting CD signals with positive (330 nm) and negative (300 nm) Cotton effects centered at the absorption peak of the ligand were observed.   This indicates that the exciton coupling of the *D*-facam ligands in Eu(*D*-facam)₃ occurred upon interaction with DNA.   In addition, the signal strength of the exciton coupling increased relative to the increase of the DNA ratio, strongly indicating that the structural chirality of Eu(*D*-facam)₃ was enhanced.
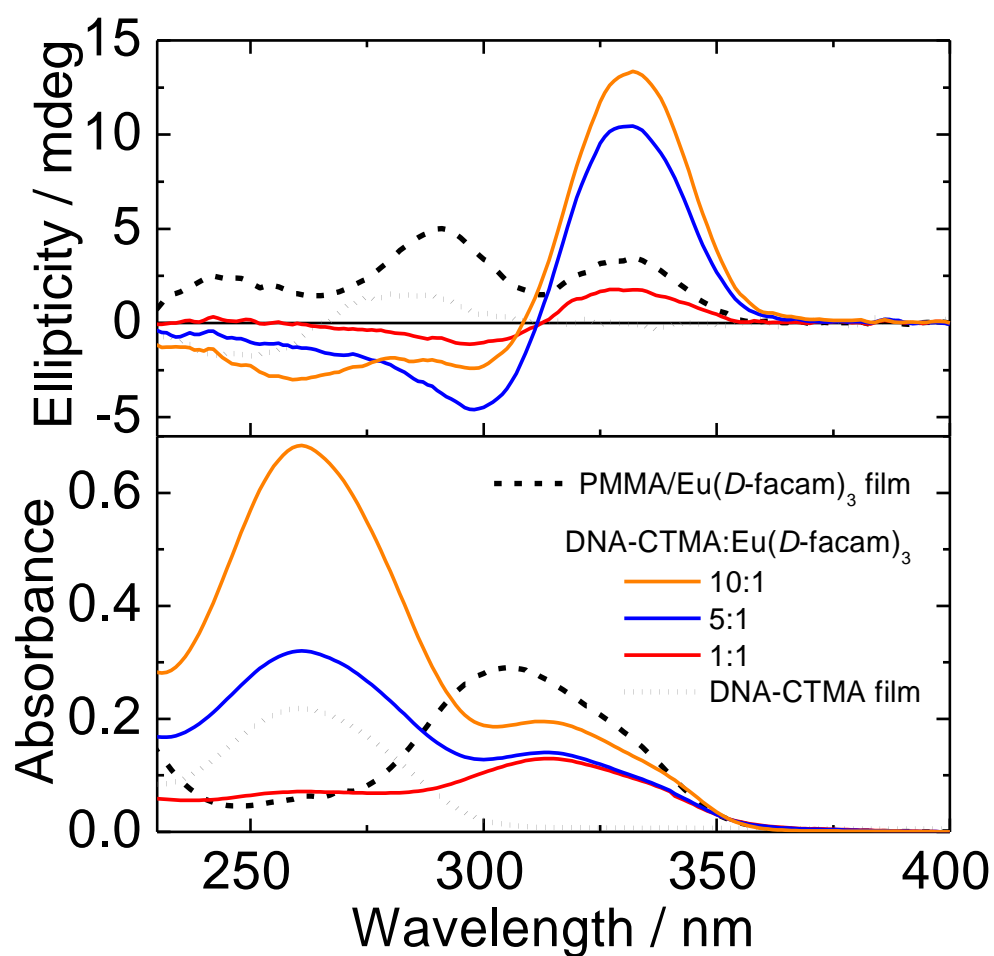
Figure 5-15. Absorbance (bottom) and circular dichroism (CD, top) spectra of DNA-CTMA/Eu(D-facam)$_3$ films at various Eu(D-facam)$_3$:DNA-CTMA molar ratios and PMMA/Eu(D-facam)$_3$ film.

Change in the VCD spectrum in the DNA film

  Vibrational circular dichroism (VCD) spectroscopy experiments were carried out to determine in more detail the structural change of Eu(*D*-facam)₃ in the presence of DNA. Figure 5-16 shows the infrared absorption (IR) and VCD spectra of the Eu(*D*-facam)₃ powder and DNA-CTMA/Eu(*D*-facam)₃ film [Eu(*D*-facam)₃:DNA-CTMA molar ratio was 1:1].   In the IR spectra (bottom), the absorption peaks corresponding to the C=O stretching vibration (around 1650 cm^{-1}) and C=C stretching vibration (around 1500-1600 cm^{-1}) of the *D*-facam ligand were observed for both the Eu(*D*-facam)₃ powder and DNA-CTMA/Eu(*D*-facam)₃ film.[7]   In the VCD spectra (top), although no significant signal was observed in the case of the Eu(*D*-facam)₃ powder, the VCD signals corresponding to the absorption bands of *D*-facam were observed for the DNA-CTMA/Eu(*D*-facam)₃ film. Especially, the absorption band due to the stretching vibration of the C=O group that was in vicinity to the central Eu(III) ion showed a significant exciton splitting pattern, indicating that the coordination symmetry of the ligand field of Eu(III) might be affected. In view of the results of the CD and VCD measurements, it was suggested that the structure of Eu(*D*-facam)₃ was distorted by the interaction with DNA, thus potentially affecting the luminescent properties of Eu(*D*-facam)₃.
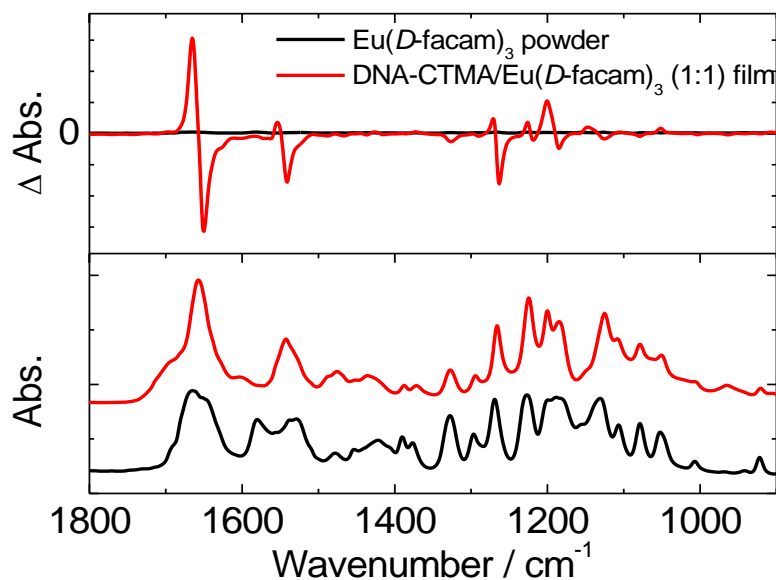
Figure 5-16. Infrared absorbance (bottom) and vibrational circular dichroism (VDC, top) spectra of the Eu(*D*-facam)₃ powder and DNA-CTMA/Eu(*D*-facam)₃ film [Eu(*D*-facam)₃:DNA-CTMA = 1:1].

5.2.3 Emission enhancement of Eu(D-facam)$_3$ within the DNA-CTMA film

Emission properties of the DNA-CTMA/Eu(D-facam)$_3$ film

In order to discuss the influence of the interaction between Eu(D-facam)$_3$ and DNA-CTMA on the luminescent properties, the emission spectra of the PMMA/Eu(D-facam)$_3$ and DNA-CTMA/Eu(D-facam)$_3$ films were examined (Figure 5-17).   For all films, a red emission with sharp peaks due to the f-f transition of the Eu(III) ion was observed upon ligand excitation (330 nm).   In the case of the PMMA/Eu(D-facam)$_3$ film, emission peaks were observed at 579, 585-600 and 613 nm; they corresponded to the $^5D_0 \rightarrow ^7F_0$, $^5D_0 \rightarrow ^7F_1$ and $^5D_0 \rightarrow ^7F_2$ transition of Eu(III) ions, respectively.[4]   Interestingly, for the DNA-CTMA/Eu(D-facam)$_3$ film, the emission peak corresponding to the $^5D_0 \rightarrow ^7F_1$ transition split into two peaks (586 and 595 nm). This change of the emission peak obviously indicated that the interaction with DNA affected the crystal field around the Eu(III) ion (Figure 5-18).   In comparison to the PMMA/Eu(D-facam)$_3$ film, the DNA-CTMA/Eu(D-facam)$_3$ films showed a stronger emission.   Their emission intensity was enhanced with increasing ratios of DNA-CTMA, suggesting that a non-radiative deactivation caused by a molecular vibration was suppressed due to the immobilization onto the DNA backbone.[18,19]
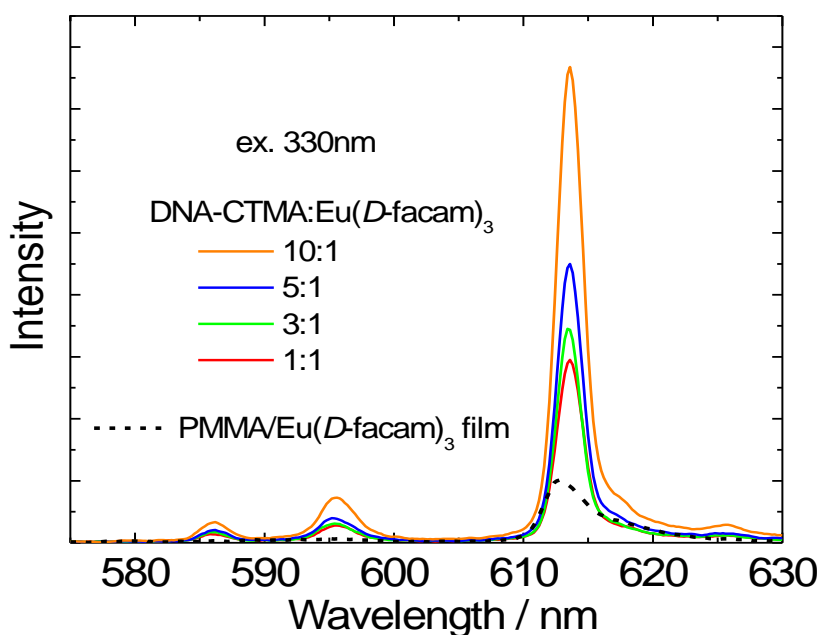
Figure 5-17. Emission spectra of DNA-CTMA/Eu(D-facam)$_3$ films at various Eu(D-facam)$_3$:DNA-CTMA molar ratios and PMMA/Eu(D-facam)$_3$ film upon excitation at 330 nm, as shown by the original emission intensities.
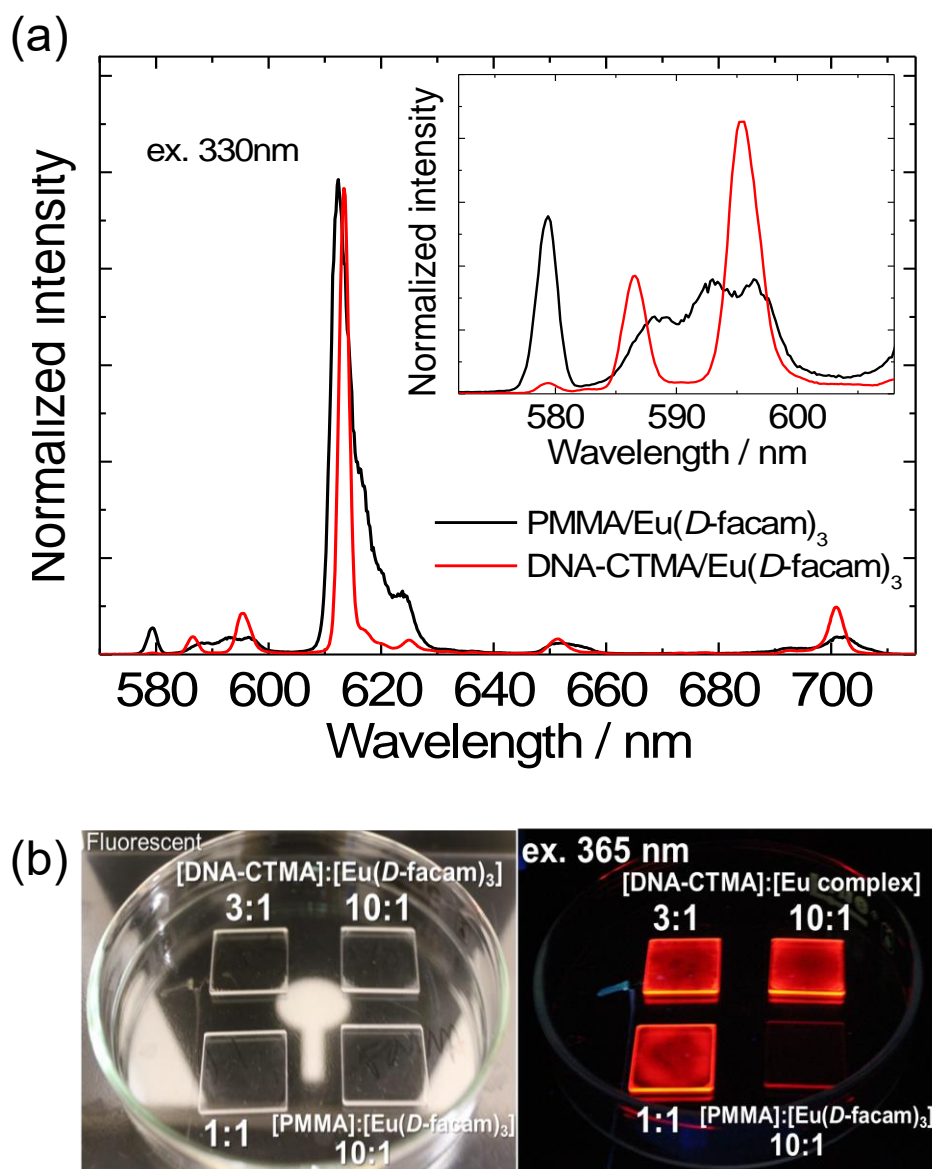
Figure 5-18. Normalized intensities (a). Photograph of the DNA-CTMA/Eu(*D*-facam)₃ films and PMMA/Eu(*D*-facam)₃ film (b).

Symmetry around Eu(III) ion in the Eu(*D*-facam)₃

The emission peak due to the $^5D_0 \rightarrow {}^7F_1$ transition derives from a magnetic dipole (MD) moment and is not easily affected by the ligand field.   On the other hand, the emission due to the $^5D_0 \rightarrow {}^7F_2$ transition is due to the electric dipole (ED) moment and its intensity obviously changes under the influence of the ligand field.   Therefore, the symmetry of Eu(*D*-facam)₃ can be discussed based on the ratio of the emission intensities obtained from the MD moment (I_{MD}) and ED moment (I_{ED}).[5]   The emission ratio ($I_{rel} = I_{ED}/I_{MD}$) of the PMMA/Eu(*D*-facam)₃ and DNA-CTMA/Eu(*D*-facam)₃ films are shown in Table 5-2.   Since the values of I_{rel} for the DNA-CTMA/Eu(*D*-facam)₃ films (5.14-5.60) were lower than that of the PMMA/Eu(*D*-facam)₃ film (7.64), it was estimated that the coordination structure around the Eu(III) ion in Eu(*D*-facam)₃ changed to a higher symmetric structure in the presence of DNA.   The changes in the structure of Eu(*D*-facam)₃ were also confirmed by CD and VCD measurements.   These results clearly suggested that Eu(*D*-facam)₃ and DNA interacted with each other and led to a stronger emission, as shown in Figure 5-17.

Table 5-2. Ratio of the emission intensity of the MD and ED moment (I_{rel}), luminescence lifetime (τ), radiative rate (k_r), non-radiative rate (k_{nr}), intrinsic quantum yield of Eu(III) ion (Φ_{Ln}), total quantum yield (Φ_{tot}), and efficiency of sensitization (η_{sens}) of the DNA-CTMA/Eu(*D*-facam)₃ and PMMA/Eu(*D*-facam)₃ films.

Sample	Polymer:Eu(III) (Weight ratio of Eu(III))	I_{rel}	τ (μs)	k_r (s⁻¹)	k_{nr} (s⁻¹)	Φ_{Ln} (%)	Φ_{tot} (%)	η_{sens} (%)
PMMA/Eu(III) film	— (12 wt%)	7.64	114	419	8353	14.9	0.5	10.5
DNA/Eu(III) film	1:1 (58 wt%)	5.15	626	317	1597	16.5	11.9	72.0
	3:1 (31 wt%)	5.14	606	316	1334	19.2	11.7	61.0
	5:1 (22 wt%)	5.62	601	341	1323	20.5	12.0	58.6
	10:1 (12 wt%)	5.60	602	340	1322	20.4	13.7	67.0

Detailed analyses of photophysical parameters of the DNA-CTMA/Eu(*D*-facam)₃ films

Generally, Eu(III) ions with a highly symmetrical structure hardly show any strong emission since the high symmetry of the Eu(III) ion results in a low radiative rate.[8] Therefore, the factors that contributed to the emission enhancement of Eu(*D*-facam)₃ in DNA-CTMA films were determined. The total quantum yield (Φ_{tot}) and luminescence lifetime (τ) of the PMMA/Eu(*D*-facam)₃ and DNA-CTMA/Eu(*D*-facam)₃ films were obtained (Table 5-2). The luminescent quantum yield was 0.5 and 11.9-13.7% for the PMMA/Eu(*D*-facam)₃ and DNA-CTMA/Eu(*D*-facam)₃ films, respectively; the luminescent quantum yield of Eu(*D*-facam)₃ was significantly increased in the case of DNA-CTMA compared to PMMA. The radiative rate constants of Eu(III) ions (k_r) was also calculated using the relation:

$$k_r = A_{MD,0} \times n^3 \times \left(\frac{I_{tot}}{I_{MD}}\right)$$

where $A_{MD,0}$ is the spontaneous emission coefficient of the $^5D_0 \rightarrow {}^7F_1$ transition (= 14.65 s^{-1}), n is the refractive index of the medium and I_{tot}/I_{MD} is the ratio of the integrated radiation corresponding to the $^5D_0 \rightarrow {}^7F_j$ transition (j = 0-6) to the peak area corresponding to the $^5D_0 \rightarrow {}^7F_1$ transition. Here, the value of n was determined to be 1.52 and 1.49 for the DNA-CTMA[20] and PMMA solid film[21], respectively. The non-radiative rate constant (k_{nr}) can be calculated from the relations:

$$\tau = \frac{1}{k_r + k_{nr}} \quad , \qquad k_{nr} = \frac{1}{\tau} - k_r$$

while the intrinsic quantum yield (Φ_{Ln}) and efficiency of sensitization of the lanthanide luminescence by the ligand (η_{sens}) can be calculated from the relations:[11]

$$\Phi_{Ln} = \frac{k_r}{k_r + k_{nr}} \quad , \qquad \eta_{sens} = \frac{\Phi_{tot}}{\Phi_{Ln}}$$

These photophysical parameters are listed in Table 1. It was evident that the k_r value of Eu(D-facam)$_3$ for the DNA-CTMA films (316-340 s^{-1}) was lower than that of the PMMA film (419 s^{-1}). This implies that the probability of light emission from the excited state decreased in the presence of DNA, which is consistent with the structural change around the Eu(III) ion towards a higher symmetry structure, as discussed above.

On the other hand, k_{nr} decreased and η_{sens} increased for the DNA-CTMA films compared to the PMMA film. The k_{nr} value of PMMA was approximately 8400 s^{-1}; it decreased to 1300 s^{-1} upon mixing with DNA. It is known that the molecular vibration can be suppressed when the molecules are immobilized on a DNA structure.[18,19] Therefore, the decrease in k_{nr} clearly indicated a suppressed vibrational deactivation of the excited states of the Eu(III) ion due to the immobilization on a DNA molecule. The decreased k_{nr} contributed to improving the intrinsic quantum yield (Φ_{Ln}); the calculated Φ_{Ln} increased from 14.9% (in PMMA) to 20.5% (in DNA-CTMA). In addition, the η_{sens} value of Eu(D-facam)$_3$ significantly improved upon interaction with DNA; it was almost 7 times higher compared to that of PMMA. This improvement of η_{sens} is believed to contribute to the emission enhancement of Eu(D-facam)$_3$.

T1 level of the *D*-facam ligand within the DNA-CTMA film

It is known that the η_{sens} value of lanthanide complexes significantly depends on the relationship between the T_1 level of the ligands and the accepting 4f level of the central metal ion.[11] An adequate energy gap between the T_1 and 4f levels encourages the energy transfer from the ligands to the metal ion. However, a close match between the T_1 and 4f levels should be avoided as it induces back energy transfer from the metal ion to the ligands. To investigate the change of the T_1 level of the *D*-facam ligand in the different polymers, the phosphorescence of Gd(D-facam)$_3$ of the PMMA and DNA-CTMA film was measured at 77 K (Figure 5-19). It is known that the first excitation energy of Gd(III) is much higher than the triplet energy of general complex ligands.[22] Thus, the energy transfer from ligands to the Gd(III) ion hardly occur, thus only the phosphorescence from the ligands can be observed. The T_1 level can be calculated from the onset wavelength of the phosphorescence spectrum. Broad phosphorescence bands due to *D*-facam were observed around 460–650 nm for both films. The onset wavelength of the phosphorescence spectrum of each film almost matched (462 nm), indicating that the T_1 level of *D*-facam was unperturbed (calculated as ca. 21600 cm^{-1}). Thus, the improvement of η_{sens} was caused by factors other than the change in the T_1 level of the

ligands. Therefore, the changes of the distance between Eu(III) and ligands as well as the angle between them, as evidenced by the CD and VCD spectra and I_{rel} values, contributed to the significant improvement of η_{sens}. In addition, the decrease of k_{nr} discussed above obviously indicates that Eu(D-facam)$_3$ was tightly immobilized onto the DNA structure. The immobilization of these molecules might suppress the vibrational deactivation of the T_1 states, and allow to improve η_{sens}, which represents the energy transfer efficiency from the ligands to the central metal ion.
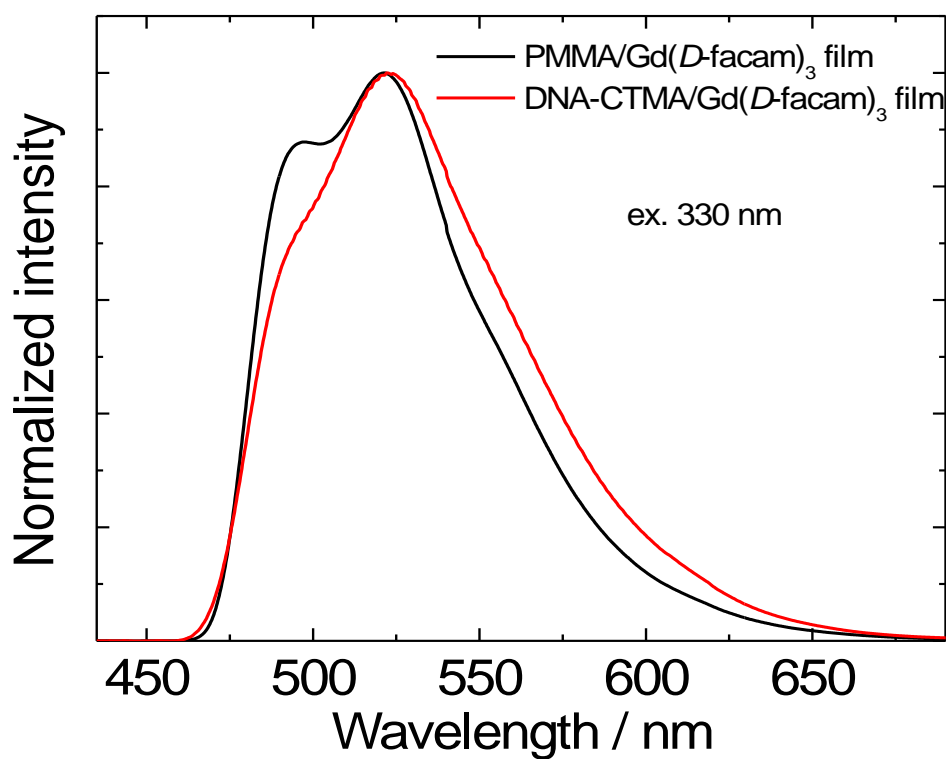
Figure 5-19. Phosphorescence spectra of the DNA-CTMA/Gd(D-facam)$_3$ and PMMA/Gd(D-facam)$_3$ films at 77 K.

5.2.4 Circularly polarized luminescence induced by DNA-CTMA

As discussed above, it was demonstrated that the structural chirality of Eu(D-facam)$_3$ significantly changed upon its interaction with DNA-CTMA. Therefore, it was assumed that CPL, which reflects the chiral luminescence, might also be greatly enhanced.[13] Therefore, the CPL spectra of the PMMA/Eu(D-facam)$_3$ and DNA-CTMA/Eu(D-facam)$_3$ films were measured and their g_{cpl} values are shown in Figure 5-20. An emission dissymmetry factor [$g_{cpl} = 2(I_L - I_R)/(I_L + I_R)$] was utilized to quantitatively evaluate the magnitude of CPL, where I_L and I_R represent the emission intensity of left-handed and right-handed circular polarized luminescence, respectively.[14] For the PMMA/Eu(D-facam)$_3$ film, the CPL intensity was very weak, and the g_{cpl} was calculated to be −0.02 at $^5D_0 \rightarrow {}^7F_1$ (598 nm, MD transition). On the other hand, in the case of the DNA-CTMA/Eu(D-facam)$_3$ films, clear CPL signals were observed at $^5D_0 \rightarrow {}^7F_1$ (598 nm, MD transition) and $^5D_0 \rightarrow {}^7F_2$ (615 nm, ED transition). The g_{cpl} at $^5D_0 \rightarrow {}^7F_1$ (598 nm) was determined to be −0.62, which resulted approximately 30 times enhanced compared to the PMMA/Eu(D-facam)$_3$ film. Such chirality enhancement of the luminescence was supposed to be due to the change of the ligand field of Eu(D-facam)$_3$ caused by the interaction with DNA-CTMA.
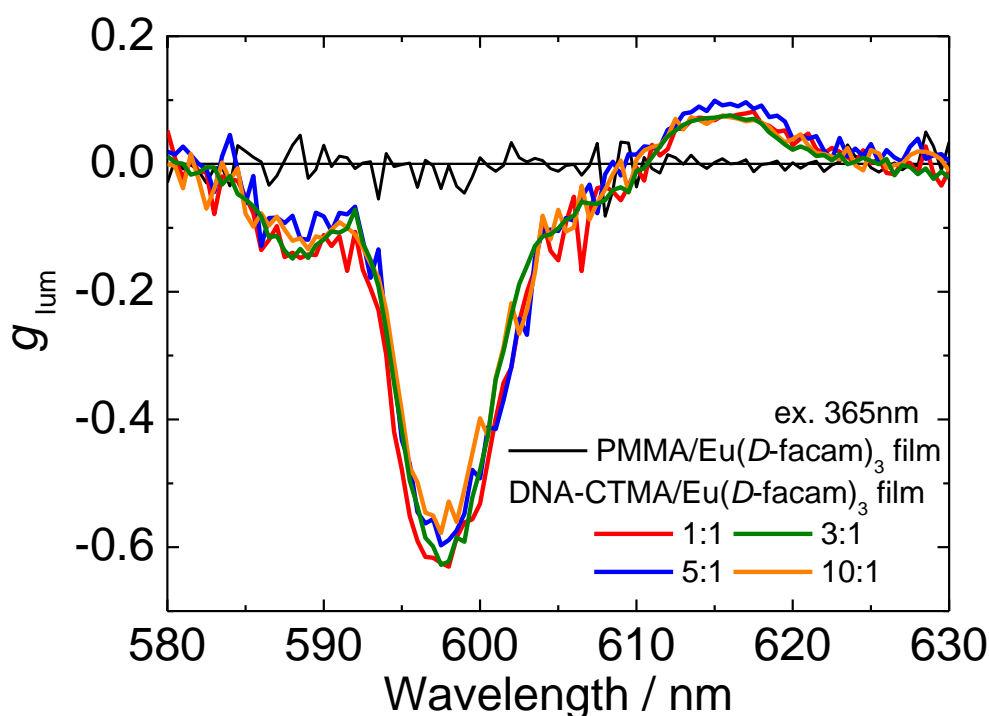
Figure 5-20. CPL spectra of the DNA-CTMA/Eu(D-facam)$_3$ films at various Eu(D-facam)$_3$:DNA-CTMA molar ratios and PMMA/Eu(D-facam)$_3$ film upon excitation at 330 nm.

5.3 Summary of Chapter 5

In this section, the influence of additives such as CTMA on the luminescent properties of Eu(III) complexes was first investigated. It was revealed that TMA^+ which is cation part of CTMA can associate with Eu(D-facam)$_3$ and improve its luminescence due to the structural change of complex. In contrast, addition of CTMA did not affect the luminescence of Eu(tta)$_3$(H$_2$O)$_2$. This indicates that the improvement of luminescence of Eu(tta)$_3$(H$_2$O)$_2$ upon the interaction with DNA-CTMA (Chapter 4) was attributed to the DNA, not CTMA. Therefore, it was suggested that DNA as well as TMACl may interact with Eu(D-facam)$_3$ and improve its luminescent properties. Then, DNA-CTMA/Eu(D-facam)$_3$ films were prepared, and their luminescent properties were investigated to develop novel photo-functional film. As a result, an emission enhancement and higher dissymmetry factor (-0.6) of Eu(D-facam)$_3$ were simultaneously achieved upon interaction with DNA. Various photophysical analyses suggested that the emission enhancement was mainly due to the increase of the sensitization efficiency (high η_{sens}) from the ligands to Eu(III) as well as suppression of the vibrational deactivation upon immobilization onto the DNA molecule. These phenomena were primarily driven by the transformation of the coordination structure of Eu(D-facam)$_3$ upon association with DNA. Luminescence from Eu(III) complexes is attributed to forbidden f-f transitions, thus the simultaneous achievement of strong emission intensity and high g_{lum} was difficult until this point. Therefore, it can be assumed that such enhancement of the optical properties of Eu(III) complexes with DNA can contribute to the development of not only luminescent devices, nanodevices and catalysts but also applications related to biological fields and DNA engineering.

References of Chapter 5

1. Shinoda, S., Miyake, H., Tsukube, H., Handbook on the Physics and Chemistry of Rare Earths, Volume 35 (ed. Gschneidner, K. A., Bunzli, J. C., Pecharsky, V.) 273-335 (Elsevier B.V., 2005).

2. Werts, M. H. V.; Duin, M. A.; Hofstraat, J. W.; Verhoeven, J. W. Bathochromicity of Michler's Ketone upon Coordination with Lanthanide(III) β-Diketonates Enables Efficient Sensitisation of Eu3+ for Luminescence under Visible Light Excitation. *Chem. Commun.* **1999**, No. 9, 799–800. https://doi.org/10.1039/a902035g.

3. Tsumatori, H.; Nakashima, T.; Kawai, T. Observation of Chiral Aggregate Growth of Perylene Derivative in Opaque Solution by Circularly Polarized Luminescence. *Org. Lett.* **2010**, *12* (10), 2362–2365. https://doi.org/10.1021/ol100701w.

4. Moore, E. G.; Samuel, A. P. S.; Raymond, K. N. From Antenna to Assay: Lessons Learned in Lanthanide Luminescence. *Acc. Chem. Res.* **2009**, *42* (4), 542–552. https://doi.org/10.1021/ar800211j.

5. Tanner, P. A. Some Misconceptions Concerning the Electronic Spectra of Tri-Positive Europium and Cerium. *Chem. Soc. Rev.* **2013**, *42* (12), 5090–5101. https://doi.org/10.1039/c3cs60033e.

6. Tsukube, H.; Onimaru, A.; Shinoda, S. Anion Sensing with Luminescent Tris(β-Diketonato)Europium(III) Complexes and Naked-Eye Detection of Fluoride Anion. *Bull. Chem. Soc. Jpn.* **2006**, *79* (5), 725–730. https://doi.org/10.1246/bcsj.79.725.

7. K. A. Gschneidner, J. C. Bunzli and V. Pecharsky, Eds., Handbook on the Physics and Chemistry of Rare Earths, North Holland, Netherland, 2005, Vol. 35.

8. Hasegawa, Y.; Yamamuro, M.; Wada, Y.; Kanehisa, N.; Kai, Y.; Yanagida, S. Luminescent Polymer Containing the Eu(III) Complex Having Fast Radiation Rate and High Emission Quantum Efficiency. *J. Phys. Chem. A* **2003**, *107* (11), 1697–1702. https://doi.org/10.1021/jp022397u.

9. Mara, D.; Artizzu, F.; Smet, P. F.; Kaczmarek, A. M.; Van Hecke, K.; Van Deun, R. Vibrational Quenching in Near-Infrared Emitting Lanthanide Complexes: A Quantitative Experimental Study and Novel Insights. *Chem. - A Eur. J.* **2019**, *25* (69), 15944–15956. https://doi.org/10.1002/chem.201904320.

10. Chauvin, A. S.; Gumy, F.; Imbert, D.; Bünzli, J. C. G. Europium and Terbium Tris(Dipicolinates) as Secondary Standards for Quantum Yield Determination. *Spectrosc. Lett.* **2004**, *37* (5), 517–532. https://doi.org/10.1081/SL-120039700.

11. Binnemans, K. Lanthanide-Based Luminescent Hybrid Materials. *Chem. Rev.* **2009**, *109* (9), 4283–4374. https://doi.org/10.1021/cr8003983.

12. Ogata, S.; Shimizu, T.; Ishibashi, T.; Ishiyone, Y.; Hanami, M.; Ito, M.; Ishii, A.; Kawaguchi, S.; Sugimoto, K.; Hasegawa, M. Water-Soluble Lanthanide Complexes with a Helical Ligand

Modified for Strong Luminescence in a Wide PH Region. *New J. Chem.* **2017**, *41* (14), 6385–6394. https://doi.org/10.1039/c7nj01444a.

13. Harada, T.; Nakano, Y.; Fujiki, M.; Naito, M.; Kawai, T.; Hasegawa, Y. Circularly Polarized Luminescence of Eu(III) Complexes with Point- And Axis-Chiral Ligands Dependent on Coordination Structures. *Inorg. Chem.* **2009**, *48* (23), 11242–11250. https://doi.org/10.1021/ic901663w.

14. Sang, Y.; Han, J.; Zhao, T.; Duan, P.; Liu, M. Circularly Polarized Luminescence in Nanoassemblies: Generation, Amplification, and Application. *Adv. Mater.* **2019**, *1900110* (11), 1–33. https://doi.org/10.1002/adma.201900110.

15. Watson, J.; Crick, F. Molecular Structure of Nucleic Acids. *Nature.* **1953**, *171* (4356), 737–738. https://doi.org/10.1038/171737a0.

16. Aslanoglu, M. Electrochemical and Spectroscopic Studies of the Interaction of Proflavine with DNA. *Anal. Sci.* **2006**, *22* (3), 439–443. https://doi.org/10.2116/analsci.22.439.

17. Annaraj, J.; Srinivasan, S.; Ponvel, K. M.; Athappan, P. R. Mixed Ligand Copper(II) Complexes of Phenanthroline/Bipyridyl and Curcumin Diketimines as DNA Intercalators and Their Electrochemical Behavior under Nafion® and Clay Modified Electrodes. *J. Inorg. Biochem.* **2005**, *99* (3), 669–676. https://doi.org/10.1016/j.jinorgbio.2004.11.018.

18. Ouyang, X.; Wang, M.; Guo, L.; Cui, C.; Liu, T.; Ren, Y.; Zhao, Y.; Ge, Z.; Guo, X.; Xie, G.; Li, J.; Fan, C.; Wang, L. DNA Nanoribbon-Templated Self-Assembly of Ultrasmall Fluorescent Copper Nanoclusters with Enhanced Luminescence. *Angew. Chemie - Int. Ed.* **2020**, *59* (29), 11836–11844. https://doi.org/10.1002/anie.202003905.

19. Minami, H.; Nakamura, K.; Kobayashi, N. Enantioselective Luminescence Enhancement of Chiral Ru(Phen)$_3^{2+}$ Complexes by Interaction with Deoxyribonucleic Acid. *J. Nanophotonics* **2018**, *12* (03), 1. https://doi.org/10.1117/1.jnp.12.033005.

20. Jung, W.; Jun, H.; Hong, S.; Paulson, B.; Nam, Y. S.; Oh, K. Cationic Lipid Binding Control in DNA Based Biopolymer and Its Impacts on Optical and Thermo-Optic Properties of Thin Solid Films. *Opt. Mater. Express* **2017**, *7* (11), 3796. https://doi.org/10.1364/ome.7.003796.

21. Song, J.; Kim, J.; Suh, K. Poly (Methyl Methacrylate) Toughening with Refractive Index-Controlled Core – Shell Composite Particles. **1998**, No. August, 1607–1614.

22. A.P.Suisalu, Valery N. Zakharov, A.L.Kamyshny, L. A. A. Effect of the Paramagnetic Ion Gd(Lll) on the Molecular Triplet State of the Organic Ligand in Complexes. *J. Chem. Inf. Model.* **1989**, *98*, 1330–1335. https://doi.org/10.1017/CBO9781107415324.004.

Conclusions

Since the 1990s, luminescent metal complexes have played an important role as a theme for various luminescent applications and academic research. However, the simultaneous achievement of both strong emission intensity and brilliant luminescent chirality was difficult in the metal complex-based systems. This thesis focused on the association of metal complex with DNA toward the development of novel photo-functional materials since the luminescent properties of the metal complexes significantly change under the alteration of the structure and ligand field around the central metal ion. As a result, unique chiral optical properties were obtained from the DNA/metal complex.

First, chiral Ru(II) complexes (Δ-, Λ-Ru(phen)$_3{}^{2+}$) were associated with DNA. Δ- and Λ-Ru(phen)$_3{}^{2+}$ formed associations with DNA thorough different interaction modes, respectively. The interaction modes of these complexes were mainly intercalation between the base pairs of DNA. From the results of various photophysical analyses, the strength and percentage of intercalation were higher in the case of Δ- form than that in Λ-form. Corresponding to this difference in the interaction mode of Δ-, Λ-Ru(phen)$_3{}^{2+}$ and DNA, CD indicated obviously different change. Such change in optical chirality is expected to apply for chemical sensors, bio-probes, and security systems. As a result of different interaction with DNA, Δ- and Λ-Ru(phen)$_3{}^{2+}$ showed enantioselective emission enhancement. The extent of emission enhancement of Δ-form (ca. 3times compared to original) was higher than that of Λ-form (2.5 times). This enantioselective emission enhancement is also suitable for various sensor systems.

However, although obvious chiral change in absorption and enantioselective emission enhancement were observed, significant CPL signal was not obtained from DNA/Ru(II) complexes. Therefore, I focused on the Eu(III) complex, which is expected to show a high degree of circularly polarization in luminescence due to the f-f transition. When the achiral Eu(III) complex (Eu(tta)$_3$(H$_2$O)$_2$) was associated with DNA-CTMA film, induced CD signal was observed, indicating the change in coordination structure. As a result of association with DNA-CTMA film, the emission intensity of Eu(tta)$_3$(H$_2$O)$_2$ was enhanced by ca. 3 times compared to in PMMA film. In addition, induced CPL was observed from DNA-CTMA/Eu(tta)$_3$(H$_2$O)$_2$ film. Like this, it was demonstrated that Eu(III) complex can exhibit induced CPL by associating with DNA. Such induced CPL is suitable for the fields of chemical sensing, bio sensing, security systems etc.

In addition, by introducing chiral ligand into the Eu(III) complex, the extent of emission enhancement and circularly polarization in luminescence of DNA/Eu(III) complex film were greatly improved.   An emission enhancement and higher dissymmetry factor (−0.6) were simultaneously observed upon association of chiral Eu(III) complex (Eu(*D*-facam)$_3$) and DNA.   These phenomena were primarily driven by the transformation of the coordination structure of Eu(*D*-facam)$_3$ by DNA.   It can be assumed that such enhancement of the optical properties of Eu(III) complexes with DNA can contribute to the development of not only luminescent devices, nanodevices and catalysts but also applications related to biological fields and DNA engineering.

Like this, this thesis reported the luminescence enhancement and expression of chiral optical properties by associating metal complexes with DNA.   By self-assembling functional materials on DNA which is a chiral backbone, I constructed novel materials that have both excellent properties due to functional materials and high emission circular polarization that reflects the chiral structure of DNA.   Currently, CPL is practically obtained by optical filters.   Therefore, the DNA-based materials that expresses high-intensity CPL constructed in this thesis are the proposal for novel chiral-optical devices and are expected to the development of applications for circularly polarized light sources. In addition, the functional DNA complex and its expression method of function invented in this research propose new design guidelines in the field of DNA materials, which have been attracting attention in Japan and overseas in recent years, and are very academically significant.   Further, I believe that addition of luminescent circularly polarization to metal complexes can greatly contribute not only to display applications but also to technologies such as various sensing applications for physiologically active substances.

List of publications

Chapter 2

1. **<u>Haruki Minami</u>**, Kazuki Nakamura, Norihisa Kobayashi, "Enantioselective luminescence enhancement of chiral Ru(phen)$_3^{2+}$ complexes by interaction with DNA", Journal of Nanophotonics, **12**(3), 033005 (2018).

2. Norihisa Kobayashi, **<u>Haruki Minami</u>**, Kazuki Nakamura, "Photonics of DNA/Ruthenium(II) complexes", Nanophotonics, **7**(8), 1373-1385 (2018).

3. <u>南　晴貴</u>，高橋　亮太，中村　一希，小林　範久，"DNA と Ru(II)錯体の組織化による特異的光学特性発現およびその電気化学素子応用"，日本画像学会誌, **59**(3), 330-340 (2020).

Chapter 3

4. **<u>Haruki Minami</u>**, Ryota Takahashi, Kazuki Nakamura, Norihisa Kobayashi, "Electrochemically triggered upconverted luminescence for light-emitting devices" Chemical Communications, **55**, 12611-12614 (2019).

Chapter 4

5. Kazuki Nakamura, **<u>Haruki Minami</u>**, Amika Sagara, Natsumi Itamoto, Norihisa Kobayashi, "Enhanced red emissions of europium(III) chelates in DNA-CTMA complexes", Journal of Materials Chemistry C, **6**, 4516-4522 (2018).

Chapter 5

6. **<u>Haruki Minami</u>**, Mayu Miyazato, Ziying Li, Kazuki Nakamura, Norihisa Kobayashi, "Alkyl ammonium ion-induced drastic emission enhancement of Eu(D-facam)$_3$ in 1-butanol", Chemical Communications, **56**, 13532-13535, (2020).

7. **<u>Haruki Minami</u>**, Natsumi Itamoto, Ziying Li, Kazuki Nakamura, Norihisa Kobayashi, "Investigation of the improved luminescent properties of a chiral Eu(III) complex within a DNA-CTMA matrix", Scientific Reports, **10**, 18917, (2020).